ROBUSTNESS AND ADAPTIVITY ENHANCED CONTROLLER DESIGN FOR SMART GRID POWER SYSTEMS WITH HIGH RENEWABLE ENERGY PENETRATION

チュク スプリヤディ アリ ナンダー

https://doi.org/10.15017/1398394

Kyushu University
Graduate School of Information Science
and Electrical Engineering

ROBUSTNESS AND ADAPTIVITY ENHANCED CONTROLLER DESIGN FOR SMART GRID POWER SYSTEMS WITH HIGH RENEWABLE ENERGY PENETRATION

by

Cuk Supriyadi ALI NANDAR

A THESIS

Submitted in partial fulfillment of

The requirements for the degree of

[DOCTOR OF ENGINEERING]

DEPARTMENT OF ELECTRICAL AND ELECTRONIC ENGINEERING

GRADUATE SCHOOL OF INFORMATION SCIENCE AND ELECTRICAL ENGINEERING

KYUSHU UNIVERSITY

2013

Thesis Title	**Robustness and Adaptivity Enhanced Controller Design for Smart Grid Power Systems with High Renewable Energy Penetration**
Student	Cuk Supriyadi Ali Nandar
Student ID.	3IE10044E
Degree	Doctor of Engineering
Program	Electrical Engineering
Year	2013
Thesis Advisor	- Prof. Dr. Tadahiro Goda - Prof. Dr. Junichi Murata

ABSTRACT

The penetration of renewable energy in power system significantly increases. However it causes some issues on power systems such as frequency deviation due to unstable power outputs of renewable energy generation units, and rotor angle instability (low frequency oscillation) caused by decrease in the total inertia constant of conventional generating plants when the electric grid receives a large amount of power from the renewable energy generation units. This thesis proposes control system design by considering robustness and adaptivity to overcome the problem. In this method, the existing controllers, most of which are PID or lead-lag controllers, are optimized, so that they can exhibit better performance and that if this alone cannot attain desirable performance, new devices will be installed. The proposed control design will be applied to solve frequency deviation in isolated power systems, and rotor angle stability in interconnected power systems with high renewable energy penetration. In isolated power systems, robust control design is enough to handle frequency deviation. However, in interconnected power system, when the variations of total inertia constants are large, giving robustness to the controllers is not enough. The controllers adaptive to

the changes in operating conditions due to the high penetration of renewable energy (RE) sources are needed. In the proposed adaptive control, the controller parameters are changed depending on the situations. Here a system identification technique and the robust controller design method are combined into an indirect adaptive controller design. The identified model is used to monitor discrepancy between the actual power system output and the expected output (model output). When a large discrepancy is detected, a new set of controller parameters is determined to adapt to the new situation. The simulation studies have been done to evaluate the effectiveness of proposed control design. The results show the proposed adaptive control scheme is able to stabilize power system under the changeable operation conditions and system uncertainties due to high penetration of renewable energy sources.

ACKNOWLEDGMENT

All praise, glory and gratitude be to Allah who said in the Holy Quran that "He who taught (the use of) the pen. Taught the man that which he knew not". Peace be upon the Prophet Mohammad, his family, his companions, and all those who followed him until the Day of Judgment.

First of all I wish to express my deepest gratitude to my thesis advisor Professor Tadahiro Goda and Professor Junichi Murata for their invaluable advice, personal attention, and continuous encouragement throughout my PhD program at Kyushu University. It was a greats experience learning with him. I am also deeply grateful to my thesis committee members Professor Taketoshi Kawabe and Professor Masataka Iwakuma for their involvement and the time they spared to review this thesis and for their constructive suggestions and comments.

I would like to thanks Assoc. Professor Hashiguchi, Kyushu Sangyo University, Japan, for giving me the support during the research of doing my Doctoral of Engineering Program.

Special thanks to AUN/SEED-Net projects that is mainly supported by the Japan International Cooperation Agency (JICA) for their financial support and giving me the opportunities and chances to publish, present, and contribute in international conferences. My appreciation is extended to Head of Electrical Engineering Department of Kyushu University and Their staff especially Assist. Professor Takano for their strong support and encouragement to complete the study.

Special and deep thanks to my wonderful parents, wife (Dewi Pusparini), children (Nur Aini Malihah, Katara Velda Naila and Muhammad Wafi Hikaru), brothers and sisters for their moral support and motivation. Last but not least, I extend my thanks and appreciation to my friends and everyone who helped to get this work done.

(Cuk Supriyadi Ali Nandar)

TABLE OF CONTENTS

LIST OF TABLES

LIST OF FIGURES

CHAPTER 1

INTRODUCTION

1.1 Background of Smart Grid Power Systems

The conventional structure of electrical power systems consist of large generating stations, transmission, distribution, and utilization of electrical energy [1]. These conventional large electric power systems have existed for more than 50 years, have been improved over the years and offered a number of advantages. However, over the last few years, the operations of power system are more challenging in security, reliability, efficiency and quality of the electric power supply due to economic, political, environmental, and social constraints. To answer the challenges in power system, transforming from the conventional structure of power systems to smart grid power systems has been started. The objective of transforming the current power grids into smart grids is to provide high quality electric power to customers in an environmentally friendly and sustainable way. This objective will be achieved through the application of combination of existing and emerging technologies for energy efficiency, renewable energy integration, demand response, monitoring and control, flexible ac transmission systems (FACTS), and so on [2].

The key differences between existing grids and smart grids are illustrated in Fig. 1.1 and 1.2. It can be observed that there is a fundamental shift in the design and operational paradigm of the grid: from central to distributed resources, from predictable power flow directions to unpredictable directions, from passive grid to an active grid. The smart grid should be accessible to distributed renewable energy generations (DREGs), comply with different forms of generation, enable local energy demand management through smart metering systems and facilitate dynamic control techniques [3]. In this context, the grid will be more dynamic in its configuration and its operational condition, which will present many opportunities not only for optimization but also many new technical challenges.

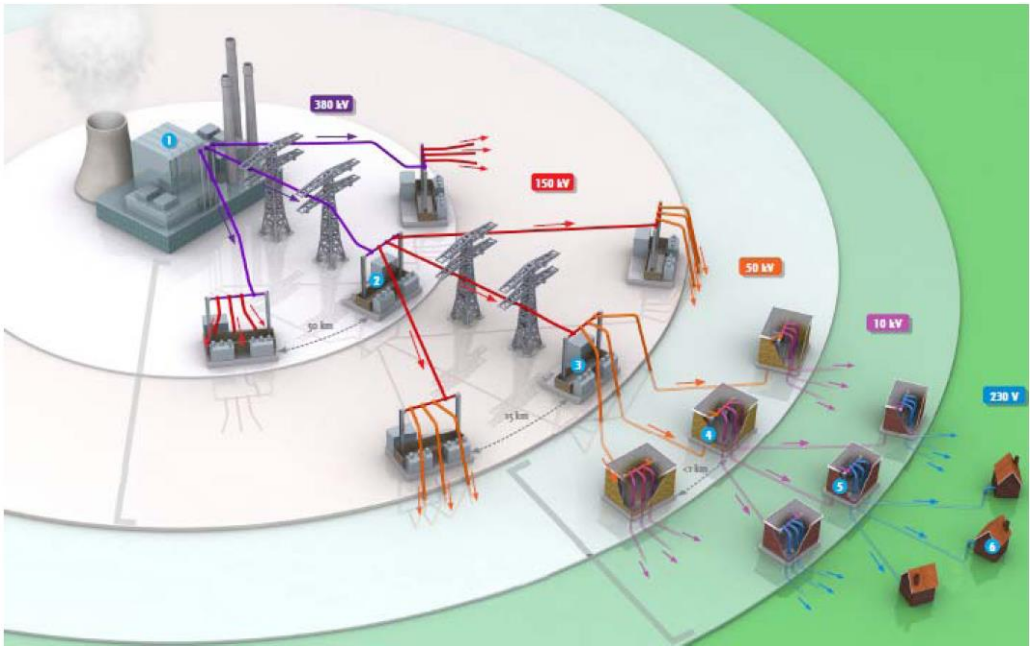

Figure 1.1 Conventional Electric Grid (illustration)

(Source: www.kennisinbeeld.nl)

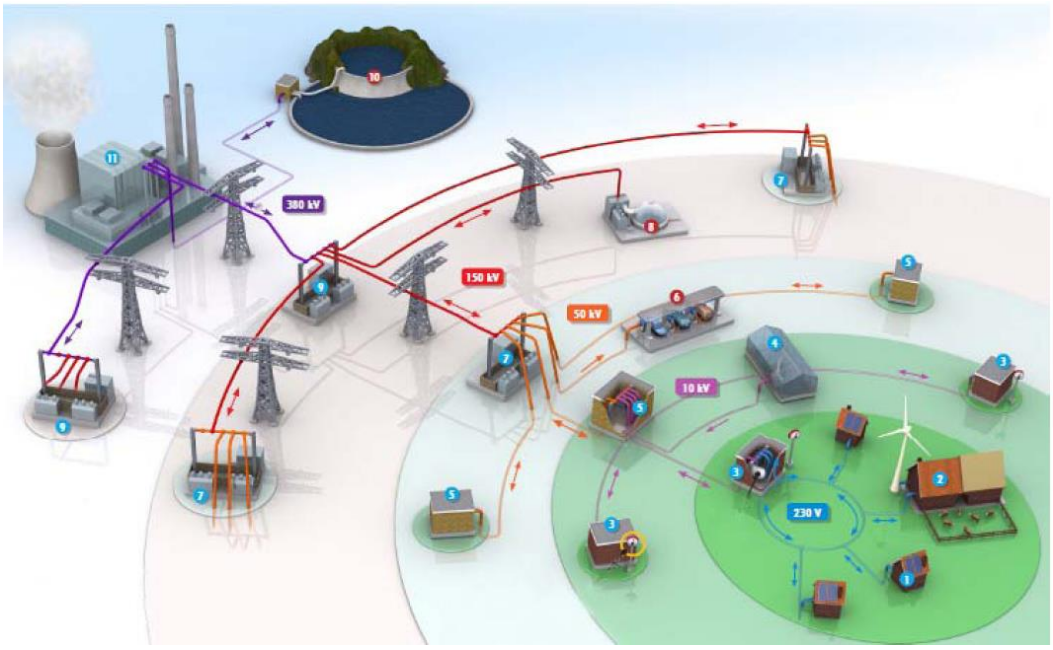

Figure 1.2 Concept of Smart Grid (illustration)

(Source: www.kennisinbeeld.nl)

1.1.1 Renewable Energy Integration

Extensive use of renewable energy for electrical power generation is expected to mitigate the environment and resources problems. Due to the variable nature of most renewable energy sources, either over seasons or within minutes, cost-effective

integration into electricity supply has proven to be challenging. It will require many fundamental changes in the ways that electric power systems are planned and operated to maintain reliability and quality of energy service. The operation challenges related to stability issues due to high DREGs penetration into electricity grid are listed as follows,

1. Voltage instability

Voltage problems typically occur in power systems which are heavily loaded faulted and/or have reactive power shortages [4]. Among the various factors which affect voltage stability issues, there is a special correlation between voltage instability problems and insufficient reactive power reserves [5]. Voltage collapse is related to reactive power demands of loads not being met because of limitations on the available reactive power reserves and transmission of reactive power [6]. It has been proved that inadequate reactive power compensation during stressed operating condition can lead to voltage instability. In the case of DREGs penetration, the voltage instability is caused by excess power output from individual renewable energy generation in the feeder.

2. Power excess

A large amount of unstable power output of DREGs at short periods may cause power excess in power systems. The condition occurs when output from photo voltaic panels is on peak power at day time and/or all wind generations receive the optimal wind speed. This power excess is likely to raise the other instability.

3. Frequency deviation

The frequency in power systems represents the balance between generated power and demand. In normal operation, small load variations occur spontaneously. In addition, more severe power imbalances might occur from power plant outages or line tripping and result in larger frequency deviations. Moreover, large intermittency of DREGs on electricity grid makes frequency control more difficult. In order to avoid these large deviations and secure a stable electrical grid, a frequency control mechanism must be implemented in power systems.

4. Rotor angle instability (low frequency oscillation)

Disturbances in an interconnected power system lead to low frequency oscillation in the grid. In the period immediately following a disturbance, the frequency deviation is primarily characterized by the amount of inertia in the system. This initial reaction of the power system to a disturbance is called inertial response of the system. It can be described as a stabilizing effect in response to a change from the equilibrium condition in the power system. Such an inertial response has long been treated as given in power systems due to the prevalence of synchronous generators. But with the increasing penetration of DREGs, often connected to the grid through power electronic devices, the overall inertial response of the system is decreasing [7] – [12].

Among the issues above, this thesis addresses (a) frequency deviation due to unstable power outputs of renewable energy generation units, and (b) rotor angle instability (low frequency oscillation) caused by decrease in the total inertia constant of conventional generating plants when the electric grid receives a large amount of power from the renewable energy generation units. In order to overcome the problems, the implementation of smart technologies and control mechanism are highly needed.

1.1.2 Smart Grid Technologies

Smart grid technologies and renewable energy technologies are important issues in regard to the global climate change problem and energy security for this century. Integrating DREGs to power systems causes several technical issues, such as power system stability and power quality. However, with the presence of smart grid technologies such as information and communication system, control system, energy storage and FACTS devices etc., there are high possibilities that these issues can be solved and minimized. The key smart grid technologies are described as follows:

- Information and communication systems

  Advanced communications are essential for enabling smart grid applications such as grid visualization, real-time load monitoring, automated demand response, advanced protection, asset monitoring, smart metering, and consumer load control.

  As one of the enabling technologies, a fast, reliable and secure communication network plays a vital role in the power system management. The network is required to connect the magnitude of electric devices in distributed locations and exchange their status information and control instructions. The system-wide intelligence is feasible only if the information exchange among the various functional units is expedient, reliable and trustable. The current communication capabilities of the existing power systems are limited to small-scale local regions that implement basic functionalities for system monitoring and control, such as power-line communications [13–16] and the Supervisory control and data acquisition (SCADA) systems [17–20], which do not yet meet the demanding communication requirements for the automated and intelligent management in the next-generation electric power systems. The future power systems comprise of a diversity of electric generators and power consumers that are located distributive over vast areas and connected all together into the same management network. Real-time bidirectional communications are the foundations to support the comprehensive power system management tasks which, in certain cases, require time-sensitive and data-intensive information exchange.

  When we develop the smart grid, it is critical to take advantage of the advancements in networking technologies to enable the automated and intelligent system management. Although the currently available networking technologies have greatly satisfied our personal communication needs,

applying them to power systems and addressing the specific requirements for power communications are challenging by all means.

- Energy storage (ES)

  Primarily, ES units are aimed to store energy during the off-peak load period and release it in the peak load period. However, energy storages also are able to supply both active and reactive powers simultaneously and quickly, to compensate the fluctuation of DREGs, and to damp the inter-area low-frequency oscillation [21-26]. The applications of the ES also include load regulation, transmission stabilization, uninterruptible power supply, power compensation, voltage control and improving customer power quality, etc. [27-29]. Moreover, the ES also has been successfully applied to solve many problems in power systems such as an improvement of power system dynamics [30,31], a frequency control in interconnected power systems [32,33], an improvement of power quality [34], a stabilization of sub-synchronous oscillation in the turbine-generator [35], a load leveling [36] etc.

- FACTS devices.

  Recent development of power electronics introduces the use of flexible ac transmission system (FACTS) controllers in power systems. FACTS controllers are capable of controlling the network condition in a very fast manner and this feature of FACTS can be exploited to improve the voltage stability, and steady state and transient stabilities of a complex power system [37]-[42]. This allows increased utilization of existing network closer to its thermal loading capacity, and thus avoiding the need to construct new transmission lines.

  Static VAR Compensator (SVC) is a first generation FACTS device that can control voltage at the required bus thereby improving the voltage profile of the system. The primary task of an SVC is to maintain the voltage at a particular bus by means of reactive power compensation [43]. SVCs have been used for high performance steady state and transient voltage control

compared with classical shunt compensation. SVCs are also used to dampen power swings, improve transient stability, and reduce system losses by optimized reactive power control [44]-[45].

Thyristor Controlled Series Capacitor (TCSC) is one of the important members of FACTS family that is increasingly applied with long transmission lines by the utilities in modern power systems. It can have various roles in the operation and control of power systems, such as scheduling power flow; decreasing unsymmetrical components; reducing net loss; providing voltage support; limiting short-circuit currents; mitigating sub synchronous resonance (SSR); damping the power oscillation; and enhancing transient stability [46]-[48].

A Static Synchronous Series Compensator (SSSC) is a member of FACTS family which is connected in series with a power system. It consists of a solid state voltage source converter which generates a controllable alternating current voltage at fundamental frequency. When the injected voltage is kept in quadrature with the line current, it can emulate as inductive or capacitive reactance so as to influence the power flow through the transmission line [49]. While the primary purpose of a SSSC is to control power flow in steady state, it can also improve transient stability of a power system.

Among the available FACTS devices, the Unified Power Flow Controller (UPFC) is the most versatile one that can be used to improve steady state stability, dynamic stability and transient stability [50]. The UPFC can independently control many parameters since it is the combination of Static Synchronous Compensator (STATCOM) and SSSC [51-53].

- Control System

High DREGs penetration into power network delivers a number of technical issues in power system. To overcome the technical issues effectively, control is one of the key enabling technologies for the deployment of renewable energy systems. Moreover, information technology, energy storage and

FACTS devices require effective use of advanced control techniques. In addition, smart grids cannot be achieved without extensive use of control technologies at all levels.

1.1.3 Control System in Power System

In this thesis, the author focuses on control system. The reasons are twofold: control plays a very significant role in power system operations; and many of power system components are already equipped with controllers whose improvement can be performed with a smaller cost comparing to installing new apparatuses.

Several approaches based on modern control theories have been successfully applied to design controllers in power systems [54-57]. In [54], the application of optimal state-feedback control has been presented, while an eigenvalue shifting technique for determining the weighing matrix in the performance index has been proposed [55]. In [56], a sequential eigenvalue assignment algorithm for selecting the parameters of controllers in multi-output/multi-input systems has been presented. In sequential tuning, the controller parameters are computed using repeated application of single-input/single-output (SISO) analysis. In [57], the eigenvalue assignment has been proposed to design the optimal controller. Besides, the new optimal linear quadratic regulator (LQR) based design has been presented [58]. It is superior to previously reported LQR approaches. However, since these techniques [54-58] do not take the presence of system uncertainties such as system nonlinear characteristics, variations of system configuration due to unpredictable disturbances, loading conditions etc. into consideration in the system modeling, the robustness of these controllers against uncertainties cannot be guaranteed.

To overcome these problems, controller designs based on self tuning control [59-61], fuzzy-logic systems [62, 63], artificial neural networks (ANN) [64-66] have been presented. Moreover, H_∞ control has been applied to design of robust controllers [67, 68]. In these works, the designed H_∞ controller via mixed sensitivity approach has confirmed the significant performance and high robustness. In this approach, however, due to the trade-off relation between sensitivity function and

complementary sensitivity function, the weighting functions in H_∞ control design cannot be selected easily. Moreover, the order of H_∞ controller depends on that of the plant which is different from the conventional lead/lag controller. Despite the significant potential of control techniques mentioned above, power system utilities still prefer the conventional controller structure, PID or lead-lag controllers. This is due to the ease of implementation, the long-term reliability, etc.

On the other hand, much research on existing/conventional controller structure design has paid attentions to tuning of controller parameters. The parameters of controllers are optimized under various operating conditions by heuristic methods such as tabu search [69], genetic algorithm [70], and simulated annealing [71] etc. Using these approaches, the controller parameters are obtained so that all of the dominant mode eigenvalues may be placed at the prescribed locations in the s-plane. In these designs, however, the uncertainty model is not embedded in the mathematical model of the power system. Furthermore, the robust stability against system uncertainties is not taken into consideration in the optimization process. Therefore, the robust stability margin of the system in these works may not be guaranteed in the face of several uncertainties.

To tackle the problem, a technique that enhances the robustness of existing/conventional controllers is necessary. The principle underlying the research described in the thesis is that we optimize the existing controllers, most of which are PID or lead-lag controllers, so that they can exhibit better performance and that if this alone cannot attain desirable performance, new devices will be installed. In other words, we do not throw away the existing controllers to replace them with new but expensive ones which the field operators may not be familiar with but enhance their performance.

The author first proposes a technique that enhances robustness of the conventional type (PID or lead-lag) controllers in power systems. The control performance is guaranteed by specifying the poles of the closed-loop systems within a desirable region, while the robustness index is optimized. This constrained optimization

problem cannot be solved analytically. Thus a meta-heuristic optimization technique (genetic algorithm) is employed. This technique is applied to both of frequency deviation problem and the rotor angle instability problem. The results show the controller can guarantee performance and robustness of its control.

Then a technique is proposed that gives adaptivity as well as robustness to the conventional type of controllers. In adaptive control, the controller parameters are changed depending on the situations. However, it is not desirable that the parameters are changed too frequently. It is preferable that the parameter alteration is done at the right moment. This demand for a method that can detect when to change the parameters and a method that determines how they should be changed. Here a system identification technique and the robust controller design method described above are combined into an in-direct adaptive controller design. The identified model is used to monitor discrepancy between the actual power system output and the expected output (model output). When a large discrepancy is detected, a new set of controller parameters is determined to adapt to the new situation. The effectively of the proposed control design is evaluated by simulation studies in both isolated and interconnected smart grid power systems.

1.2 Research Methodologies and Techniques.

This research aims to find out the performance of smart grid power systems, especially to examine power system stability when large DREGs are coupled to the grids. The research was done by designing power system configuration of both isolated and interconnected smart grid power systems with renewable energy generation and simulated using Simulink/Matlab and ObjectStab/Dymola Software. The details of proposed methods and techniques to investigate the impact of high renewable energy penetration on smart grids power system are as follows:

1. **Study of high renewable energy penetration impact on power system network:** This part of the study was intended to collect information and review the impact of high renewable energy penetration on power system

networks, such as in terms of an isolated smart grid and an interconnected smart grid power system.

2. **Developing the configuration of isolated smart grid power system and interconnected power system with high renewable penetration:** Isolated and interconnected smart grid power system configuration was developed through the use of control devices. The system simulation work allows measurement of the frequency and primary grid parameters and analysis of the system‘s behavior at particular points in normal and extreme conditions, especially when small and large output power of DREGs are connected to the smart grid power system.
3. **Designing the controller by considering robustness and adaptivity**: First, this part proposes a technique that enhances robustness of the conventional type (PID or lead-lag) controllers in power systems. Then a technique is proposed that gives adaptivity as well as robustness to the conventional type of controllers.
4. **Performance analysis:** The final system configuration was performed to obtain results. The simulation results were validated by several case studies on both isolated and interconnected smart grid power systems through the following scenarios:
    - Parameter system variations analysis, which is used to investigate the potential impact of renewable energy generation penetrations on network performance, particularly to check the frequency deviation and rotor angle pattern. Moreover, it is used to evaluate the robustness of controller, especially to identify and determine whether the development of adaptive control design is necessary or not.
    - Smart grid power system stability analysis to check whether the system remains stable or not after sudden changes in large power output of renewable energy and load. The system stability analysis also has been done by examining sudden faults in the system.

1.3 Summary of Contribution/Originality of The Thesis

This research will contribute to the knowledge in renewable energy penetration on both distributed generation and interconnected smart grid power system areas, as it addresses major concerns in smart grid stability.

The summary of contributions and originalities of this research are mentioned below:

1. Designing existing structure (PID or Lead/lag) of controller by considering robustness and adaptivity. The existing structure of controller is easy to be implemented in utility and costless. In adaptive control, the controller parameters are changed depending on the situations. By considering the robustness, it is not desirable that the parameters are changed too frequently. It is preferable that the parameter alteration is done at the right moment.
2. The identified model is equipped with virtual controller. The advantage of the feature is the parameters tuning of the controller can be done without disturbing the real controller. The virtual controller is modeled by mathematical model for more flexibility and low cost.
3. The proposed control design method is able to store several good models and corresponding controller parameter sets in memory, and re-uses them in the similar situations without model identification and controllers parameters re-tuning, then we have "Model and Controller Bank".
4. The each control device is able to identify and tune controller parameters independently. As a result, no communication system is necessary and cost of investment can be reduced.
5. Further, this research will contribute to knowledge since smart grids have become a leading concern in the field of power systems, in particular with its development in industry.

1.4 Outline of The Thesis

This section presents an outline of the thesis.

Chapter 1 - A brief description of smart grid power systems is provided and challenges of smart grid application on power systems are discussed. The challenge of smart grids on control scheme is specially highlighted. Furthermore, robustness and adaptivity of control system design due to renewable energy penetration on smart grid power systems to improve performance in power system stability are introduced.

Chapter 2 - The general theories of conventional robust control design are presented. The classification of system uncertainties modeling is provided. Then the conventional control system design considering system uncertainties to guarantee robustness of controller are given. The example of application of conventional control design on a single machine infinite bus power system is presented.

Chapter 3 - This chapter introduces conventional adaptive control designs. First, direct adaptive control design, especially MIT rule, to adjust parameters of controller is explained. The example of MIT rule direct adaptive control design in simple plant is presented. Then, this chapter presents indirect adaptive control systems using iterative identification and control design method, and multi model adaptive control scheme. The several methods for identification and control system design are briefly explained.

Chapter 4 - This chapter shows the proposed robust control design and adaptive control scheme. The proposed robust control design using conventional control structure is described. Furthermore, the example of application of the proposed robust control design to a single machine infinite bus power system is presented to shows comparison results of both the proposed robust control and the conventional robust control. The weakness of robust control design due to high renewable energy penetration in power system is discussed. Next, the proposed indirect adaptive robust control design is described.

Chapter 5 - This chapter presents the robustness and adaptivity enhanced controller design in isolated smart grid power systems. The details of power system model, pitch controller model and principal operation of energy storage are given. To check the performance and robustness of proposed energy storage controller in comparison with that of conventional energy storage controller, eigenvalues analysis and non linear simulation using Simulink/Matlab are applied.

Chapter 6 - This chapter concentrates on the application of proposed method to design of adaptive robust power system stabilizer (PSS) in two areas four machines power system. First, system modeling such as generator model, exciter model, and power system equipped with PSS is described. Then non-linear simulation studies using ObjectStab are applied to evaluate damping performance and robustness of the proposed PSS in comparison with those of PSSs designed without considering robustness and adaptivity against several system uncertainties.

Chapter 7 - General conclusion and recommendations for further research are given.

REFERENCES

[1] P.H Schavemaker and L. van der Sluis, " Electrical power system essentials", Wiley & sons, Chichester, United Kingdom, 2008.

[2] Edison Electric Institute," Understanding smart grid. From definition to development" Washington, D.C., March 2009.

[3] European Smart Grids Technology Platform. Vision and strategy for Europe's electricity networks of the future. Technical report, European Smart Grids Technology Platform.

[4] P. Kundur, Power System Stability and Control. New York: McGraw-Hill, 1994.

[5] A.M. Abed., "WSCC voltage stability criteria, under voltage load shedding strategy, and reactive power reserve monitoring methodology," Power Engineering Society Summer Meeting, 1999. IEEE , vol.1, no., pp.191-197 vol.1, 18-22 Jul 1999.

[6] L. Bao, Z. Huang, W. Xu, "Online voltage stability monitoring using VAr reserves," Power Systems, IEEE Transactions on , vol.18, no.4, pp. 1461-1469, Nov. 2003.

[7] J. Morren, J. Pierik, S.W.H. de Haan, "Inertial Response of Variable Speed Wind Turbines" Electric Power Systems Research, 2005.

[8] A. Mullane, M. O'Malley, "The Inertial Response of Induction - Machine - Based Wind Turbines" IEEE Transactions on Power Systems, 2005.

[9] A. Mullane, M. O'Malley, "Kinetic Energy and Frequency Response Comparisons for Renewable Generation Systems" International Conference on Future Power Systems, 2005.

[10] G. Lalor, A. Mullane, M. O'Malley, " Frequency Control and Wind Turbine Technologies" Dublin, Ireland. IEEE Transactions on Power Systems, 2005.

[11] Y. Lei, A. Mullane, G. Lightbody, R. Yacamini, "Modeling of the Wind Turbine with a Doubly Fed Induction Generator for Grid Integration Studies" IEEE Transactions on Energy Conversion, 2006.

[12] A. Mullane, M. O'Malley, " Modifying the Inertial Response of Power - Converter Based Wind Turbine Generators" The 3rd IET International Conference on Power Electronics, Machines and Drives, 2006.

[13] N. Ginot, M.A. Mannah, C. Batard, M. Machmoum, "Application of power line communication for data transmission over PWM network", IEEE Transactions on Smart Grid 1 (2), 178–185, 2010.

[14] J. Anatory, N. Theethayi, R. Thottappillil, Channel characterization for indoor power-line networks, IEEE Transactions on Power Delivery 24, 4, 1883–1888, 2009.

[15] V.K. Chandna, M. Zahida, Effect of varying topologies on the performance of broadband over power line, IEEE Transactions on Power Delivery, 25, 4, 2371–2375, 2010.

[16] C. Konate, A. Kosonen, J. Ahola, M. Machmoum, J.-F. Diouris, Powerline communication in motor cables of inverter-fed electric drives, IEEE Transactions on Power Delivery, 25, 1, 125–131, 2010.

[17] V.I. Nguyen, W. Benjapolakul, K. Visavateeranon, A high-speed, low cost and secure implementation based on embedded Ethernet and internet for SCADA Systems, in: Proceedings of SICE Annual Conference, 2007.

[18] J.D. McDonald, Developing and defining basic SCADA system concepts, in: Proceedings of Rural Electric Power Conference, 1993.

[19] I. Ali, M.S. Thomas, Substation communication networks architecture, in: Proceedings of Joint International Conference on Power System Technology and IEEE Power India Conference, 2008.

[20] Q. Yang, J.A. Barria, C.A.H. Aramburo, A communication system architecture for regional control of power distribution networks, Proceedings of IEEE International Conference on Industrial Informatics, 2009.

[21] S. Banerjee, J.K. Chatterjee and S.C. Tripathy "Application of Magnetic Energy Storage Unit as Load-frequency Stabilizer," IEEE Trans. on Energy Conversion, Vol. 5, No.1, pp.46–51, 1990.

[22] F. Irie, M. Takeo and S. Sato, " A Field Experiment on Power Line Stabilization by a SMES System," IEEE Trans. on Magnetics, Vol. 28, pp.426–429, 1992.

[23] X. Jiang and X. Chu, " SMES System for Study on Utility and Customer Power Applications," IEEE Trans. on Applied Superconductivity, Vol. 11, pp. 1765–1768, 2001.

[24] J.B. Simo and I. Kamwa, " Exploratory Assessment of the Dynamic Behavior of Multi-machine System Stabilized by a SMES Unit," IEEE Trans. on Power Systems, Vol.10, No.3, pp. 1566–1571, 1995.

[25] C.J. Wu and Y.S. Lee, "Application of Simultaneous Active and Reactive Power Modulation of Superconducting Magnetic Energy Storage Unit to Damp Turbine-Generator Subsynchronous Oscillations," IEEE Trans. on Energy Conversion, Vol.8, No.1, pp. 63–70, 1993.

[26] J. Maschowski and D. Nelles, “Power System Transient Stability Enhancement by Optimal Simultaneous Control of Active and Reactive Power,” IFAC symposium on power system and power plant control, Munich, pp. 271–276, 1992

[27] W. Buckles and W.V. Hassenzahl, “ Superconducting Magnetic Energy Storage,“ IEEE Power Engineering Review, pp.16–20, 2000.

[28] K.P. Juengst, ”SMES Progress,” Proc. of 15th International Conference on Magnet Technology, Science Press, pp. 18–23, 1998.

[29] C.A. Luongo,“ Superconducting Storage Systems: An Overview,” IEEE Trans. on Magnetics, Vol. 32, No.4, pp.2214–2223, 1996.

[30] M.G. Rabbani, J.B.X. Devotta and S. Elangovan, “An Adaptive Fuzzy Controlled Superconducting Magnetic Energy Storage Unit for Power Systems,” Energy Conversion and Management , Vol. 39, pp.931-942, 1998.

[31] J.B.X. Devotta and M.G. Rabbani, “Application of Superconducting Magnetic Energy Storage Unit in Multi-machine Power Systems,” Energy Conversion and Management, Vol. 41, pp. 493-504, 2000.

[32] S.C. Tripathy, “Dynamic Simulation of Hybrid Wind-diesel Power Generation System with Superconducting Magnetic Energy Storage,” Energy Conversion and Management, Vol.38 , pp.919-930, 1997.

[33] I. Ngamroo, “An Optimization Technique of Robust Load Frequency Stabilizers for Superconducting Magnetic Energy Storage,” Energy Conversion and Management, Vol.46, pp.3060-3090, 2005.

[34] X. Chu, X. Jiang, Y. Lai , X. Wu and W. Liu, “SMES Control Algorithms for Improving Customer Power Quality,” IEEE Trans. on Applied Superconductivity, Vol. 11, pp.1769-1772, 2001.

[35] J.B.X. Devotta, M.G. Rabbani and S. Elangovan, “Application of Superconducting Magnetic Energy Storage Unit for Damping of Subsynchronous Oscillations in Power Systems,” Energy Conversion and Management, Vol.40, pp.23-37, 1999.

[36] M.K. Abdelsalam, R.W. Boom and H.A. Perterson, " Operation Aspects of Superconducting Magnetic Energy Storage (SMES)," IEEE Trans. on Magnetics, Vol.23, pp. 3275-3277, 1987.

[37] Igor Papic, Peter Zunko, 2002, "Mathematical Model and Steady State Operational Characteristics of a Unified Power Flow Controller,"Electro-technical Review, Slovenija, 69(5), pp. 285-290.

[38] Prechanon Kumkratug, 2009, "Application of UPFC to Increase Transient Stability of Inter-Area Power System," Journal of Computers, 4(4), pp. 283-287.

[39] Prechanon Kumkratug, Panthep Laohachai, "Direct Method of Transient Stability Assessment of a Power System with a SSSC," Journal of Computers, 2(8), pp. 77-82, 2007.

[40] S.V. Ravi Kumar, S. Siva Nagaraju, "Transient Stability Improvement using UPFC and SVC," ARPN Journal of Engineering and Applied Sciences, 2(3), pp. 38-45, 2007.

[41] A. Kazemi, F. Mahamnia, "Improving of Transient Stability of Power Systems by Supplementary Controllers of UPFC using Different Fault Conditions," WSEAS Transactions on Power Systems, 3(7), pp. 547-556, 2008.

[42] S. Panda, Ramnarayan N. Patel, "Improving Power System Transient Stability with an off-centre Location of Shunt FACTS Devices," Journal of Electrical Engineering, 57(6), pp. 365-368, 2006.

[43] N.G. Hingorani, L. Gyugyi, "Understanding FACTS: Concepts and Technology of Flexible AC Transmission Systems," IEEE Press, New York, 1999.

[44] N. Mithulananthan, C.A. Canizares, J. Reeve, Graham J. Rogers, "Comparison of PSS, SVC and STATCOM Controllers for Damping Power System Oscillations," IEEE Transactions on Power Systems, 18(2), pp. 786-792, 2003.

[45] E.Z. Zhou, "Application of Static Var Compensators to Increase Power System damping," IEEE Transactions on Power Systems, 8(2), pp. 655-661, 1993.

[46] P. Mattavelli, G.C. Verghese, A.M. Stankovic "Phasor Dynamics of Thyristor-Controlled Series Capacitor Systems," IEEE Transactions on Power Systems, 12(3), pp. 1259-1267, 1997.

[47] B.H. Li, Q.H. Wu, D.R. Turner, P.Y. Wang, X.X. Zhou, "Modeling of TCSC Dynamics for Control and Analysis of Power System Stability," Electrical Power & Energy Systems, 22(1), pp. 43-49, 2000.

[48] A.D. Del Rosso, C.A. Canizares, V.M. Dona, "A Study of TCSC Controller Design for Power System Stability Improvement," IEEE Transactions on Power Systems, 18(4), pp. 1487-1496, 2003.

[49] L. Gyugyi, "Dynamic Compensation of AC Transmission Line by Solid State Synchronous Voltage Sources," IEEE Transactions on Power Delivery, 9(22), pp. 904-911, 1994.

[50] M. Noroozian, L. Angquist, M. Ghandhari, G. Andersson, "Use of UPFC for Optimal Power Flow Control," IEEE Transactions on Power Delivery, 12(4), pp. 1629-1634, 1997.

[51] M. Ghandhari, G. Andersson, I.A. Hiskens, "Control Lyapunov Functions for Series Devices," IEEE Transactions on Power Delivery, 16(4), pp. 689-694, 2001.

[52] P. Kumkratug, M.H. Haque, "Versatile Model of a Unified Power Flow Controller in Simple System," IEE Proc. Gener. Transm. & Distrib., 150(2), pp. 155-161, 2003.

[53] V. Vittal, N. Bhatia, A.A. Fouad, "Analysis of the Inter-area Mode Phenomenon in Power Systems Following Large Disturbances," IEEE Transactions on Power Systems, 6(4), pp. 1515-1521, 1991.

[54] Larsen E, Swarm D. Applying power system stabilisers. IEEE Trans. on PAS. 1981; 100: 3017-46. Zhou E.Z. Design of stabilizers for a multimachine power system based on the sensitivity of PSS effect. IEEE Power & Energy Society 1992; 7: 3: 606 - 13.

[55] Aldeen M. Multimachine power system stabilizers design based on new LQR

approach. Proc. of IEE Proc.-Gen. Tran. Dist. 1995; 142: 494-502.

[56] Chen S. H_∞ optimization-based power system stabilizer design. Procs. of IEE.-Gen. Tran. Dist. 1995; 142: 179-84.

[57] Yan T.C. Applying optimization method to power system stabilizer design – Parts 1 & 2. Int. J. of Elect. Pwr. & Ener. Syst. 1997; 19: 29-43.

[58] S.J. Cheng, Y.S. Chow, O.P. Malik and G.S. Hope, "An Adaptive Synchronous Machine Stabilizer," IEEE Trans. on Power Systems, Vol. 1, pp.101-109, August 1986.

[59] S.J. Cheng, O.P. Malik and G.S. Hope, "Damping of Multi-modal Oscillations in Power Systems using a Dual-rate Adaptive Stabilizer," IEEE Trans. on Power Systems, Vol.3, pp. 101-108, February 1988.

[60] C.M. Lim, "A Self-tuning Stabilizer for Excitation or Governor Control of Power Systems," IEEE Trans. on Energy Conversion, Vol. 4, pp. 152-159, June 1989.

[61] Y.Y. Hsu and C.H. Cheng, "Design of Fuzzy Power System Stabilisers for Multimachine Power Systems," Proc. of IEEE, Vol. 137, No. 3, May 1990.

[62] P. Hoang and K. Tomsovic, "Design and Analysis of an Adaptive Fuzzy Power System Stabilizer," IEEE Trans. on Energy Conversion, Vol. 11, pp. 455 – 461, Dec. 1996.

[63] Y. Zhang, G.P. Chen, O.P. Malik and G.S. Hope, "An Artificial Neural Network Based Adaptive Power System Stabilizer," IEEE Trans. on Energy Conversion, Vol. 8, No.1, March 1993.

[64] R. Segal, M.L. Kothari and S. Madnani, " Radial Basis Function (RBF) Network Adaptive Power System Stabilizer," IEEE Trans. on Power Systems, Vol. 15, pp. 722-727, May 2000.

[65] M.A. Abido and Y.L. Abdel-Magid, "A Hybrid Neuro-fuzzy Power System Stabilizer for Multimachine Power Systems," IEEE Trans. on Power Systems, Vol. 13, No. 4, November 1998.

[66] S. Chen and O.P. Malik, " H_∞ Optimisation-based Power System Stabilizer

Design," Proc. of IEE Generation Transmission and Distribution, Vol. 142, pp.179-184, 1995.

[67] T.C. Yan, "Applying Optimisation Method to Power System Stabiliser Design – Parts 1 & 2," Electrical Power and Energy System, Vol. 19, pp. 29-43, 1997.

[68] Y.L. Abdel-Magid, M. A. Abido and A. H. Mantawy, "Robust Tuning of Power System Stabilizers in Multimachine Power Systems," IEEE Trans. on Power Systems, Vol. 15, pp.735-740, 2001.

[69] Y.L. Abdel-Magid, M. A. Abido, S. Al-Baiyat and A. H. Mantawy, "Simultaneous Stabilisation of Multimachine Power Systems via Genetic Algorithms, " IEEE Trans. on Power Systems, Vol. 14, pp. 1428-1437, 1999.

[71] M.A Abido," Robust Design of Multi-machine Power System Stabilisers using Simulated Annealing, " IEEE Trans. on Energy Conversion, Vol. 15, pp. 297-304, 2000.

CHAPTER 2

CONVENTIONAL ROBUST CONTROL DESIGN

We know that a primary objective of a control is to make the output of a dynamic process behave in a certain manner. The design procedure of a control system usually involves a mathematical model of dynamic process, the plant model or nominal model. Consequently, many aspects of the real plant behavior cannot be captured in an accurate way with the plant model leading to uncertainties. Usually, high performance specifications are given in terms of the plant model. For this reason, model uncertainties characterization should be incorporated to the design procedure in order to provide a reliable control system capable to deal with the real process and to ensure the fulfillment of the performance requirements. The term robustness is used to denote the ability of a control system to cope with the uncertain scenario.

With robust control, we want to develop a controller which can deal with predefined process uncertainties in an explicit manner. That is, we can still guarantee certain performance objectives, regardless of these uncertainties. In this chapter, we introduce the robustness of control design method.

2.1 Feedback Configuration

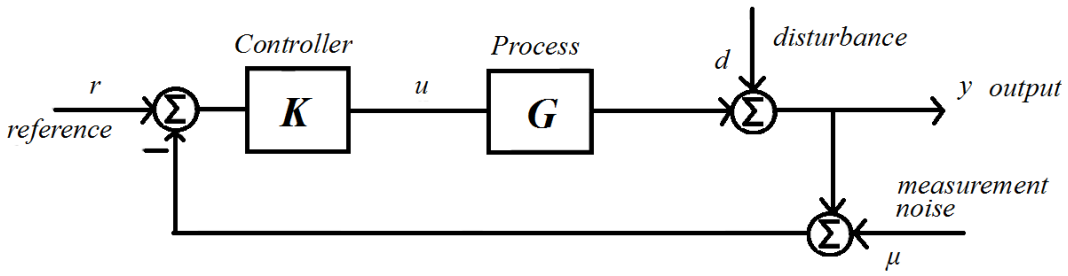

Figure 2.1 Feedback control configuration.

Figure 2.1 shows the basic feedback control configuration [1]. Based on the figure, we can derive the following:

$$y = T(r-\mu) + Sd, \tag{2.1}$$

$$e \overset{\Delta}{=} r - y = S(r-d) + T\mu, \tag{2.2}$$

$$u = R(r - \mu - d)\,, \tag{2.3}$$

where

$$T = GK(I + GK)^{-1}, \tag{2.4}$$

$$S = (I + GK)^{-1}, \tag{2.5}$$

$$R = G(I + GK)^{-1}. \tag{2.6}$$

Here *T, S* and *R* are the complementary sensitivity, the sensitivity, and the control sensitivity functions, respectively. By minimizing sensitivity function (*S*), the good disturbance error reduction will be achieved. To get a good measurement error reduction, the complementary sensitivity functions should be small, and for the "disturbances" *r-d* and the noise μ to affect the control input *u* to the least extent, *R* should be small. As a result, we have to minimize *S, T* and *R* to get good performance.

2.2 System uncertainties

The uncertainty can be classified into two categories: disturbances signals and dynamic perturbations [2]. The disturbances signal includes input and output disturbance, sensor noise and actuator noise, etc. The dynamic perturbation uncertainty represents the discrepancy between the mathematic model and the actual dynamics of the system in operation. It is well known that a mathematical model of any system is always just an approximation of the true system. Modeling errors may adversely affect the stability and performance of a control system. Here we will discuss how to model the dynamic perturbations uncertainty in the control design.

The uncertainty of dynamic perturbations can be represented into single perturbation block Δ. This uncertainty representation is referred to as "unstructured" uncertainty. The unstructured dynamic uncertainty in a control system can be described in many ways as follows,

- Additive perturbation

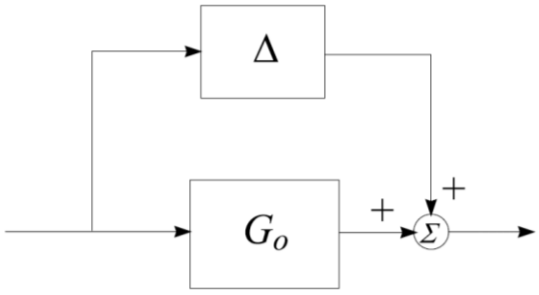

Figure 2.2 Additive perturbation configuration.

Figure 2.2 shows the configuration of additive perturbation. Therefore, the perturbed system dynamics can be written as follows:

$$G_P(s) = G_0(s) + \Delta(s)\,. \tag{2.6}$$

where $G_p(s)$ is the actual perturbed system dynamic, $G_0(s)$ is a nominal model, and $\Delta(s)$ is unstructured uncertainty.

- Inverse additive perturbation

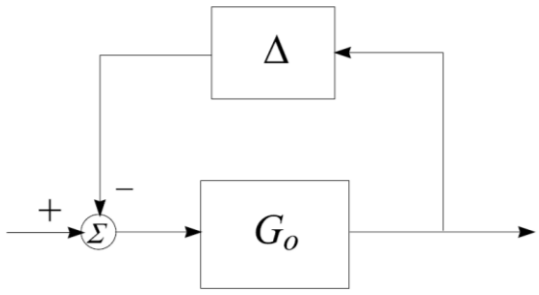

Figure 2.3 Inverse additive perturbation configuration.

The following equation is perturbed system of inverse additive perturbation configuration in Fig. 2.3,

$$(G_P(s))^{-1} = (G_0(s))^{-1} + \Delta(s)\,. \tag{2.7}$$

- Input multiplicative perturbation

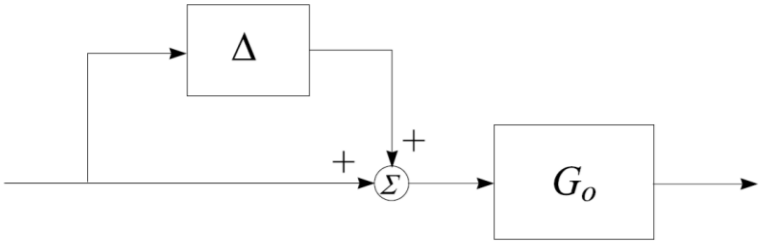

Figure 2.4 Input multiplicative perturbation configuration.

The perturbed system of input multiplicative perturbation configuration in Fig. 2.4 can be derived as

$$G_P(s) = G_0(s)[I + \Delta(s)]. \tag{2.8}$$

- Output multiplicative perturbation

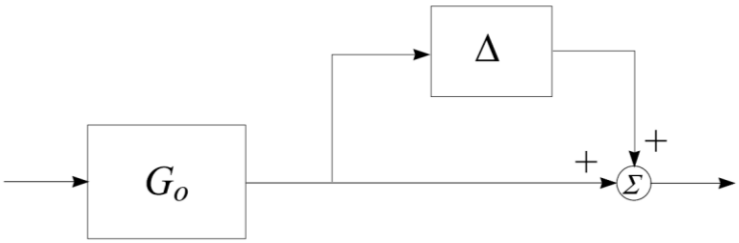

Figure 2.5 Output multiplicative perturbation configuration.

Figure 2.5 depicts output multiplicative perturbation configuration, the following equation is the perturbed system dynamics of the configurations,

$$G_P(s) = [I + \Delta(s)]G_0(s). \tag{2.9}$$

- Inverse input multiplicative perturbation

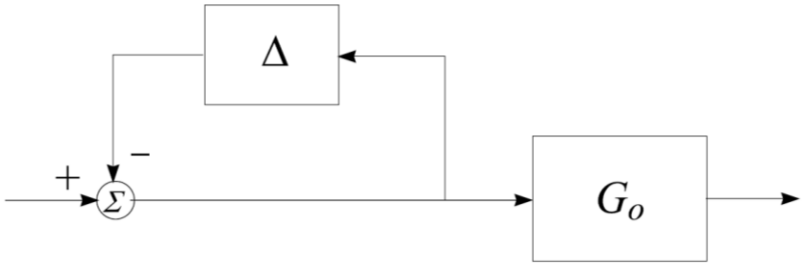

Figure 2.6 Inverse input multiplicative perturbation configuration.

The perturbed system of inverse input multiplicative perturbation configuration in Fig. 2.6 can be derived as

$$(G_P(s))^{-1} = [I + \Delta(s)](G_0(s))^{-1}. \tag{2.10}$$

- Inverse Output multiplicative perturbation

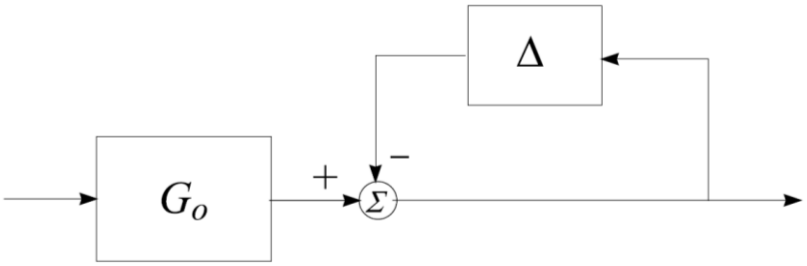

Figure 2.7 Inverse output multiplicative perturbation configuration.

The perturbed system of inverse output multiplicative perturbation configuration in Fig. 2.7 can be calculated as follows:

$$(G_P(s))^{-1} = (G_0(s))^{-1}[I + \Delta(s)]. \tag{2.11}$$

- Left coprime factor perturbations

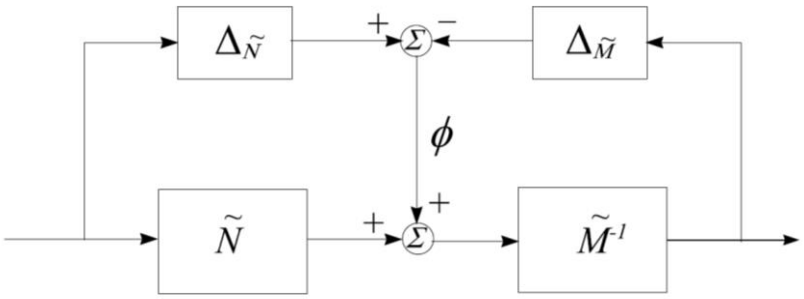

Figure 2.8 Left coprime factor perturbation configuration.

Figure 2.8 shows the configuration of left coprime factor perturbation. Therefore, the perturbed system dynamics can be written as follows:

$$G_P(s) = (\tilde{M} + \Delta_{\tilde{M}})^{-1}(\tilde{N} + \Delta_{\tilde{N}}). \tag{2.12}$$

where $(\tilde{M}, \tilde{N})$ is left coprime factorization of the nominal system model $G_0(s)$; and $(\Delta_{\tilde{M}}, \Delta_{\tilde{N}})$ is the perturbation on the corresponding factors.

- Right coprime factor perturbations

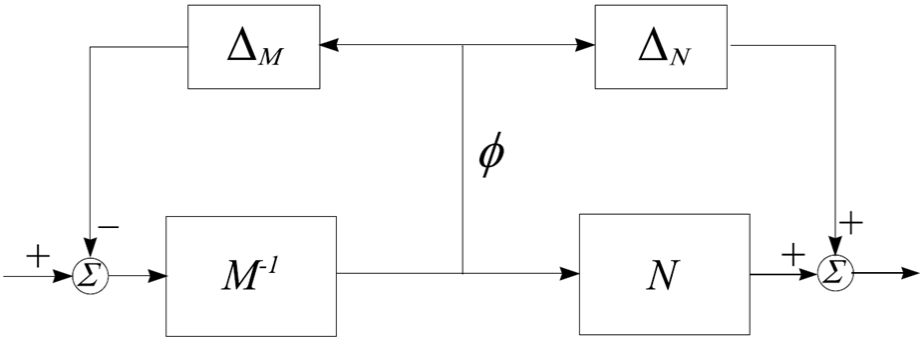

Figure 2.9 Right coprime factor perturbation configuration.

Figure 2.9 describes the configuration of right coprime factor perturbation, and the perturbed system dynamic can be derived as follows:

$$G_P(s) = (N + \Delta_N)(M + \Delta_M)^{-1}. \tag{2.13}$$

where (M, N) is right coprime factorization of the nominal system model $G_0(s)$; and (Δ_M, Δ_N) is the perturbations on the corresponding factors.

2.3 Robust Control Design

Robustness of controller can be achieved by considering system uncertainties, and the system with unstructured uncertainty has been discussed in section 2.2. This section introduces robust control design; it means how to find a controller by considering system uncertainties into account, for a given system, such that the closed loop system is robust. But, in this thesis, we only focus on the H_∞ optimization approach to design robust control for each model of system uncertainty. To design robust control using the H_∞ optimization approach, the small gain theorem is an important role in the derivation of many stabilization tests.

Let us consider a closed loop feedback control with each system uncertainties in the previous section.

1. Closed loop feedback control with additive perturbation.

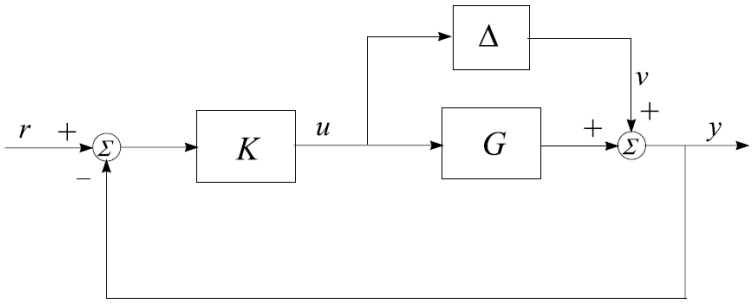

Figure 2.10 Configuration of closed loop feedback control with additive perturbation.

Controller K is robustly stable if the controller remains stable for nominal plant G and perturbation Δ. In the case of additive perturbation as shown in Fig. 2.10, the transfer function from signal v to u is $T_{uv} = -K(I+GK)^{-1}$. Based on small gain theorem, for stable Δ(s), the closed loop system is robustly if K stabilizes the nominal plant G and the following holds

$$\left\| \Delta K(I+GK)^{-1} \right\|_\infty < 1. \tag{2.14}$$

then

$$\left\| K(I+GK)^{-1}\Delta \right\|_\infty < 1. \tag{2.15}$$

We can derive the equation (15) as

$$\left\| K(I+GK)^{-1} \right\|_\infty < \frac{1}{\left\| \Delta \right\|_\infty}. \tag{2.16}$$

The robust controller $K(s)$ can be achieved in the largest possible set of perturbations $\Delta(s)$, in the sense of ∞-norm by the following minimization problem,

$$\min_{K\text{stabilizing}} \left\| K(I+GK)^{-1} \right\|_{\infty} . \tag{2.17}$$

2. Closed loop feedback control with inverse additive perturbation.

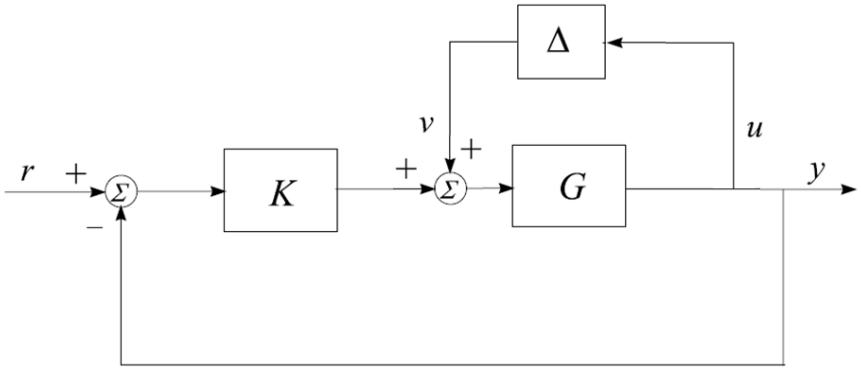

Figure 2.11 Configuration of feedback control with inverse additive perturbation.

Fig. 2.11 shows the feedback control with inverse additive perturbation. Transfer function from signal v to u is $T_{uv} = -G(I+GK)^{-1}$. Therefore, the closed loop system is robustly if $K(s)$ stabilizes the nominal plant $G(s)$ and the following holds

$$\left\| G(I+GK)^{-1} \right\|_{\infty} < \frac{1}{\|\Delta\|_{\infty}} . \tag{2.18}$$

The robust controller $K(s)$ can be achieved in the largest possible set of perturbations $\Delta(s)$ by the following minimization problem:

$$\min_{K\text{stabilizing}} \left\| G(I+GK)^{-1} \right\|_{\infty} . \tag{2.19}$$

3. Closed loop feedback control with input multiplicative perturbation.

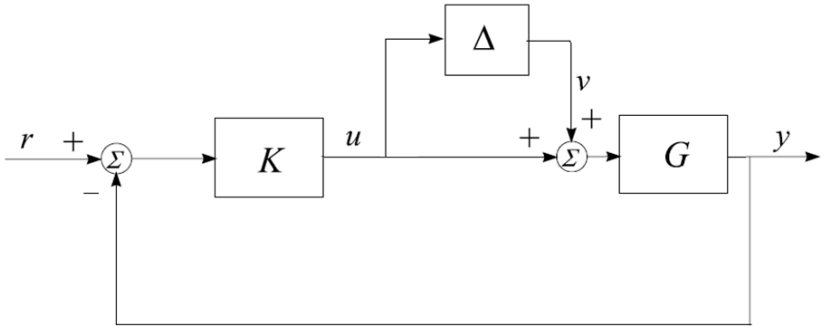

Figure 2.12 The configuration of feedback control with input multiplicative perturbation.

Same as the previous calculation, the robustness of controller in the case of feedback control with input multiplicative perturbation in Fig. 2.12 can be achieved by the following minimization problem:

$$\left\| KG(I+GK)^{-1} \right\|_{\infty} < \frac{1}{\left\| \Delta \right\|_{\infty}}, \tag{2.20}$$

then

$$\min_{K\text{stabilizing}} \left\| KG(I+GK)^{-1} \right\|_{\infty}. \tag{2.21}$$

4. Closed loop feedback control with output multiplicative perturbation.

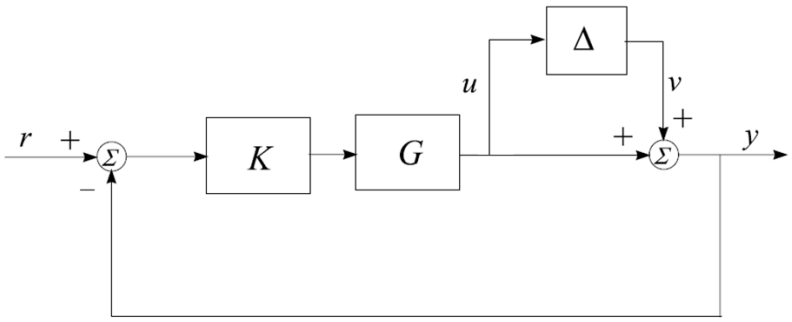

Figure 2.13 The configuration of feedback control with output multiplicative perturbation.

We can get a robust control of output multiplicative perturbation in Fig. 2.13 by the minimization problem as follows:

$$\left\| GK(I+GK)^{-1} \right\|_{\infty} < \frac{1}{\left\| \Delta \right\|_{\infty}}, \tag{2.22}$$

and

$$\min_{K\text{stabilizing}} \left\| GK(I+GK)^{-1} \right\|_{\infty}. \tag{2.23}$$

5. Closed loop feedback control with inverse input multiplicative perturbation.

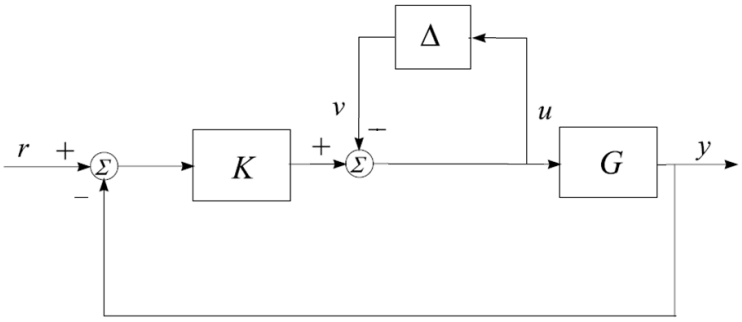

Figure 2.14 Configuration of feedback control with inverse input multiplicative perturbation.

In the case of additive perturbation as shown in Fig. 2.14, the robust controller $K(s)$ can be achieved in the largest possible set of perturbations $\Delta(s)$, in the sense of ∞-norm by the following minimization problem:

$$\left\|(I+KG)^{-1}\right\|_{\infty} < \frac{1}{\|\Delta\|_{\infty}}, \tag{2.24}$$

then

$$\min_{K\text{stabilizing}} \left\|(I+KG)^{-1}\right\|_{\infty}. \tag{2.25}$$

6. Closed loop feedback control with inverse output multiplicative perturbation.

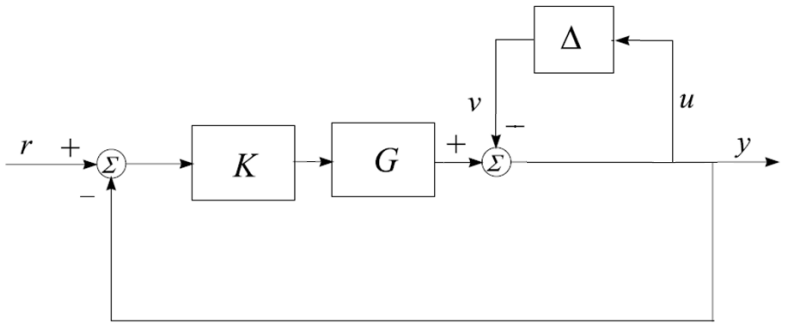

Figure 2.15 Configuration of feedback control with inverse output multiplicative perturbation.

Fig. 2.15 shows the feedback control with inverse output multiplicative perturbation. The closed loop system is robust if $K(s)$ stabilizes the nominal plant $G(s)$ and the following holds

$$\left\|(I+GK)^{-1}\right\|_{\infty} < \frac{1}{\|\Delta\|_{\infty}}. \tag{2.26}$$

Then the minimization problem can be constructed by the following equation,

$$\min_{K\text{stabilizing}} \left\|(I+GK)^{-1}\right\|_{\infty}. \tag{2.27}$$

2.4 Conventional Robust Control Design Application to Power System

This section presents a conventional robust control design of power system stabilizer (PSS) for enhancement of power system dynamic stability. The normalized coprime factorization is used to represent unstructured uncertainties in the system such as variations of system parameters, system generating and loading conditions etc. The H_{∞} loop shaping technique is applied to design robust PSS controllers.

2.4.1 System Modeling

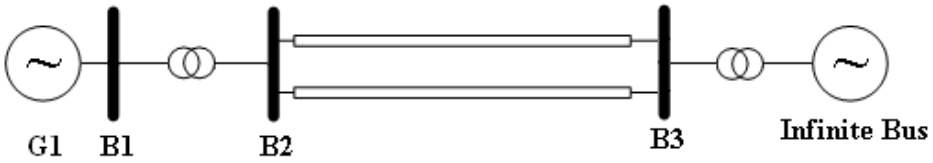

Figure 2.16 Single machine infinite bus (SMIB) system.

A single machine infinite bus (SMIB) system as shown in Fig. 2.16 is used in this study. The automatic voltage regulator (AVR), an excitation system, and the PSS are installed in the Generator G1. A detailed linearized model for an exciter, power system stabilizer, and overall power system model are explained below.

2.4.1.1 SMIB System

Figure 2.17 depicts a linearized power system model in Fig. 2.16. It is represented by the Heffron-Phillips model [3]. This system is modelled by a forth-order model with the small deviation of the power angle $\Delta\delta$, the rotor speed $\Delta\omega$, the internal voltage of generator $\Delta e'_q$ and the field voltage ΔE_{fd}, as the state variables. The initial condition used as the design condition of the proposed PSS is P_e = 0.8 p.u., x_e = 0.2 p.u. from [4].

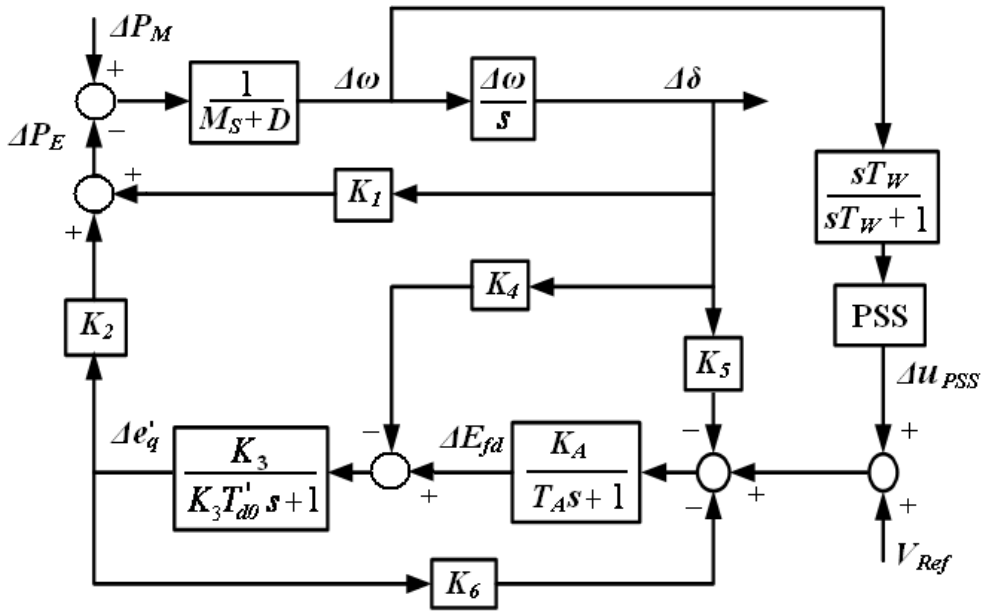

Figure 2.17 Linearized model of SMIB system.

2.4.1.2 Exciter

The linearized excitation system model that is used in this study is shown in figure 2.18 below,

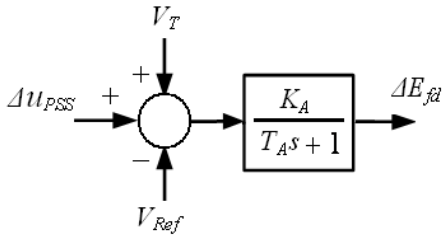

Figure 2.18 Exciter model

The exciter is modeled by the first-order transfer function with gain K_A = 50, and time constant T_A =0.05 s.

2.4.1.3 Power System Stabilizer (PSS)

The block diagram of PSS is shown in Fig. 2.19. In this study, the PSS is modeled by two block diagram. The first block is wash out with time constant T_W = 2 s, the second block is controller which is represented by H_∞ controller.

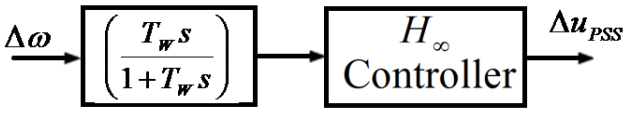

Figure 2.19 PSS model with H_∞ controller.

Here $\Delta\omega$ is angular velocity deviation as input signal of PSS and Δu_{PSS} is the control output signal of the PSS controller.

2.4.1.4 State Space Equation

The state equation of the overall power system model in Fig. 2.17 can be expressed as

$$\Delta\dot{X} = A\Delta X + B\Delta u_{pss}, \tag{2.28}$$

$$\Delta Y = C\Delta X + D\Delta u_{pss}, \tag{2.29}$$

$$\Delta u_{pss} = K(s)\Delta\omega, \tag{2.30}$$

2.4.1.2 Exciter

The linearized excitation system model that is used in this study is shown in figure 2.18 below,

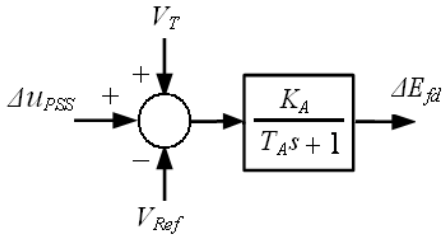

Figure 2.18 Exciter model

The exciter is modeled by the first-order transfer function with gain K_A = 50, and time constant T_A =0.05 s.

2.4.1.3 Power System Stabilizer (PSS)

The block diagram of PSS is shown in Fig. 2.19. In this study, the PSS is modeled by two block diagram. The first block is wash out with time constant T_W = 2 s, the second block is controller which is represented by H_∞ controller.

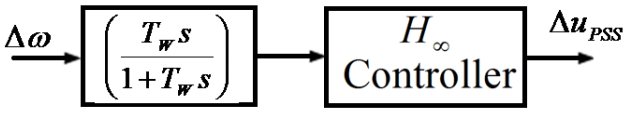

Figure 2.19 PSS model with H_∞ controller.

Here $\Delta\omega$ is angular velocity deviation as input signal of PSS and Δu_{PSS} is the control output signal of the PSS controller.

2.4.1.4 State Space Equation

The state equation of the overall power system model in Fig. 2.17 can be expressed as

$$\Delta\dot{X} = A\Delta X + B\Delta u_{pss}, \tag{2.28}$$

$$\Delta Y = C\Delta X + D\Delta u_{pss}, \tag{2.29}$$

$$\Delta u_{pss} = K(s)\Delta\omega, \tag{2.30}$$

where the state vector $\Delta X = \left[\Delta\delta \quad \Delta\omega \quad \Delta e_q^{'} \quad \Delta E_{fd}\right]^T$, the output vector $\Delta Y = \left[\Delta\omega\right]$, Δu_{pss} is the control output signal of the PSS ($K(s)$), which uses only the angular velocity deviation ($\Delta\omega$) as a feedback input signal. Note that the system (28) is a single-input single-output (SISO) system. The proposed method is applied to design a robust PSS.

The state equation of system in Fig. 2.17 can be expressed as

$$\begin{bmatrix} \Delta\dot{\delta} \\ \Delta\dot{\omega} \\ \Delta\dot{e}_q^{'} \\ \Delta\dot{E}_{fd} \end{bmatrix} = \begin{bmatrix} 0 & \omega_B & 0 & 0 \\ -\frac{K_1}{M} & -\frac{D}{M} & -\frac{K_2}{M} & 0 \\ -\frac{K_4}{T_{d0}^{'}} & 0 & -\frac{1}{K_3 T_{d0}^{'}} & \frac{1}{T_{d0}^{'}} \\ -\frac{K_a K_5}{T_a} & 0 & -\frac{K_a K_6}{T_a} & -\frac{1}{T_{a\,a}} \end{bmatrix} \begin{bmatrix} \Delta\delta \\ \Delta\omega \\ \Delta e_q^{'} \\ \Delta E_{fd} \end{bmatrix} + \begin{bmatrix} 0 \\ 0 \\ 0 \\ \frac{K_a}{T_a} \end{bmatrix} u_{PSS}, \qquad (2.31)$$

$$\Delta Y = \begin{bmatrix} 0 & 1 & 0 & 0 \end{bmatrix} \begin{bmatrix} \Delta\delta \\ \Delta\omega \\ \Delta e_q^{'} \\ \Delta E_{fd} \end{bmatrix} + \begin{bmatrix} 0 & 0 \end{bmatrix} \Delta u, \qquad (2.32)$$

$$\Delta u = K(s)_{PSS} \Delta\omega. \qquad (2.33)$$

Here, the $H\infty$ loop shaping approach is applied to design a robust PSS in (2.31) that is referred to as the nominal plant G.

2.4.2 Robust PSS Design

The robust PSS is designed based on H_∞ loop shaping control [5, 6]. The design procedure is divided into 3 steps as follows.

Step 1 Loop shaping

As shown in Fig. 2.20, a pre compensator (W_1) and a post compensator (W_2) are employed to form the augmented plant $G_s=W_2GW_1$, which is enclosed by a solid line. The designed robust stabilizer $K=W_1K_\infty W_2$ is enclosed by a dotted line where K_∞ is the H_∞ controller. The weighting function can be selected as $W_1 = W$ and $W_2 = 1$.

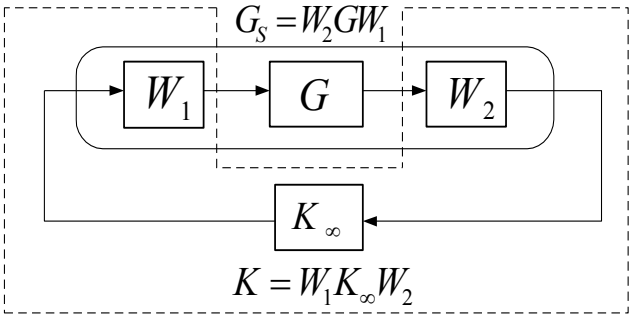

Figure 2.20 Shaped plant G_s and designed robust controller *K*.

Step 2 Formulation of H_∞ robust stabilization problem

A shaped plant G_s is expressed in form of normalized left coprime factor $G_s = M_s^{-1} N_s$, when the perturbed plant G_Δ is defined as

$$G_\Delta = \left\{ (M_s + \Delta M_s)^{-1} (N_s + \Delta N_s) : \left\| \begin{bmatrix} \Delta N_s & \Delta M_s \end{bmatrix} \right\|_\infty \le 1/\gamma \right\}. \tag{2.34}$$

where ΔM_s and ΔN_s are stable unknown transfer functions which represent uncertainties in the nominal plant model *G*. Based on this definition, the H_∞ robust stabilization problem can be established by G_Δ and *K* as depicted in Fig. 2.21. The objective of robust control design is to stabilize not only the nominal plan *G* but also the family of perturbed plant G_Δ. In (2.34), $1/\gamma$ is defined as the robust stability margin.

The maximum stability margin in the face of system uncertainties is given by the lowest achievable value of γ, i.e. $\gamma_{\min}$. Hence, $\gamma_{\min}$ implies the largest size of system uncertainties that can exist without destabilizing the closed-loop system in Fig. 2.21. The value of $\gamma_{\min}$ can be easily calculated from

$$\gamma_{\min} = \sqrt{1 + \lambda_{\max}(XZ)} \,. \tag{2.35}$$

Where $\lambda_{\max}(XZ)$ denotes the maximum eigenvalue of XZ. For minimal state-space realization *(A, B, C, D)* of G_s, the values of *X* and *Z* are unique positive solutions to the generalized control algebraic Riccati equation

$$(A - BS^{-1}D^T C)^T X + X(A - BS^{-1}D^T C) - XBS^{-1}B^T X + C^T R^{-1} C = 0\,, \tag{2.36}$$

and the generalized filtering algebraic Riccati equation

$$(A - BS^{-1}D^{T}C)Z + Z(A - BS^{-1}D^{T}C)^{T} - ZC^{T}R^{-1}CZ + BS^{-1}B^{T} = 0, \tag{2.37}$$

where $R = I + DD^{T}$ and $S = I + D^{T}D$. Note that no iteration on γ is needed to solve for $\gamma_{\min}$. To ensure the robust stability of the nominal plant, the weighting function is selected so that $\gamma_{\min} \le 4.0$ [6]. If $\gamma_{\min}$ is not satisfied, then we adjust the weighting function.

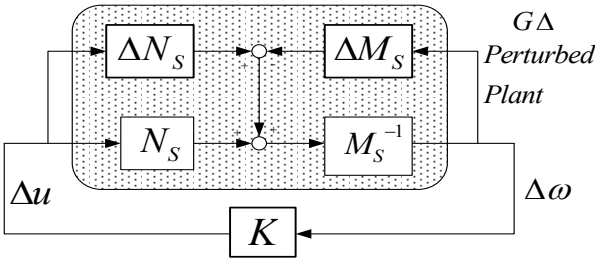

Designed Robust Controller

Figure 2.21 H_{∞} robust stabilization problem.

Step 3 Determination of Robust controller.

The K_{∞} controller in Fig. 2.21 can be determined by

$$K_{\infty} = \begin{bmatrix} A + BF + \gamma^{2}(L^{T})^{-1}ZC^{T}(C + DF) & \gamma^{2}(L^{T})^{-1}ZC^{T} \\ B^{T}X & -D^{T} \end{bmatrix}, \tag{2.38}$$

Where $F = -S^{-1}(D^{T}C + B^{T}X)$ and $L = (1 - \gamma^{2})I + XZ$.

Next, find robust controller $K(s) = W_1 K_{\infty} W_2$ that satisfies the necessary condition

$$\left\| \begin{bmatrix} I \\ K_{\infty} \end{bmatrix} (I - G_s K_{\infty})^{-1} \begin{bmatrix} I & G_s \end{bmatrix} \right\|_{\infty} \le \gamma \cdot \tag{2.39}$$

2.4.3 Simulation Studies

In this section, simulation studies in an SMIB system are carried out. The weighting functions are appropriately selected as

$$W_1 = 168\,\frac{s+16}{s+19},\ W_2 = I. \tag{2.40}$$

Consequently, the shaped plant G_S can be established by (34). As a result, the sixth-order of robust controller of PSS is obtained as follows,

$$PSS = 100\frac{0.00022s^5 + 0.0189s^4 + 0.574s^3 + 7.27s^2 + 31.72s - 57.4}{0.0000001s^6 + 0.00145s^5 + 0.094s^4 + 0.364s^3 + 8.083s^2 + 75.9s + 5.88}. \quad (2.41)$$

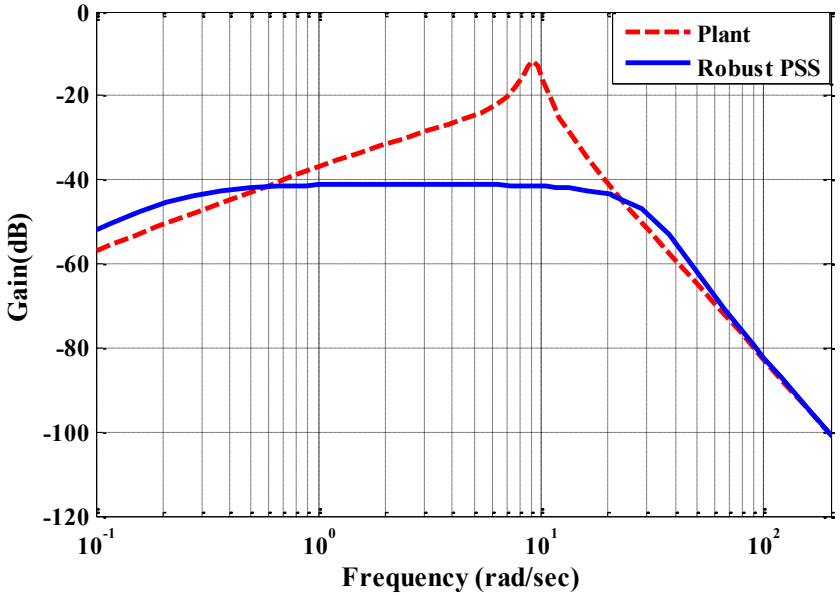

Figure 2.22 System with and without robust PSS.

Fig. 2.22 depicts the bode plot of the plant (system without PSS) and robust PSS. Without PSS, the peak resonance of the oscillation mode occurs at frequency about 1 Hz. For system with robust PSS, the peak resonance is reduced significantly. This signifies the stabilizing effects of robust PSS.

The performance and robustness of the proposed controller is compared with that of the conventional lead-lag controller (CPSS) obtained from [4], that is

$$(CPSS)K(s) = 5.5\frac{(1+0.1732s)^2}{(1+0.0577s)^2}. \quad (2.42)$$

In simulation studies, the limit on each PSS output (Δu_{pss}) is ±0.05 p.u and the limit on ΔE_{fd} is ±6.0 p.u. The system responses with PSSs are examined under three case studies as in Table 2.1, while a small disturbance of 5 % (0.05 p.u.) step response of ΔV_{ref} is applied to the system at $t = 0$ s.

Table 2.1 Operating Conditions.

System Parameters	$P(p.u)$	$Q(p.u)$	$x_e\ (p.u)$
Case 1 : Normal Condition	0.8	0.4	0.2
Case 2 : Weak Line	0.8	0.4	**0.8**
Case 3 : Heavy Load &Weak line	**0.95**	0.4	0.8

Figure 2.23 shows the responses of electrical power output deviation in case 1. CPSS and the robust PSS are able to damp power oscillations. Nevertheless, the overshoot and setting time of power oscillations in the cases of the robust PSS are much lower than those of CPSS.

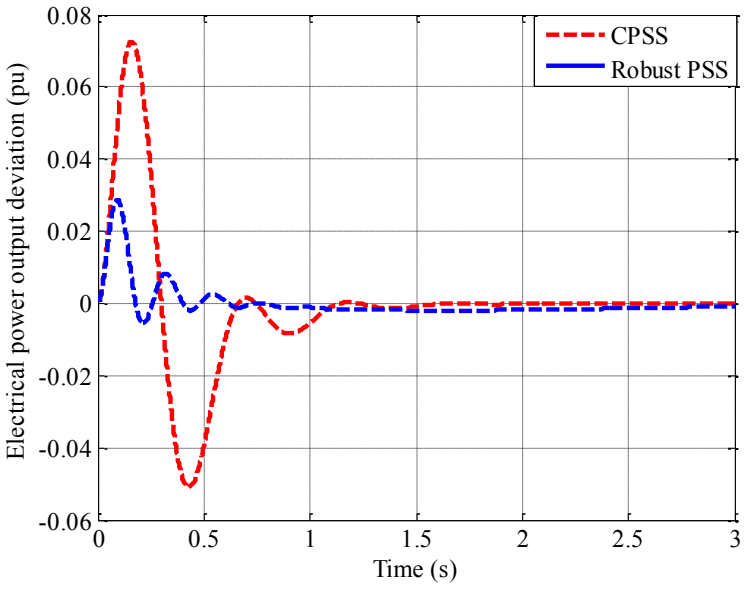

Figure 2.23 Simulation results of case 1.

In case 2 as shown in Fig. 2.24, the damping effect of CPSS is deteriorated by the increase in transmission line reactance. On the other hand, the power oscillation is effectively stabilized by the robust PSS. The robust PSS is rarely sensitive to the weak line condition.

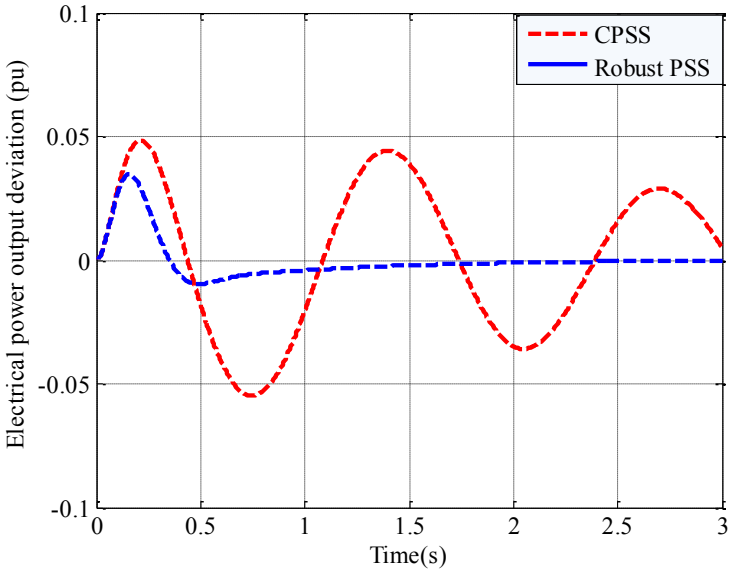

Figure 2.24 Simulation results of case 2.

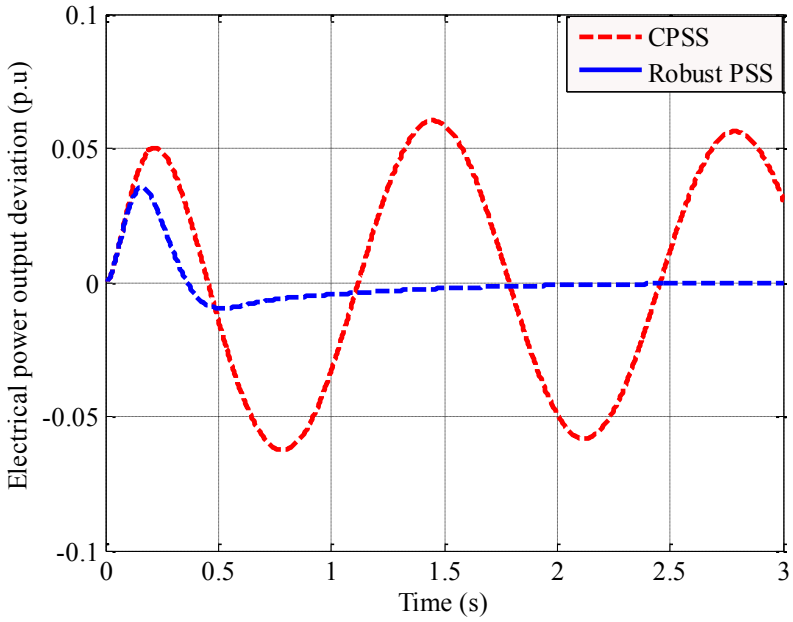

Figure 2.25 Simulation results of case 3.

In addition to the weak line condition in case 2, the electrical power output is increased in case 3. Fig. 2.25 shows that the CPSS fails to damp power system. The power oscillation gradually increases and diverges. In contrast, the robust PSS can tolerate this situation. The power oscillations are significantly damped.

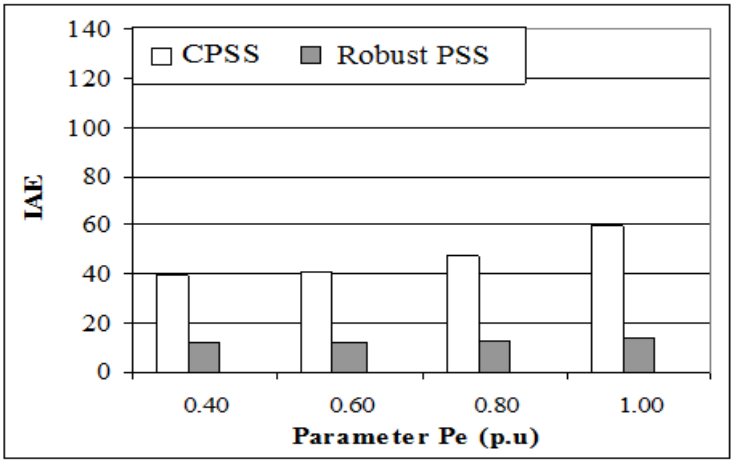

Figure 2.26 Variation of IAE against variations of power.

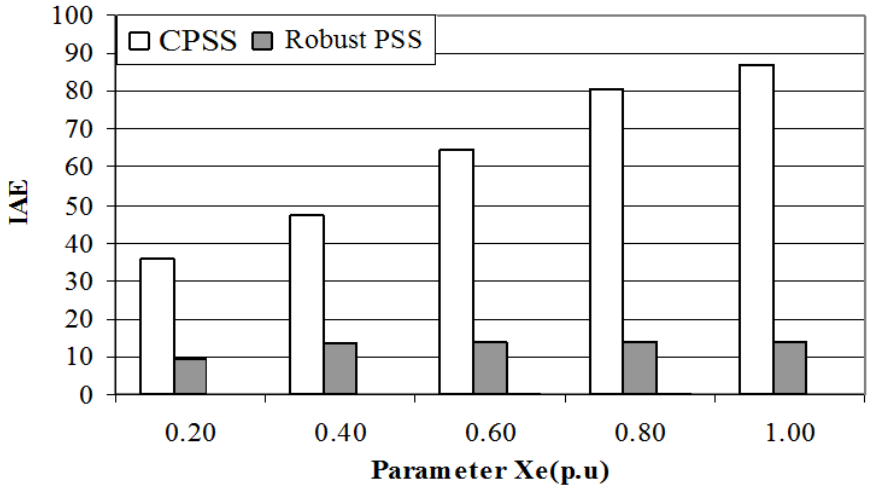

Figure 2.27 Variation of IAE against variation of reactance.

Next, the robustness of the proposed PSS against the variations of system parameters is evaluated by an integral absolute error (IAE). For 3 s. of simulation study, the IAE of electrical power output deviation ΔP_e is defined as,

$$\text{IAE of } \Delta P_e = \int_0^3 |\Delta P_e| dt. \qquad (2.43)$$

Fig. 2.26 shows the variation of IAE when the electrical power is varied from 0.4 to 1.0 p.u. The IAE in the case of CPSS considerably increases as the electrical power becomes larger. This shows that the CPSS is very sensitive to variations of electrical power output. On the other hand, the IAE in case of the robust PSS is much lower than that of CPSS and rarely change. This signifies that the robust PSS is able to guarantee the robustness of the system against the heavy loading condition.

Fig. 2.27 shows the variation of IAE when the line reactance x_e is increased from 0.2 p.u to 1.0 p.u. Clearly, the CPSS is very sensitive to the variation of reactance. The values of IAE become larger when the reactance increases. On the contrary, the value of IAE in the case of robust PSS is much lower and almost constant. These results confirm that the robust PSS has very high robustness to weak line condition. However, the order of H_∞ controller depends on that of the plant. This leads to the complex structure PSS which is different from the conventional lead/lag PSS. Despite the significant potential of control techniques mentioned above, power system utilities still prefer the conventional lead/lag PSS structure. This is due to the ease of implementation, the long-term reliability, etc. To overcome the problem, new technique that gives robustness to conventional structure of controller is needed. With the simple structure and easy implementation, the robustness of controller is guaranteed. The technique will be discussed in chapter 4.

REFERENCES

[1] K. Ogata. Modern Control Engineering. Englewood Cliffs, N.J: Prentice-Hall, 1970.

[2] D.W. Gu, et al., " Robust control design with MATLAB, "Springer, London, 2005.

[3] F. P. DeMello, et al., . Concepts of synchronous machine stability as affected by excitation control, "IEEE Trans. on PAS., Vol. 88, pp. 316-329, 1969.

[4] P.S. Rao, et al,. " Robust tuning of power system stabilizers using QFT. " IEEE-Trans. on Control Systems Technology. Vol. 4, pp. 478-486, 1999.

[5] D.C. Mcfarlane and K. Glover. " Robust controller design using normalized coprime factor plant descriptions." Lecture notes in control and information science, Springer-Verlage, Vol. 138, 1990.

[6] S. Skogestad, and I. Postlethwaite. Multivariable Feedback Control: Analysis and Design. 2nd edition. John Wiely, 2005.

CHAPTER 3

ADAPTIVE CONTROL DESIGN

This chapter introduces adaptive control systems. An **a**daptive control system is an automatic (process) control system that uses adaptation as part of its prediction of process behavior in order to optimize the control [1]. It means a system will modify its control algorithm as the system's operating conditions change so that optimal performance can be achieved. This chapter explains briefly two different approaches of adaptive control system, direct adaptive control and indirect adaptive control. In the direct adaptive control configuration, the system parameters result directly from calculations of the controller parameters. On the other hand, indirect adaptive control allows different algorithms to calculate the system parameters from the plant or the controller signals.

3.1 Direct Adaptive Control.

This section uses model reference adaptive control to explain a direct adaptive control. Model reference adaptive control (MRAC) attempts to match the output of a plant to a given reference model output representing the desired output of the controlled plant. Briefly, the output of the controlled plant is compared to the reference model output. The difference between the two outputs becomes the error that control engineers aim to minimize. This error and the control signal drive the adjustment mechanism to optimally adjust the controller parameters to force the controlled plant to exactly match the desired reference model output [2].

3.1.1 Model Reference Adaptive Control (MRAC) Configuration.

A MRAC configuration is shown in Figure 3.1. This technique was first introduced by Whitacher in 1958. Initial examination of this design scheme begins with the reference model, normally represented as a second order system for ease in modeling and analysis. This equation is very popular in control systems and is shown below in (1) [3].

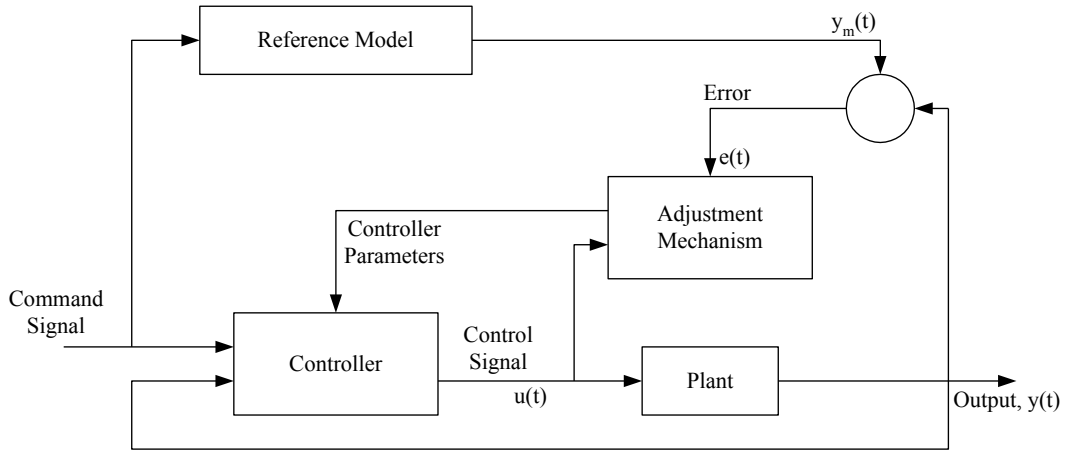

Figure 3.1 Block diagram for conventional model reference adaptive control.

$$W_{ref}(s) = \frac{Y(s)}{R(s)} = \frac{\omega_n^2}{s^2 + 2\zeta\omega_n s + \omega_n^2}, \tag{3.1}$$

where W_{ref} is the reference model transfer function, Y and R are numerator and denominator of reference model, respectively, and ω_n and ζ are natural frequency and damping ratio of reference model, respectively. The reference model equation in (1) is the basic form that the plant's output will be forced to match. The industry standard for the value of damping ratio is 0.707 since this value has been proven to be optimum for performance.

Then an adjustment mechanism compares the real plant output $y(t)$ with the reference model output $y_m(t)$, and correctly reevaluates the controller parameters. MRAC begins by defining the tracking error (e), where the error can be expressed as follow:

$$e = y(t) - y_m(t), \tag{3.2}$$

Then a cost function of theta ($J(\theta)$) can be constructed by the error as the following equation:

$$J(\theta) = \frac{1}{2}e^2(\theta), \tag{3.3}$$

where theta (θ) is the parameter that will be adapted inside the controller. To find out how to update the parameter theta, the derivative of theta is equal to the negative change in J. Then the result for the cost function chosen above is:

$$\frac{d\theta}{dt} = -\gamma\frac{\delta J}{\delta\theta} = -\gamma e\frac{\delta e}{\delta\theta} \tag{3.4}$$

By finding the minimum of the expected value, the next control signal calculated in (3.4) minimizes the time for the error to become zero.

The core problem of adaptive control is parameter estimation. To estimate parameter of controller, the several methods can be applied. Here, we give example of parameter estimation by gradient method or MIT Rule.

3.1.2 MIT rule for Direct Adaptive Control.

The MIT rule is a scalar parameter adjustment law which was proposed around 1960 for the adaptive control of a linear system modeled as a cascade of a linear stable plant and a single unknown gain [4, 5]. The adjustment law involves approximating a gradient-descent procedure seeking the minimum of an integral-squared performance criterion. The initial intended application was to the control of aircraft dynamics where the single unknown parameter was related to dynamic pressure.

In the history of adaptive control, the MIT Rule represented a watershed; it offered the possibility of adaptation for a useful application, the method was simply formulated, and apparently straightforward to apprehend in an intellectual sense. Performance however turned out to be unpredictable; explanations (as opposed to mere reporting of the performance) took some time to be achieved [6].

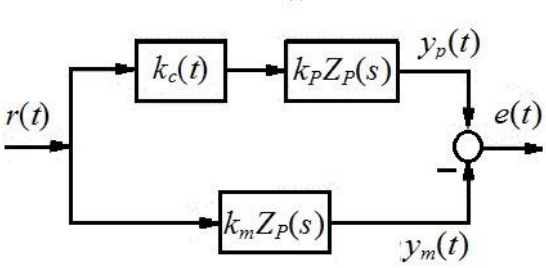

Figure 3.2 MIT rule.

The basic set up of MIT rule is shown in Figure 3.2 The plant is $k_p Z_p(s)$, where k_p is unknown apart from its sign, and $Z_p(s)$ is a known stable transfer function. The basis of identification is that a cascade adjustable positive known gain k_c is introduced as shown, and the output of the upper arm is compared to the output of $k_m Z_p(s)$ when the same driving signal is applied; here, k_m is a known gain, with the same sign as k_p. Of course, if $k_p k_c(t) = k_m$ for all t, zero error will result and k_p will be given as k_m/k_c. If the

error $e(t)$ is nonzero the idea is to adjust k_c to cause it to go to zero. The MIT rule is the rule of adjustment for k_c. The idea is to use gradient descendent to adjust k_c (.) which leads to

$$K_c = -g(y_P - y_m)y_m, \tag{3.5}$$

where g is a positive gain constant. The rule is appealing due to its simplicity but it often leads to instabilities. The mechanism is one where the fast dynamics of the adaptation destabilizes the closed loop system.

3.1.3 Application of MIT Direct Adaptive Control to Simple Model.

Assumed that we have a driven pendulum system [7], the transfer function of the system is given below:

$$F(s) = \frac{1.89}{s^2 + 0.0389s + 10.77} \tag{3.6}$$

The system was modeled in Simulink/Matlab. Figure 3.3 depicts the open loop step response of the system, the system response illustrates that the system has a lack damping, and settling time of the system is upwards of 100 seconds, therefore the system needs a controller. Theta is the parameter that will be adapted inside the controller.

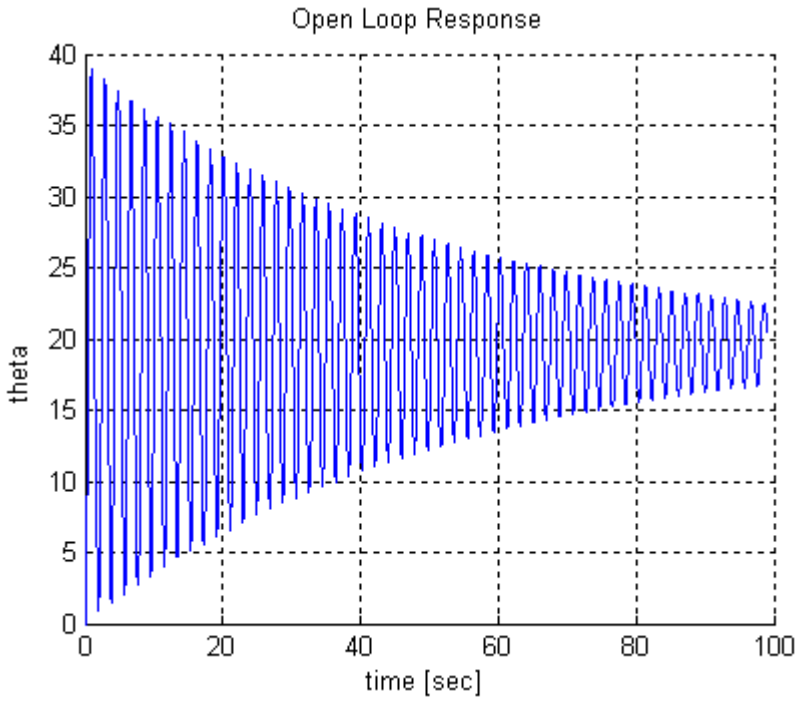

Figure 3.3 The open loop step response of the driven pendulum system.

The simulink model with MIT rule direct adaptive control is shown in Fig. 3.4. It is then assumed that the controller has both an adaptive feed forward (*Theta1*) and an adaptive feedback (*Theta2*) gain. Then the designed MIT rule controllers are applied. Figure 3.5 depicts the response of the system plant with direct adaptive control. The simulation result shows that the system response obviously doesn't match the reference model. The value of theta is gradually increases and becomes unstable in the case of gamma value 0.001. Tuning of gamma does not solve the problem. By decreasing gamma value, the controller is able to damp the oscillation of theta. But the response becomes very slow to reach steady state condition.

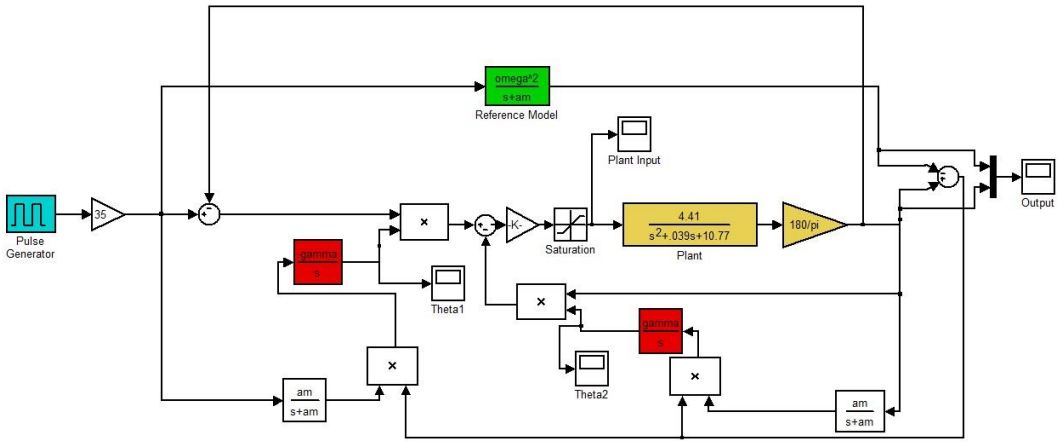

Figure 3.4 Simulink block diagram of MIT direct adaptive control.

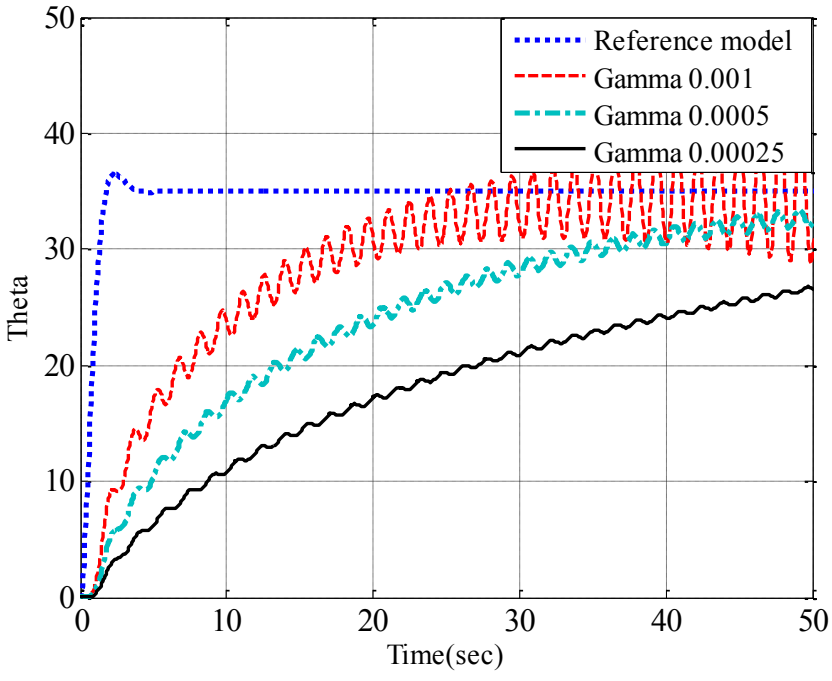

Figure 3.5 system response of system with various gamma value.

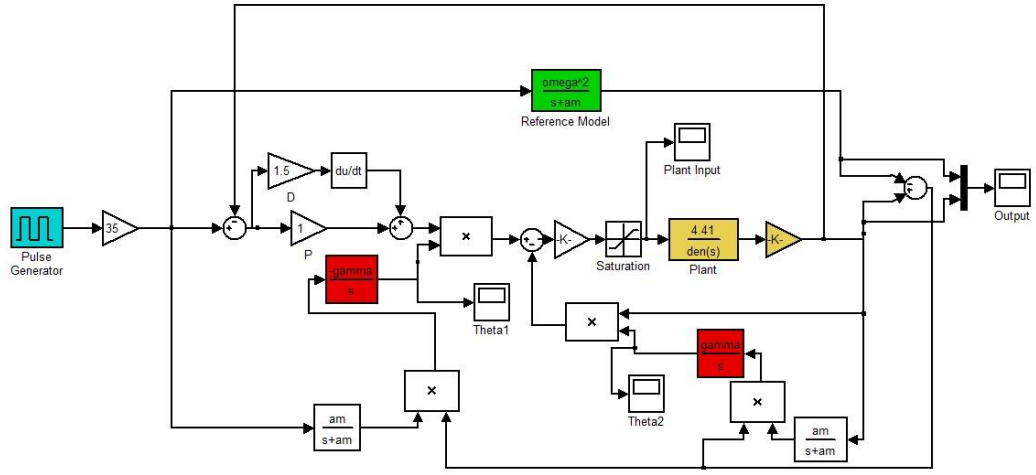

Figure 3.6 Simulink model of system with MIT rule direct adaptive control and PD controller.

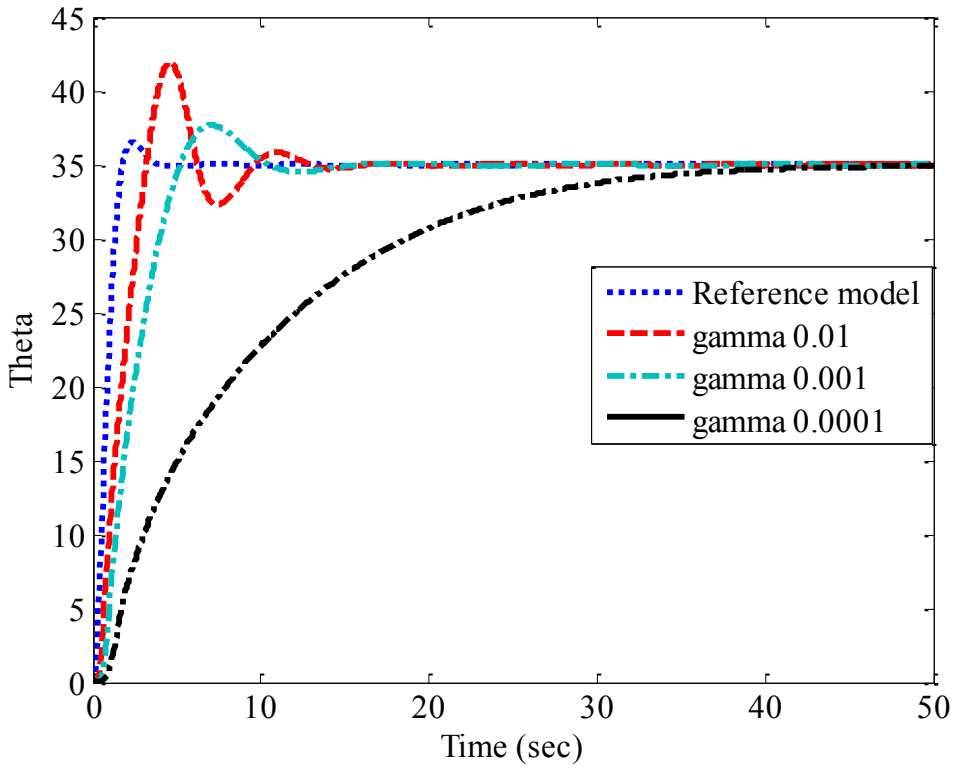

Figure 3.7 system response of system with direct adaptive and PD controller for several different values of gamma.

To solve the problem and to kill the oscillations, proportional and derivative (PD) control is applied across the plant. The simulink model and simulation result for several different values of gamma are shown in Fig. 3.6 and Fig. 3.7, respectively. By installing PD control across the plant, the system response can be improved. When

the value of gamma is increased, the system responses much faster, but the system response becomes unstable. On the other hand, a smaller value of gamma leads to longer adaptation times, but a less volatile response. Tuning of gamma with proper value is able to improve performance of system.

However, the direct adaptive control has some issues to be solved. This method sometimes works, and sometimes it does not work [8]. An instability being displayed is a result of interaction of the adaptive loop dynamics with the plant dynamics, a phenomenon that is occurring when the time scales are comparable, but does not occur otherwise. Another issue is bursting phenomenon. In the early 1980s, scattered reports appeared of adaptive control systems which worked well for a long period, say a week, and then unexpectedly burst into an oscillation which then died away. Figure 3.8 shows the phenomenon; an adaptive controller is connected to a first order plant, and set-point control is sought.

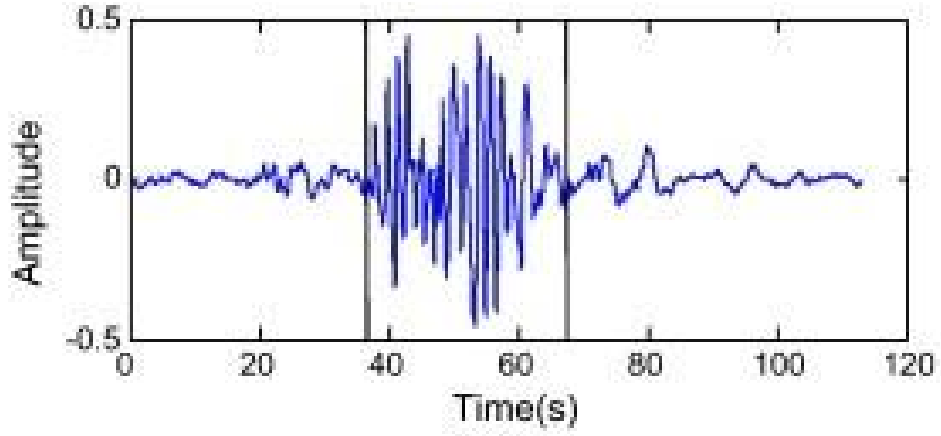

Figure 3.8 Plant Output with Adaptive Controller connection during a ”Burst”.

Instability is observed when the signals become steady. After a furious phase, the system goes back to steady state again. This reason behind this behavior is that when the signals are near zero the adaptive algorithm does not have enough information in order to identify all parameters simultaneously. This leads to divergence of the estimates. The consequence of that is a faulty controller rendering the plant unstable. Once the signals become rich enough though, the adaptive algorithm begins to deliver good estimates of the parameters. Now, just in time, the controller begins to

perform well, leading to plant recovery. Eventually, the problem appears again. Clearly, in industrial applications bursting must not occur.

3.2 Indirect Adaptive Control

3.2.1 Basic Work of Indirect Adaptive Control

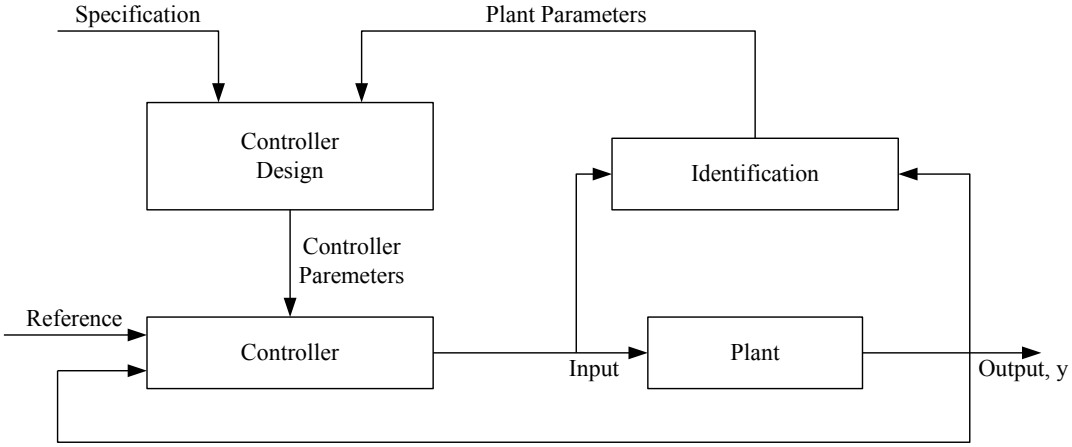

Figure 3.9 Block diagram for classical indirect adaptive control.

Figure 3.9 depicts conventional/classical indirect adaptive control. Generally, indirect adaptive control design approach is iterative identification and controller redesign [9-11]. This is a form of adaptive control in which the tasks of identification and control are separated. There is usually an underlying performance index which is to be minimized. One iteration comprises:

a) Identifying the plant with the current controller. The identification block takes as its inputs the control signal and the plant output. Using a variety of methods of evaluation, the parameters of the plant are estimated and sent to the controller design block to update the controller parameters. In conventional indirect adaptive control, with the possible combinations of the many identification model algorithms coupled with the different controller designs, researchers continuously experiment with multiple couplings in search of better responses. Most take the recursive least squares approach as the method for identification, even though extended least squares (ELS) and recursive maximum likelihood (RML) have also been explored [12]. RLS as the simplest model was proven by Warwick to be just as effective as its more

complex counterparts [13]. Recently, attempts have been made to implement multiple identification models, but in this case, multiple corresponding controllers must also be implemented [14].

b) Redefining the controller on the basis of the identified model of the plant. The controller block for indirect adaptive control assemblies, which calculates the control signal, can also be modeled by a variety of methods. The three popular methods for this evaluation are minimum variance (MV), generalized minimum variance (GMV), and parameter optimization. The advantages of minimum variance control lie in its simplicity [15]. It offers absolute performance limits to form a basis for design of all self tuning regulators (STRs). However, its disadvantages include its instability to handle non-minimum phase systems [9] and its use of excessive inputs that can lead to stability problems in some operating conditions [10]. Other variations can handle these problems, but for the purposes of simplicity, minimum variance is a common choice. Also, the focus of current research relies on slightly altering the methods of minimum variance and generalized minimum variance due to the complexity of changing parameter optimization.

However, in conventional indirect adaptive control with iterative identification and control, the average rate of controller variations is almost much slower than the underlying closed-loop dynamics [16]. Each identification interval is normally long enough that transients associated with any controller switching at the start of the interval die out early in the interval. Thus, despite the fact that the controller undergoes step changes, one cannot explain unsatisfactory behavior as a consequence of violating the separation of time scales dictum. It is however true that unsatisfactory behavior is more likely to be observed when the controller changes are large.

3.2.2 Multi Model Indirect Adaptive Control

To improve the conventional indirect adaptive control, some researchers propose multi model adaptive control to improve performance of previous adaptive control [17,18]. The basic structure of multi model adaptive control is shown in Fig. 3.10.

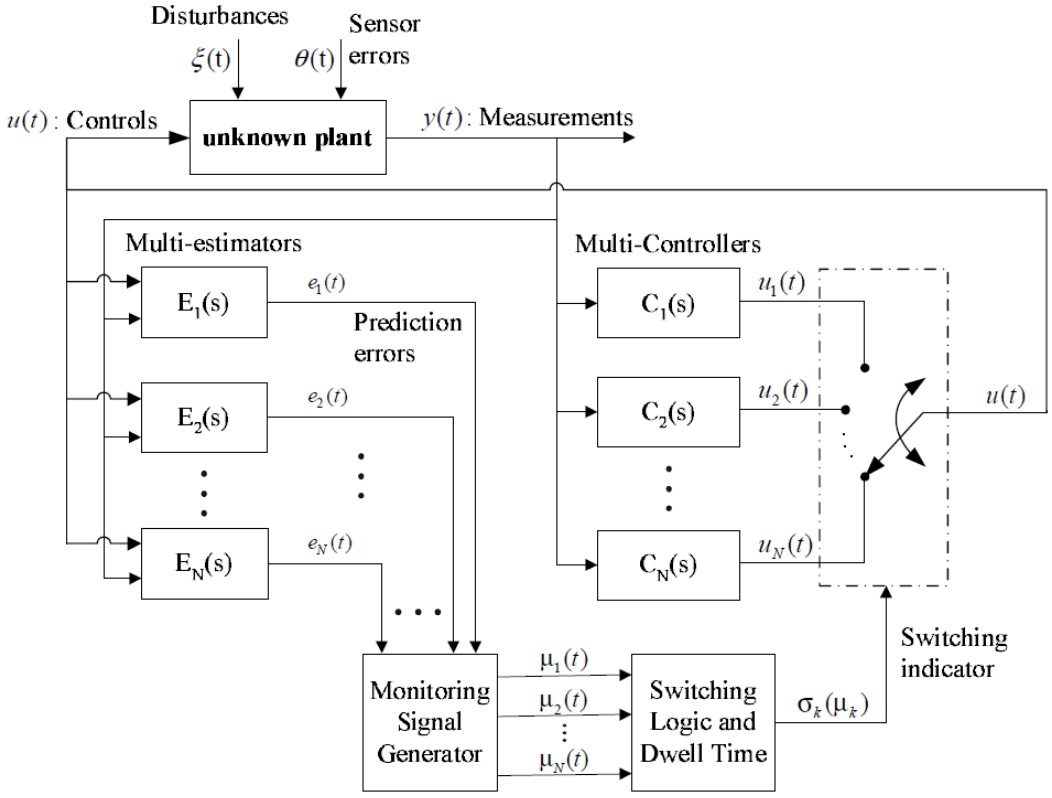

Figure 3.10 Basic structure of multi model adaptive control.

In these methods, the identification process is completely separated from the control process. One of the advantages is infrequent controller-switching. The estimated model is identified by identification via hypothesis testing [16]. Controllers are designed to give good performance with corresponding estimated model. These methods are able to improve conventional indirect adaptive control, especially to overcome the average rate of controller variations. However, some problems appear in these methods. First, the complexity of the adaptive system will depend on the number of estimated models that are required to implement. Ideally, the number of estimated models and corresponding controller should be as small as possible. But the small number of models may reduce the performance of controller [19]. There is no clear guidance on how many models should be chosen. Second, the numerical

simulations have been reported for only a couple of SISO plants. Another issue is the utility needs to install many controllers, it is costly.

REFERENCES

[1] D. John and W. Edmund, " A Dictionary of Computing (6 ed.)", Oxford University Press, 2008

[2] K. Al-Olimat and A.Ghandakly. “Using Multiple Identification Models In Adaptive Power System Stabilizers,” *North American Power Symposium (NAPS)*, pp. 474-480. Cleveland, OH: October 19-20, 1998.

[3] K. Ogata. Modern Control Engineering. Englewood Cliffs, N.J: Prentice-Hall, 1970.

[4] HP Whitaker, An Adaptive System for Control of the Dynamics Performances of Aircraft and Spacecraft, Inst Aeronautical Services, Paper 59-100, 1959.

[5] PV Osbourne, HP Whitaker, and A Kezer, New Developments in the Design of Model Reference Adaptive Control Systems, Inst Aeronautical Services, Paper 61-39, 1961.

[6] IMY Mareels, BDO Anderson, RR Bitmead, M Bodson, and S Sastry, Revisiting the MIT Rule for Adaptive Control, Proc 2nd IFAC Workshop on Adaptive Systems in Control and Signal Processing, 1986, pp. 161-166.

[7] Keith Sevcik, " Model Reference Adaptive Control" Online available : http://www.pages.drexel.edu/~kws23/tutorials/MRAC/MRAC.html

[8] D. O. Brian, Anderson, "Failures of adaptive control theory and their solution" Communications in Information and Systems, Vol. 5, No. 1, pp. 1-20, 2005

[9] P Albertos, Model-based Iterative Control Design, in: Iterative Identification and Control, Springer 2002, pp. 121-142.

[10] RR Bitmead, Iterative Optimal Control Design, in: Iterative Identification and Control, Springer 2002, pp. 167-184.

[11] M Gevers, Identification and Validation for Robust Control, in: Iterative Identification and Control, Springer 2002, 185-208.

[12] K.J. Åström, and B. Wittenmark. Adaptive Control: Second Edition. Reading, MA: Addison-Wesley, 1995.

[13] K. Warwick. Implementation of Self-Tuning Controllers. England: Billing and Sons, Ltd. 1988.

[14] K. Al-Olimat and A.Ghandakly. "Using Multiple Identification Models In Adaptive Power System Stabilizers," *North American Power Symposium (NAPS)*, pp. 474-480. Cleveland, OH: October 19-20, 1998.

[15] RR Bitmead, Iterative Optimal Control Design, in: Iterative Identification and Control, Springer 2002, pp. 167-184.

[16] D.O Brian, Anderson, Arvin D, " Challenges of Adaptive Control-Past, Permanent and Future" Annual Reviews in Control, Elsevier, Vol. 32, 1123-135, 2008.

[17] M. Gevers, "Identification for control: From the early achievements to the revival of experiment design. European Journal of Control, 11(4–5),335–352, 2005.

[18] P. M. J. Van den Hof and R. J. P. Schrama, Identification and control:Closed-loop issues. Automatica, 31(12), 1751–1770, 1995.

[19] A. Michael, F. Sajjad, P. Antonio " Issues on Robust Adaptive Feedback Control" International Federation of Automatic Control (IFAC), 2005.

CHAPTER 4

PROPOSED ROBUSTNES AND ADAPTIVITY ENHANCED CONTROLLER DESIGN

This chapter explains a proposed robustness and adaptivity enhanced controller design. First, a robust control design is explained to stabilize smart grid power systems due to negative impact of the power fluctuation of distributed renewable energy generations (DREGs), especially the small fluctuation of RE. When sudden change of large power output of DREGs occurs, the performance of robust controller may deteriorate. Therefore, an adaptive robust control design is necessary. In this chapter, the author focuses on indirect adaptive control design which applies iterative identification and parameter tuning. System identification is used to construct an estimated model, and it will be updated whenever the estimated mismatch exceeds predetermined bound. Then the controller parameters are tuned by using the estimated model.

4.1 Robust Control Design

4.1.1 System Uncertainty Modeling

System nonlinear characteristics, variations of system configuration due to unpredictable disturbances, loading conditions, measurement uncertainty, complex behavior, the inherent changing nature of power systems etc., cause various uncertainties in the power system. The system uncertainties will increase when the electricity grid is connected to intermittent DREGs which produce more than 20% of total electricity [1,2]. It is caused by the fact that DREGs typically deliver power with no inertial response. Replacing conventional generation by DREGs, especially wind and solar power, will thus result in lower system inertia. The system inertia is often considered as one of the vital system parameters upon which the synchronized operation of power systems [3]. Lower system inertia makes the power system

stability weak. The relationship between power output of generator and other parameters can be expressed as follows [4],

$$M = M_0 \frac{P_G}{P_{G0}}, \tag{4.1}$$

where M is current generator inertial constant, M_0 is generator inertia constant on rated output, P_G is output of generator, P_{G0} is rated output of generator,

$$D = D_0 \frac{P_G}{P_{G0}}, \tag{4.2}$$

where D is current damping ration of generator, D_0 is generator damping ratio on rated output, and

$$X = X_0 \frac{P_G}{P_{G0}}. \tag{4.3}$$

where X is current reactance of generator, X_0 is generator reactance on rated output.

The equations above show that the high penetration of DREGs causes the total inertia, damping ratio and reactance of generator decrease. Moreover, the application of smart technology in transmission and distribution network is rising significantly, it makes the structure of transmission and distribution more complex and dynamic, and it cause uncertainties in the network also increase. Therefore, a controller which is designed without considering the system uncertainties in the system modeling, the robustness of the controller against system uncertainties cannot be guaranteed. As a result, the controller may fail to operate and lose stabilizing effect under various operating conditions.

To overcome this problem, improvement in the damping factor must be done. In order to achieve this, controller should be properly controlled where robustness against system uncertainties is much desirable. To enhance the robustness of power system damping controller against system uncertainties, the inverse additive perturbation [5] is applied to represent all possible unstructured system uncertainties. However, when the variations of total system inertia are large, giving robustness to the controllers is not enough. The power control designer need to make the controllers adaptive to the changes in operating conditions due to the high penetration of RE sources.

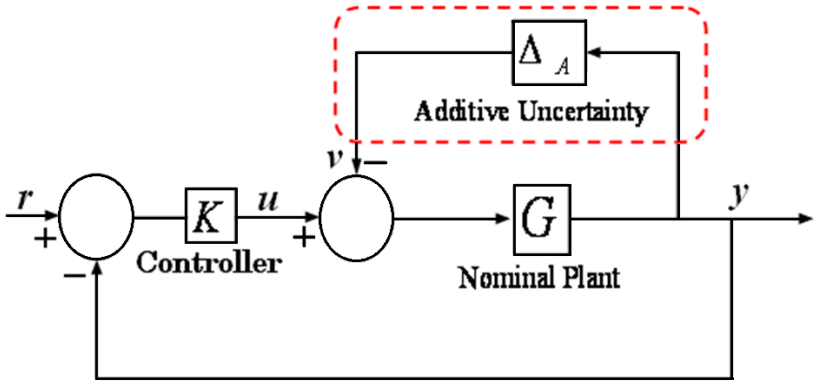

Figure 4.1 Feedback system with inverse additive perturbation.

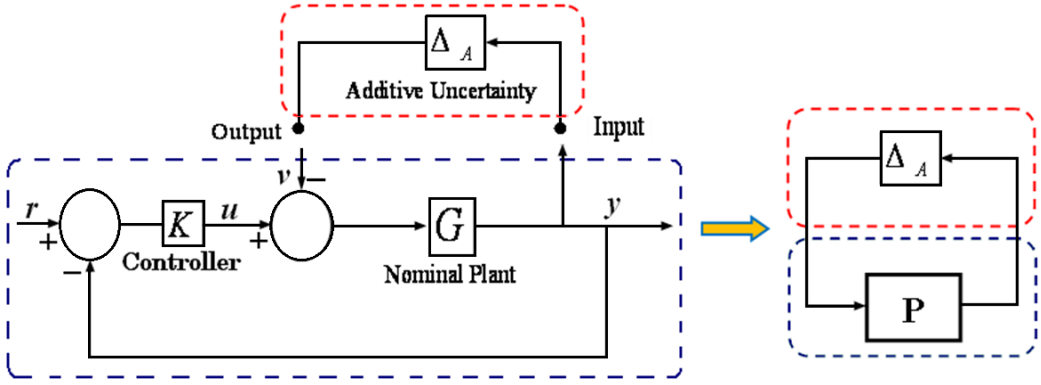

Figure 4.2 Configuration of nominal plant and controller with additive uncertainty.

The feedback control system with the inverse additive perturbation is shown in Fig. 4.1 where G is the nominal plant and K is the controller to be designed. v, r, u and y are the output of additive uncertainty, the reference input, the control signal and the output, respectively. The purpose of the controller K is to stabilize the nominal plant G, and unstructured system uncertainties are represented by Δ_A which is the additive uncertainty model.

Next, the relationship between additive uncertainties with the system will be explained. Fig. 4.2 shows the configuration of nominal plant (G) and controller (K) with additive uncertainty model (Δ_A). The transfer function of P (nominal plant and controller) in the right hand side of Fig. 4.2 can be expressed as

$$P(s) = \frac{-G(s)}{1+G(s)K(s)}. \tag{4.4}$$

Based on the small gain theorem, for a stable additive uncertainty Δ_A, the closed loop system will be robustly stable if

$$\left\|\Delta_A(s)P(s)\right\|_\infty < 1. \tag{4.5}$$

The equation (2) can be modified as follows,

$$\left\|\Delta_A(s)\right\|_\infty < \frac{1}{\left\|P(s)\right\|_\infty}. \tag{4.6}$$

By substituting P, the equation (3) becomes,

$$\left\|\Delta_A(s)\right\|_\infty < \frac{1}{\left\|G(s)/(1+G(s)K(s))\right\|_\infty}. \tag{4.7}$$

The right hand side of equation (4) implies the size of system uncertainties or the robust stability margin against system uncertainties. By minimizing $\|G/(1+GK)\|_\infty$, the robustness of the closed-loop system is near optimum.

4.1.2 Performance Improvement

In this study, the problem constraints are the controller parameters bounds. In addition to enhance the robust stability, another objective is to increase the damping ratio and place the closed-loop eigenvalues of the electromechanical mode in a D-shape region. The D-shape region can be established to achieve the following objectives.

1) To have some degree of relative stability [6].

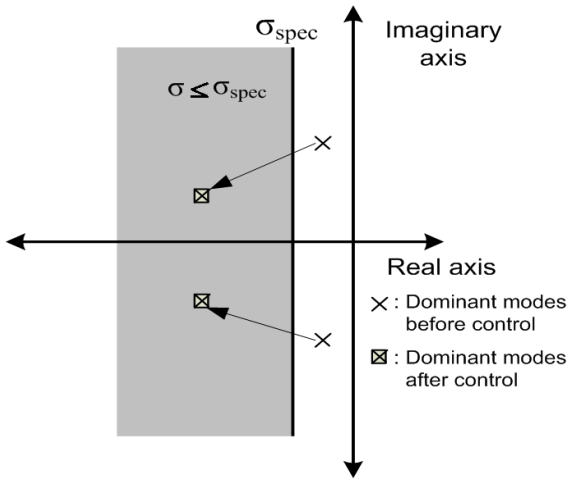

Figure 4.3 Region in the left-side of the s-plane where $\sigma \le \sigma_{spec}$.

The parameters of the controller may be selected to place the electromechanical mode eigenvalue in the left-side of the s-plane by the following function,

$$J_1 = \sigma \le \sigma_{spec}, \tag{4.8}$$

where σ is the actual real part of eigenvalue and σ_{spec} is desired real part of the dominant inter-area oscillation mode, respectively. The relative stability is determined by the value of σ_{spec}. This will place the closed-loop eigenvalues in a region as shown in Fig. 4.3.

2) To limit the maximum overshoot, the parameters of the controller may be selected by the following function

$$J_2 = \zeta \geq \zeta_{spec}, \tag{4.9}$$

where ζ and ζ_{spec} are the actual and desired damping ratio of the dominant inter-area oscillation mode, respectively. This will place the closed-loop eigenvalues in a wedge-shape region in which as shown in Fig. 4.4.

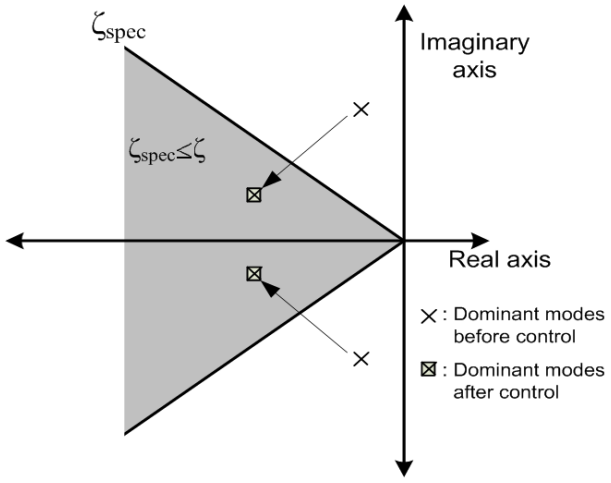

Figure 4.4 Wedge-shape region in the s-plane where $\zeta \geq \zeta_{spec}$.

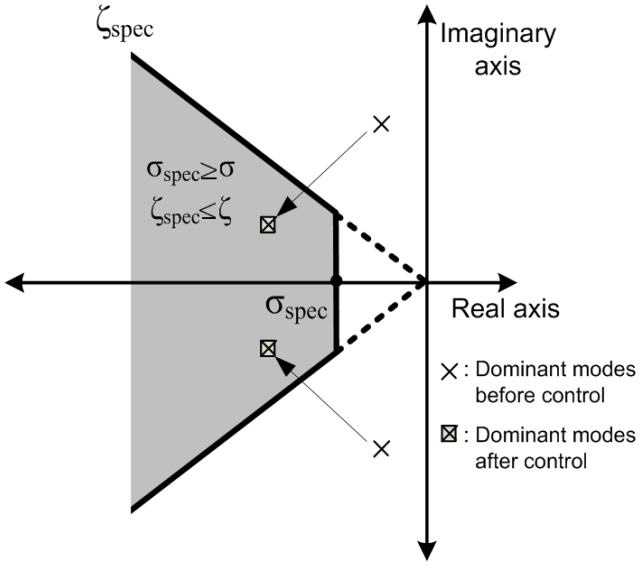

Figure 4.5 D-shape region in the s-plane where $\sigma \leq \sigma_{spec}$ and $\zeta \geq \zeta_{spec}$.

Next, the conditions J_1 and J_2 are imposed simultaneously and will place the system closed-loop eigenvalues in the D-shape region characterized by $\zeta \geq \zeta_{spec}$ and $\sigma \leq \sigma_{spec}$ as shown in Fig. 4.5. It is necessary to mention here that only the unstable or lightly damped electromechanical modes of oscillations are relocated.

4.13. Optimization Problem Formulation

4.1.3.1 Objective Function

To optimize the stabilizer parameters, an inverse additive perturbation based-objective function is considered. The objective function is formulated to minimize the infinite norm of $\|G/(1+GK)\|_\infty$. Therefore, the robust stability margin of the closed-loop system will increase to achieve near optimum and the robust stability of the power system will be improved. As a result, the objective function can be defined as

$$\text{Minimize} \quad \|G/(1+GK)\|_\infty, \tag{4.10}$$

It is clear that the objective function will identify the minimum value of $\|G/(1+GK)\|_\infty$ for nominal operating conditions considered in the design process.

4.1.3.2 Optimization Problem

In this study, the problem constraints are the controller parameter bounds and place the closed-loop eigenvalues of the system in a D-shape region in the s-plane characterized by $\zeta \geq \zeta_{spec}$ and $\sigma \leq \sigma_{spec}$. The constraints are applied to limit the maximum overshoot by increasing the damping ratio of the system.

Therefore, the design problem can be formulated as the following optimization problem.

$$\text{Minimize} \quad \|G/(1+GK)\|_\infty, \tag{4.11}$$

$$\text{Subject to} \quad \zeta \geq \zeta_{spec}, \sigma \leq \sigma_{spec}, \tag{4.12}$$

This optimization problem is solved by genetic algorithm (GA) [7] to search the controller parameters. The author uses GA in this study because the following reason: (a) GA is capable of successful global optimization in the presence of multiple local minima in the parameter space, (b) GA is a method which is very easy to understand and it practically does not demand the knowledge of mathematics, (c) Genetic

algorithms are easily transferred to existing simulations and models. Therefore, it is important to note that the GA provides a number of potential solutions to a given problem and the choice of final solution is left to the user.

4.1.4 Parameters Tuning

In this section, GA is applied to search the controller parameters of controllers with off line tuning. The flow chart of the proposed method is illustrated in Fig. 4.6. Each step is explained as follows.

Step 1 Generate the objective function for GA optimization.

In this study, the performance and robust stability conditions in inverse additive perturbation design approach is adopted to design a robust controller. The control parameters are optimized by GA based on the optimization problem in sub section 4.1.3.2.

Step 2 Initialize the search parameters for GA. Define genetic parameters such as population size, crossover, mutation rates, and maximum generation.

Step 3 Randomly generate the initial solutions.

Step 4 Evaluate objective function of each individual in (4.11) and (4.12).

Step 5 Select the best individual in the current generation. Check the maximum generation.

Step 6 Increase the generation.

Step 7 While the current generation is less than the maximum generation, create new population using genetic operators and go to step 4. If the current generation is the maximum generation, then stop.

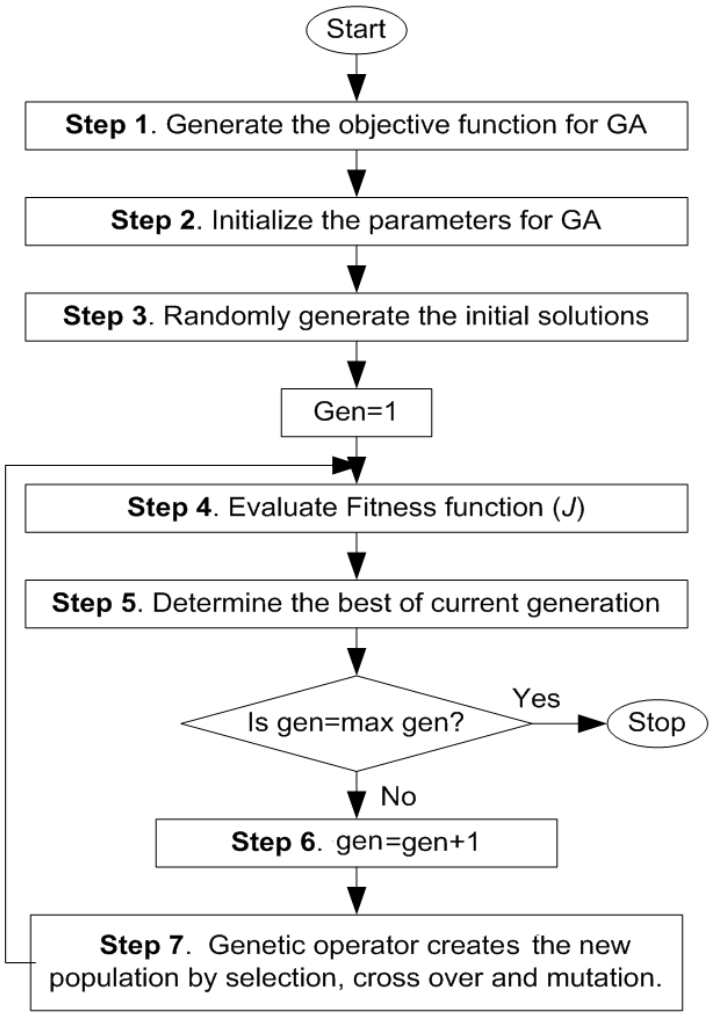

Figure 4.6 Flow chart of the proposed robust control design.

The proposed robust control method will be applied to design battery controller in isolated hybrid wind-diesel power system in chapter 5. Additionally, the robust PSS design will be carried out to stabilize the inter-area oscillation in interconnected power systems with high DREGs penetration in Chapter 6.

This method is able to guarantee the robustness controller with conventional structure PID or lead-lag controller. It is different with those of conventional robust controllers in Chapter 2, where the conventional robust controller has high order and unstructured controller, and it is difficult to be applied in the real system. On the other hand, the proposed robust controller is able to guarantee robustness by using existing conventional controller structure. However, when the high DREGs penetration occurs in power system, very extreme conditions may appear and the

system stability becomes weak. The high penetration of unpredictable renewable energy power outputs cause inertia constant of conventional generator decreases significantly, and it gives impact on system stability. To examine the condition, let us use the example of SMIB system in chapter 2.

4.1.5 Application of Proposed Robust Control Design in Power System

In this section, the proposed robust control design as described in section 4.1 above is applied. In the optimization, the ranges of search parameters and GA parameters are set as follows: $K_P \in [1 \quad 50]$, T_1 and $T_2 \in [0.001 \quad 1]$, ζ_{Spec} =0.4, σ_{Spec} = -0.5, population size is 200, and maximum generation is 100. Consequently, the designed PSS is given as follow,

$$K(s) = 18.27\left(\frac{0.3243s+1}{0.0658s+1}\right). \tag{4.13}$$

Table 4.1 Comparison of oscillation mode.

	Without PSS	With proposed PSS
Eigenvalue	-0.1281±j9.134	-2.502±j 0.859
Damping ratio	0.014	0.94

The eigenvalues corresponding to the electromechanical mode without PSS and with the proposed PSS are listed in Table 4.1. Clearly, the desired damping ratio and the desired real part of the oscillation mode are achieved by the proposed PSS. In simulation studies, the performance and robustness of the proposed controllers are compared with those of the PSS designed by fixed structured H_∞ loop shaping method (FH PSS) obtained from chapter 2, that is

$$PSS = 100\frac{0.0002s^5 + 0.0189s^4 + 0.574s^3 + 7.27s^2 + 31.72s - 57.4}{0.0000003s^6 + 0.00014s^5 + 0.0094s^4 + 0.364s^3 + 8.083s^2 + 75.9s + 5.88}, \tag{4.14}$$

and the conventional lead-lag controller (CPSS) obtained from [8], that is

$$(CPSS)K(s) = 5.5\frac{(1+0.1732s)^2}{(1+0.0577s)^2}, \tag{4.15}$$

Table 4.2 Operating Condition.

System Parameters	$P(p.u)$	$Q(p.u)$	$x_e\ (p.u)$
Case 1 : Normal Condition	0.8	0.4	0.2
Case 2 : Heavy Load &Weak line	**0.95**	0.4	0.8

In simulation studies, the system responses with PSSs are examined under two case studies as in Table 4.2, while a small disturbance of 5 % (0.05 p.u.) step response of ΔV_{ref} is applied to the system at $t = 0$ s.

Fig. 4.7 shows the responses of electrical power output deviation and power output of PSS in case 1. CPSS, FH PSS and the proposed PSS are able to damp power oscillations. Nevertheless, the overshoot of power oscillations in cases of FH PSS and the proposed PSS are much lower than that of CPSS. By simple structure of controller, the proposed controller can guarantee the performance and robustness of controller. It is one of the advantages of the proposed controller.

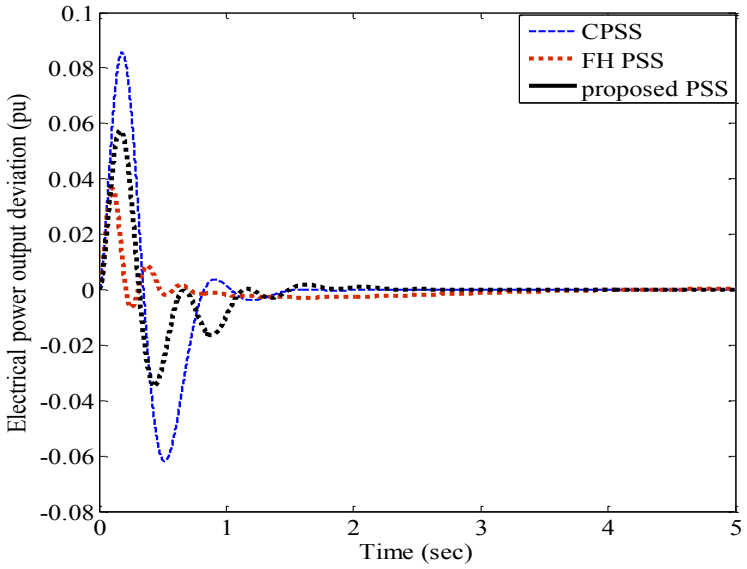

Figure 4.7 Simulation results of case 1.

Next, the electrical power output is increased in case 2 to get heavy load and weak line condition. The simulation results are shown in Fig. 4.8. The results shows that the CPSS fails to damp power system. The power oscillation gradually increases and diverges. In contrast, the FH PSS and the proposed PSS can tolerate this situation. The power oscillations are significantly damped.

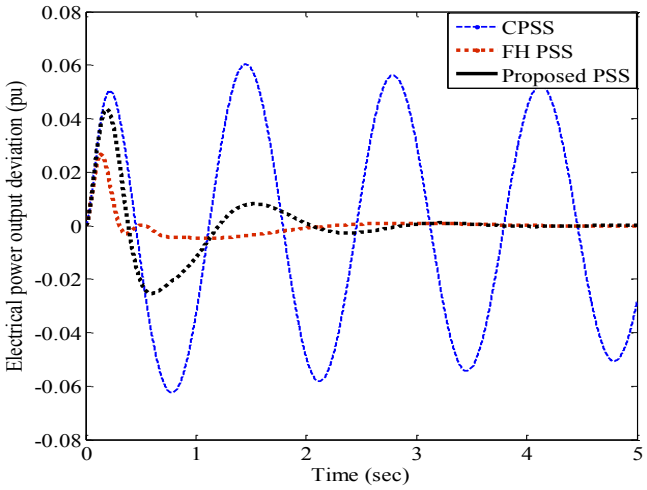

Figure 4.8 Simulation results of case 2.

The simulation results above depict the system response without renewable energy generation penetration. After large renewable energy generations are connected to the system, some of system parameters change, especially inertia constant, damping ratio and reactance of generator. It is assumed that large DREGs are connected to the system above. The maximum capacity of renewable energy is 0.4 pu or about 40% of the total system capacity. Therefore, the new inertia constant, damping ratio and reactance of generator are decreased significantly.

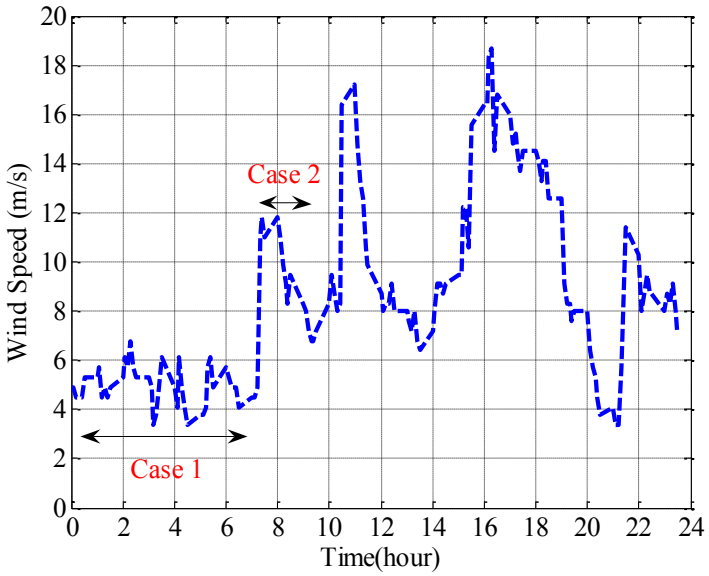

Figure 4.9 Sample of wind speed in Indonesia for a day.

For example, the wind speed in Fig. 4.9 applied in the SIMB system. We can see that from 0:00 to 07.00 am, the wind speed is very low; it means that the conventional generator has a large portion to deliver power to demand. But from 07.00 to 08.30 am, the wind power output is increase, and it causes the conventional generator will reduces the power output. Consequently, inertia constant, generator reactance and damping ratio also will go down.

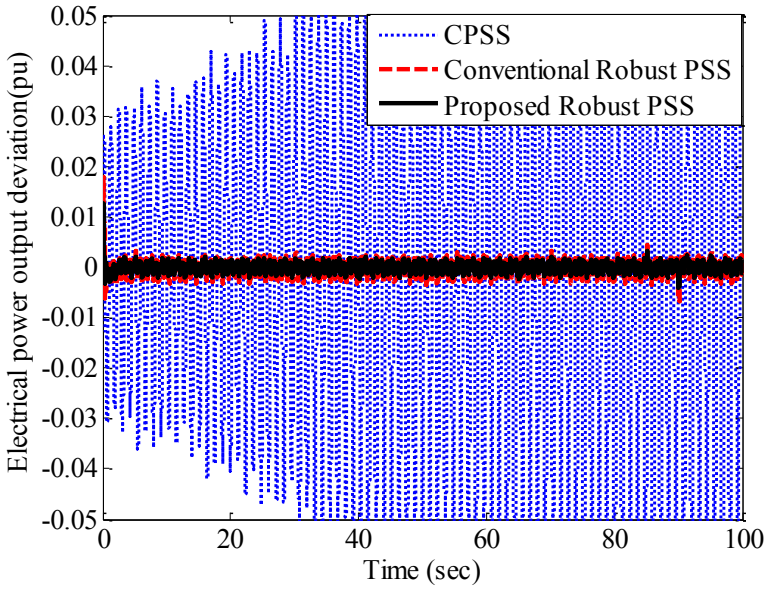

Figure 4.10 Simulation result in the case of heavy load condition and low wind power output.

The performance of system against the change of wind power output is shown in Fig. 4.10 and 4.11. Figure 4.10 depicts the electrical power response during low wind power output in the case that the system works on heavy load condition. CPSS fails to damp power oscillation. On the other hand, FH PSS and proposed robust PSS are able to stabilize the system.

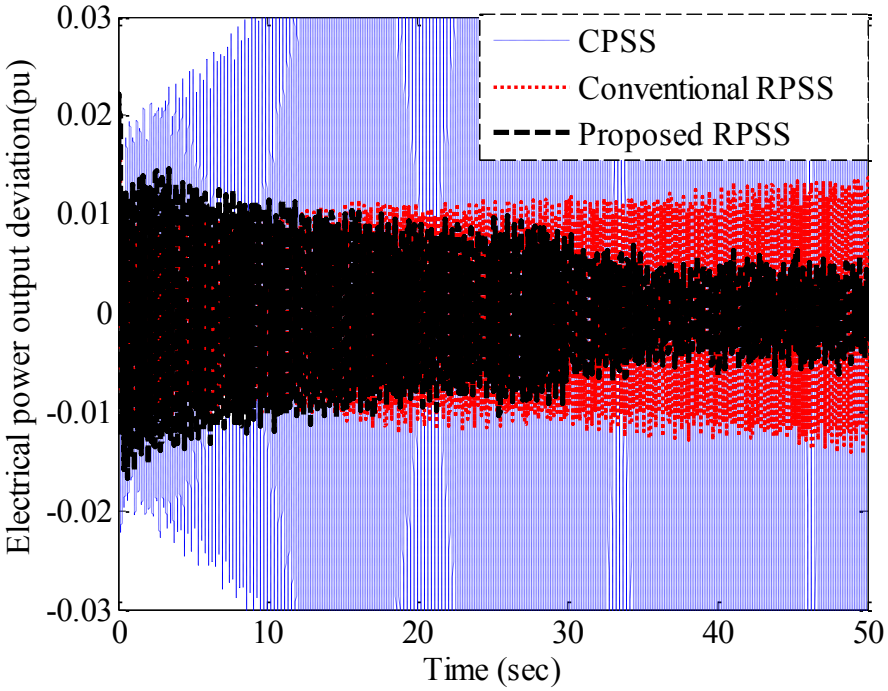

Figure 4.11 Simulation result in the case of heavy load condition and large wind power output.

Simulation result of system in the case of heavy load condition and large wind power output is shown in Fig. 4.11. In this case, inertia constant is reduced significantly. The simulation results show that the damping effect of all controllers are deteriorated by the decrease of inertia constant, and the peak oscillations become large. As a result, in the case that the high penetration of renewable energy is applied, the performance of robustness is not enough; we need to combine the robustness with adaptivity to stabilize extreme conditions, and it will be explained in the next section.

4.2. Proposed Adaptive Robust Controller Design

4.2.1 Introduction

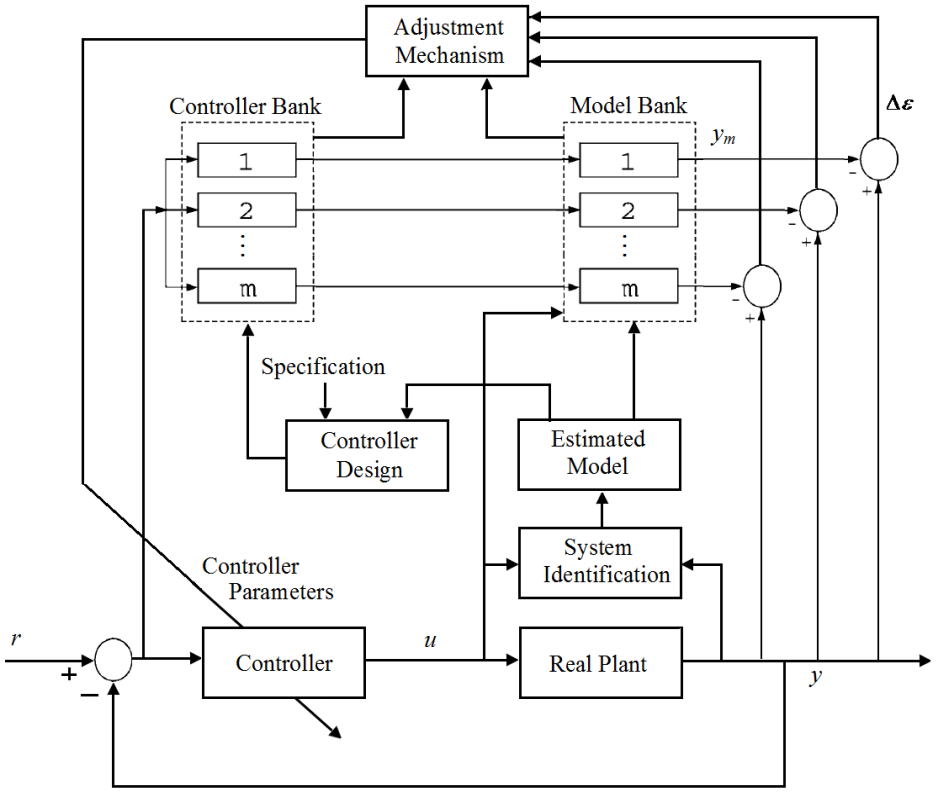

Figure 4.12 Architecture diagram of proposed indirect adaptive control.

Large unstable outputs of DREGs cause frequency deviation from the rated value. If the most loads are supplied by the power from the renewable energy, the power output of conventional generators should be decreased. It causes the reduction of total inertia constant and makes the power system stability weak. To overcome this problem, improvement in the damping factor must be done. In order to achieve this, controller (PSS, energy storage, FACTS device etc.) should be properly controlled where robustness against system uncertainties such as various generating and loading conditions, unpredictable network structures, variations of system parameters etc. is much desirable. When the variations of total inertia constants are large, giving robustness to the controllers is not enough. We need to make the controllers adaptive to the changes in operating conditions due to the high penetration of RE sources. This section proposes adaptivity as well as robustness to the conventional type of

controllers. Diagram of the proposed adaptive robust control design is shown in Fig. 4.12.

In the proposed adaptive control, a system identification technique and the robust controller design method described above are combined into an indirect adaptive controller design. The identified model is used to monitor discrepancy between the actual power system output and the expected output (model output). When a large discrepancy is detected, a new set of controller parameters is determined to adapt to the new situation. The robust control design is applied to guarantee robustness of controller. The several given identified models and corresponding controller parameters will be stored in memory, so that we have model and controller banks. The model and controller bank have an advantage, the system re-uses them in the similar situations without model identification and controller parameters re-tuning.

4.2.2 System Identification

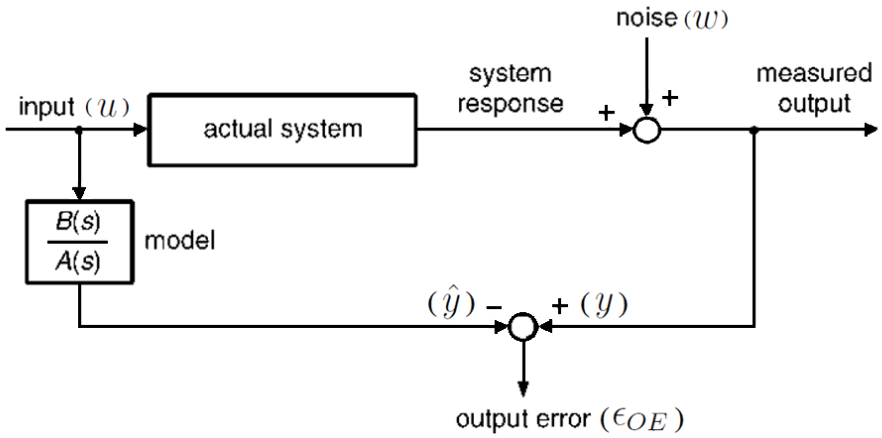

Figure 4.13 Structure of Output Error (OE) model identification.

The goal of system identification is to characterize the dynamic input-output relation of the underlying process [9]. Many methods have been successfully applied to identify systems. In this study, we use output error (OE) identification to construct the estimated model of each generator because the OE model is easily computed, familiarly used and has high accuracy. The model structure is the conventional transfer function, but the parameters of the transfer function are unknown, and OE

identification is applied to identify the parameters. The OE structure is represented in Fig. 4.13 [10], the error is defined by

$$\in_{OE} = y - \hat{y} = y - \left(\frac{B}{A}\right)u, \tag{4.16}$$

where u is the input signal of the real system, y is the measured output of the real system and $\hat{y}$ is the output of the estimated model. $B(s)/A(s)$ is the transfer function of the estimated model. W is the output disturbance or noise. The OE method deals with minimizing an objective function, usually a quadratic criterion, which is based on the output error ϵ_{OE}. This is the error between the measured output y of the system and the output $\hat{y}$ of the transfer function model.

4.2.3 Robust Control design

In this study, the purposes of the controller design are to guarantee robustness and good damping. The robust controller can be designed by considering the system uncertainties in the modeling with constraints which correspond to guaranteeing good damping. In this study, an inverse additive perturbation model [5] is applied to represent all possible unstructured system uncertainties.

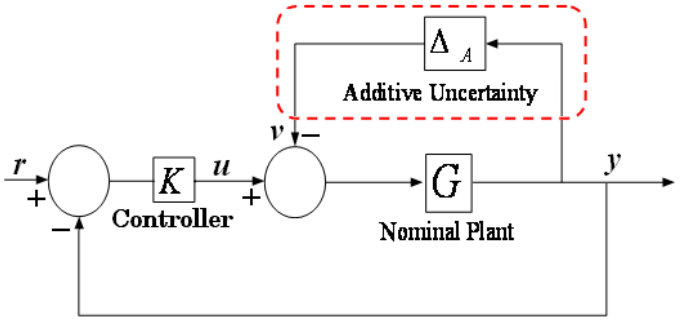

Figure 4.14 Feedback system with inverse additive perturbation.

The feedback control system with the inverse additive perturbation is shown in Fig. 4.14 where G is the nominal plant and K is the controller to be designed. v, r, u and y are the output of additive uncertainty, the reference input, the control signal and the output, respectively. The purpose of the controller K is to stabilize the nominal plant G, and unstructured system uncertainties are represented by Δ_A which is the additive uncertainty model. Then the transfer function from signal v to y is

T_{uv}= $\|G(s)/(1+G(s)K(s))\|$. Based on the small gain theorem, for a stable additive uncertainty Δ_A, the closed loop system is robustly stable if the controller *K(s)* stabilizes the nominal plant *G(s)* by the following form,

$$\|\Delta_A G(s)/(1+G(s)K(s))\|_\infty < 1. \quad (4.17)$$

Then

$$\|\Delta_A\| < \frac{1}{\|G(s)/(1+G(s)K(s))\|_\infty}. \quad (4.18)$$

By minimizing $\|G(s)/(1+G(s)K(s))\|_\infty$, the robust stability value of the closed-loop system is near optimum. The infinity sign in the equation means the amplitude or peak value of $\|G(s)/(1+G(s)K(s))\|_\infty$.

4.2.4 Adaptive Robust Control Design

In practice, we often do not know all system parameters. Therefore, the identification system to get an estimated model is highly needed. However, extreme operating conditions of the system may alter the parameters of mathematical structure of the plant model. The estimated model that was designed in normal operating condition may no longer match with the real plant model, and the estimated model must be redesigned to make the matching conditions again. To determine when re-estimation is needed, it is necessary to calculate the plant-model mismatch. Based on the new estimated model, controller parameters should be re-tuned to get suitable performance. This research presents an adaptive robust control using the estimated model to enhance smart grid stability under high RE penetration. The flow chart of the proposed method is shown in Fig. 4.15. Each step of the proposed method for model identification, and adaptive robust controller design is explained as follows,

Step 1. Comparison of the real system and the estimated model

In this step, we compare the output signal of both the real and the estimated system. The result of the comparison between the real and estimated model is called 'mismatch error'. The estimated model will be updated whenever the mismatch exceeds predetermined bound ($\Delta\varepsilon$). $\Delta\varepsilon$ is predetermined by the power control

designer according to the error tolerance required. As mentioned in the introduction that the system has memory to store a new estimated model and controller parameters. When the operating condition of the real system move to a new condition and the mismatch exceeds the predetermined bound, the system will look at memory to check the availability of the matching estimated model. If the memory has the matching estimated model, then the system will re-uses it directly without model identification and controller parameters tuning. Otherwise, the system will develop a new estimated model and tune controller parameter.

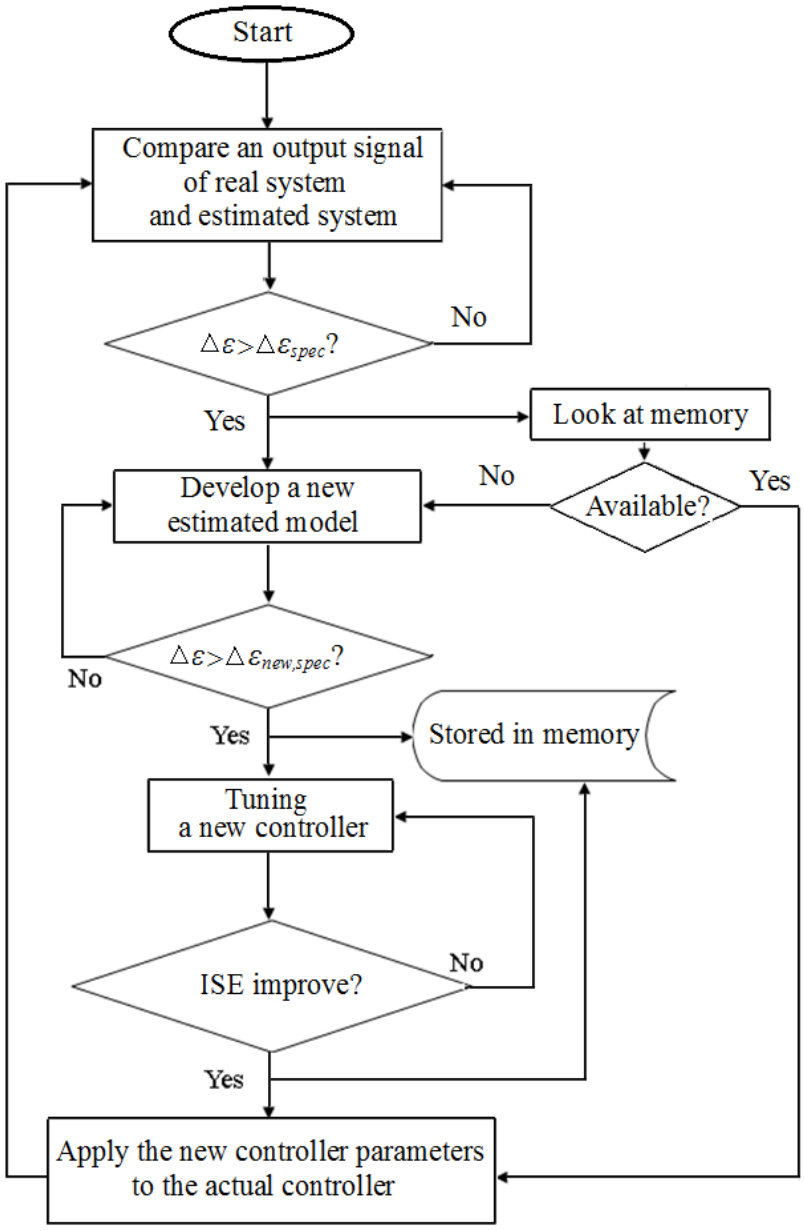

Figure 4.15 Flow chart of the proposed adaptive control method.

Step 2. Develop a new estimated model

We develop a new estimated model using output error (OE) system identification so that the mismatch error be less than or same as specification. If the mismatch error is greater than specification, we need to develop a new estimated model again using another set of data. There are two sets of data. The first set of data is used to model identification, and the second set of data is needed as model validation. The length of each data is 60 s or 1 minute.

Step 3. Controller parameters tuning

Based on the new estimated model, parameters of the 'virtual controller' will be tuned by considering system uncertainties and increasing the damping ratio of the dominant mode of the power system. Note that, the 'virtual controller' parameters are tuned and that therefore the actual system behavior is not affected by the tuning.

Here, there are two kinds of conventional controller structure that the author applies in this study; each controller structure is shown in the following equation:

PI controller : $K_{PI} = K_P + \frac{K_I}{s}$, (4.19)

Lead lag controller : $K_{LeadLag} = K\left(\frac{T_1 s + 1}{T_2 s + 1}\right)\left(\frac{T_3 s + 1}{T_4 s + 1}\right)$, (4.20)

where K_P is a controller gain of PI controller; K_I is an integral parameter of PI controller. K is a controller gain of lead/lag controller, and T_1 , .., T_4 are time constants of lead/lag controller.

Then to tune controller parameters, the following optimization problem is applied

Minimize $\|G/(1+GK)\|_\infty$ (4.21)

Subject to $\zeta \geq \zeta_{spec}, \sigma \leq \sigma_{spec}$ (4.22)

$K_{P,\min} \leq K_P \leq K_{P,\max}$, or $K_{\min} \leq K \leq K_{\max}$

$K_{I,\min} \leq K_I \leq K_{I,\max}$, or $T_{1,\min} \leq T_i \leq T_{i,\max}$

where ζ and ζ_{spec} are the actual and desired damping ratio of the dominant mode, respectively; σ and σ_{spec} are the actual and desired real part of the dominant mode,

respectively. This optimization problem is solved by meta-heuristic method (genetic algorithm).

Step 4. Store the new estimated model and the new controller parameters in the memory.

After the new controller parameter is successfully to improve the robustness and performance of the system, the new estimated model and the new controller parameters will be stored in the memory to be used in the similar situations in the future without model identification and controller parameters tuning.

Step 5. Apply the new controller parameters to the actual controller, and return to step 1.

During controller parameters changes, overshoot may occur. To eliminate the problem, incremental changes in the controller parameters are applied until the final value is achieved and the performance is optimized. In this thesis, the author use 5-10 step in incremental controller parameters changes.

The proposed indirect adaptive robust control method will applied to design battery controller in isolated hybrid wind-diesel power system in chapter 5. Additionally, the robust PSS design will be carried out to stabilize the inter-area oscillation in interconnected power systems with high wind farms and PV generations penetration in Chapter 6.

REFERENCES

[1] National Conference of State Legislatures, "Integrating Wind power into the electric grid" pp. 1-4, 2009.

[2] Emmanuel S. Karapidakis, "Wind Power Impact on Power System Dynamic Performance", Wind Power, pp. 395-414, InTech, 2010.

[3] Pieter Tielens, Dirk Van Hertem," Grid Inertia and Frequency Control in Power Systems with High Penetration of Renewables" Young Researchers Symposium in Electrical Power Engineering edition: 6, Delft, The Netherlands,16-17 April 2012.

[4] R. Watanabe, T. Tsuji, T. Oyama, T. Hashiguchi, T. Goda, " A study on multiswing stability under a large penetration of PV generations, The International Conference on Electrical Engineering 2012, Kanazawa, Japan.

[5] Gu D.W, et al., " Robust control design with MATLAB, "Springer, London, 2005.

[6] Y. L. Abdel-Magid, M. A. Abido, S. AI-Baiyat and A. H. Mantawy, “Simultaneous Stabilization of Multimachine Power Systems via Genetic Algorithm, ” IEEE Trans. on Power Systems, Vol. 14, No. 4, pp. 1428-1439, 1999

[7] GAOT , " A Genetic Algorithm for Function Optimization: A Matlab Implementation, " 1995

[Online] Available: http://www.ie.ncsu.edu/mirage/GAToolBox/gaot/

[8] P.S. Rao, et al,. " Robust tuning of power system stabilizers using QFT. " IEEE-Trans. on Control Systems Technology. Vol. 4, pp. 478-486, 1999.

[9] T. Elie, T. Poinot, R. Ouvrard, A. Abche, "Initialization of Output Error Identification Algorithms". PhD Thesis 2008; The university of Balamand, Lebanon.

[10] G.P. Rao, H. Unbehauen, "Identification of continous-time systems". IEE proc.-control theory Appl. 2006; 153: 185-220.

CHAPTER 5

ROBUSTNESS AND ADAPTIVITY ENHANCED ENERGY STORAGE CONTROL DESIGN FOR STABILIZATION OF SMART MICRO GRID POWER SYSTEM

This chapter applies the proposed control design method to battery energy storage controllers for stabilization smart micro grid. First, the power system model, pitch controller, governor and energy storage model are explained. Next, the proposed robust controller is applied to design pitch, governor and battery controller. Subsequently, eigenvalue analysis is used to evaluate whether controller design by considering adaptivity is needed or not. Simulation studies are carried out in hybrid wind-diesel power systems to show the superior robustness and damping effect of the proposed robust battery controller in comparison with that of conventional controller.

5. 1. Introduction

Wind power as one of renewable energy sources is expected to be economically attractive when the wind speed of the proposed site is considerable for electrical generation and electric energy is not easily available from the grid [1]. However, the intermittence and fluctuation of output power of wind power generation may cause a serious problem of frequency fluctuation of the isolated micro grid [2]. To guarantee high quality power system, the applications of smart grid technologies such as distributed energy storage and FACTS devices for mitigating impacts and allowing the integration of renewable energy generation are highly needed [3].

Several control methods for frequency stabilization by applying pitch angle of wind power generation have been reported [4-6]. In these works, however, they only focus on the design of pitch controller in the wind site without considering governor controller in the diesel side. To enhance the frequency stability in isolated power

system, some research works have successfully proposed control design methods of the pitch controller in the wind side and the governor in the diesel side simultaneously. To damp the frequency fluctuation, optimization of controller parameters using ISE technique [7] and fuzzy logic [8] etc have been proposed. In [9,10], the authors proposed new load frequency control method combining a PID controller and a disturbance observer for large penetration of wind power generations. This work can significantly improve the performance of the controllers and power system. Nevertheless, under the sudden change of load demands and random wind power input, the pitch controller of the wind side and the governor of the diesel side may no longer be able to effectively control the system frequency due to their slow response.

Energy storages such as battery, flywheel, superconducting magnetic energy storage (SMES), fuel cell etc, which are able to supply and absorb active power rapidly [11,12], have been highly expected as the most effective controllers of system frequency. SMES has been successfully applied to solve many problems in power systems such as an improvement of power system dynamics [13,14], a load leveling [15], a frequency control in hybrid wind-diesel power systems [16,17] etc. SMES may provide satisfactory control affect. However, SMES is very costly in comparison with the common energy storage such as battery energy storage, flywheel etc. Despite the significant potential of SMES mentioned above, power system utilities still prefer to use the common storage such as battery energy storage.

In [18], design of robust battery controller in a hybrid wind-diesel power system by H_∞ control has been proposed. In this work, the controller has high robustness against various uncertainties. However, the weighting functions in H_∞ control design cannot be selected easily. Moreover, the order of H_∞ controller depends on that of the plant. This leads to the complex structure controller which is different from conventional PI or lead/lag compensator, and also the pitch and battery controller in this work have been designed separately while the control parameters of governor are fixed. This method may not be able to guarantee the well coordinated control

between governor, pitch and battery controller. To enhance the coordinated control, the simultaneous optimization of robust governor, pitch and battery controller is highly expected.

This chapter presents a design on the robust PI-based coordinated control of governor, pitch and battery on isolated hybrid wind-diesel power system to control frequency fluctuation. The simple 1st order PI controller is used in this study, it is easy to implement in industry. To take system uncertainties into account in the control design, the inverse additive perturbation [19] is applied to represent all unstructured uncertainties in the system modeling. Moreover, to improve performance of the system, another objective is to increase the damping ratio and place the closed-loop eigenvalues of the electromechanical mode in a D-shape region. Then the genetic algorithm (GA) is used to solve the optimization problem. Then eigenvalue analysis against variation of fluid coupling parameter is applied to check whether adaptivity enhanced controller design is necessary or not. The simulation studies have been done to evaluate performance, effectiveness and robustness of proposed control design in comparison with that of conventional controller design against various operating conditions.

5.2. Problem Formulation

Figure 5.1 depicts the basic system configuration of an isolated hybrid wind-diesel power system which will be used to design the coordinated robust frequency controller of governor, pitch and battery controllers. The base capacity of the system is 300 kW. This system consists of a diesel generator, a wind power generation and the load [7]. The rated capacities of diesel and wind power generation are 150 kW and 150 kW, respectively. The wind power generation produces a random active power, and the diesel is used to supply power to system when wind power could not adequately provide power to customer.

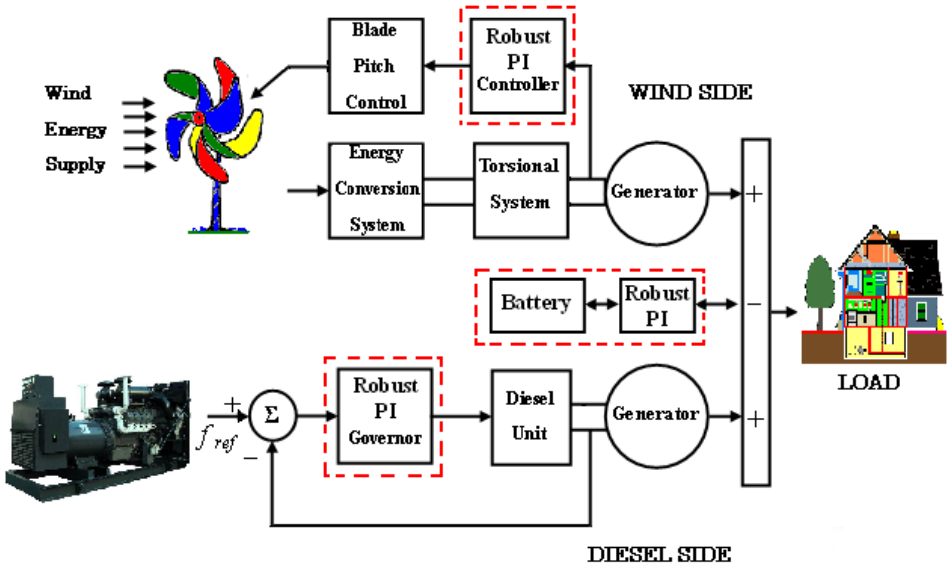

Figure 5.1 Basic configuration of an isolated power system with governor, pitch and battery controllers.

The fluctuation of real power in the system can be expressed as follow:

$$\Delta P = P_{GD} + P_{GW} - P_L - P_{BATT}, \tag{5.1}$$

where ΔP is deviation of real power, P_{GD} is real active of diesel generation, P_{GW} is real power of wind power generation, P_L is real power consumption in the costumer side, and P_{BATT} is real power which is absorbed or supplied by battery energy storage. The deviation of real power may cause the serious problem of large frequency deviation in the system [17]. Furthermore, the life time of machine apparatuses on the load side affected by large frequency deviations will be reduced. To overcome this problem, maintaining the balance of real power between supply and demand in the system is highly needed. In this study, the real power deviation is suppressed by the diesel generator, the wind power generation, and the battery. Governor and pitch controller are equipped in the diesel side and the wind side, respectively, to help balance the distribution of real power in the system. However, the ability of the governor and pitch controllers to provide frequency control is not adequate due to their slow response. Accordingly, the battery energy storage is installed in the system to fast compensate for surplus or insufficient power demands, and minimize frequency deviation.

Here, the proposed control design method is applied to design the coordinated control of governor, pitch and battery. The coordinated controllers are able to improve the performance and also minimize the interaction of the controllers.

5.3. Mathematical Modeling of Studied Power System

For mathematical modeling, the transfer function block diagram of the isolated power system used in this study is shown in Fig. 5.2. This model consists of the following subsystems: the wind dynamic model, the diesel dynamic model, the governor control of diesel side, the battery unit, the pitch control of wind side, and the power network model. However, this model is primarily based on the frequency problem in the system hence do not take the voltage deviation into account in the system modeling.

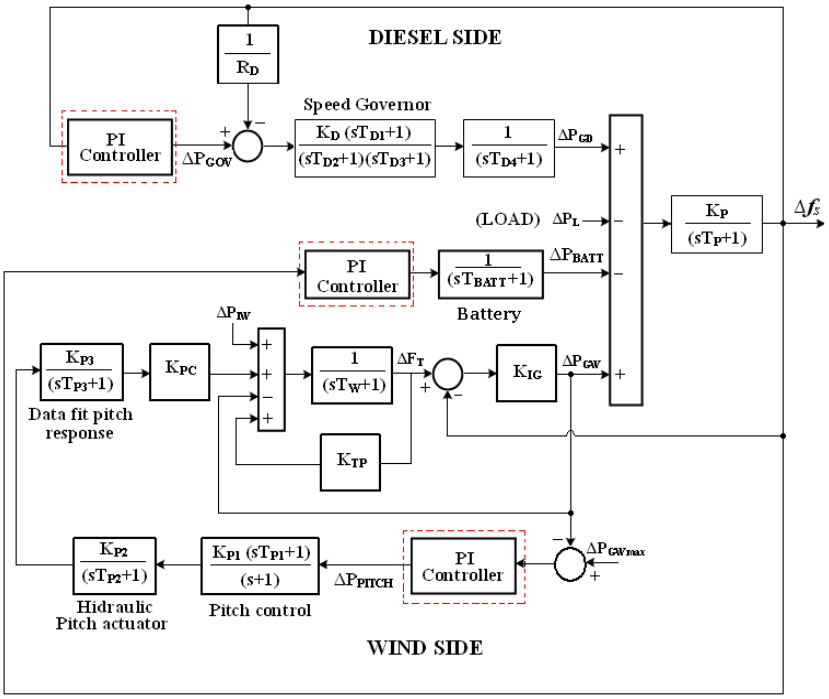

Figure 5.2 Block diagram of a hybrid wind-diesel power generation with battery controllers.

The linearized state equation of the hybrid wind-diesel power system shown in Fig. 5.2 can be expressed as

$$\Delta \dot{X} = A\Delta X + B\Delta u\,, \tag{5.2}$$

$$\Delta Y = C\Delta X + D\Delta u\,, \tag{5.3}$$

where the state vector $\Delta X = [\Delta f_S \quad \Delta P_{GD} \quad \Delta P_{D1} \quad \Delta F_T \quad \Delta PF_1 \quad \Delta PF_2 \quad \Delta PF_3]^T$, the output vector $\Delta Y = [\Delta f_s \quad -\Delta P_{GW}]^T$, the output vector consists of the deviation of output power of wind power (ΔP_{GW}), and the system frequency deviation (Δf_S). The input (or control) vector $\Delta u = [\Delta u_{GOV} \quad \Delta u_{PITCH} \quad \Delta u_{BATT}]^T$, where Δu_{GOV}, Δu_{PITCH} and Δu_{BATT} are the control signal of the governor, the pitch controller and the battery controller, respectively.

5.4. Configuration of Governor, Pitch and Battery Controllers

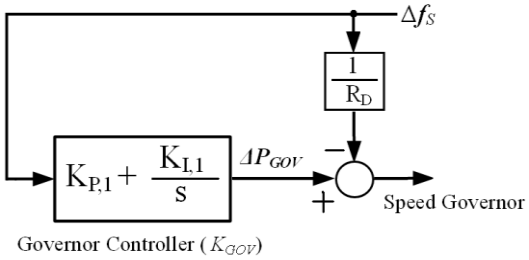

Figure 5.3 Block diagram of governor controller (K_{GOV}).

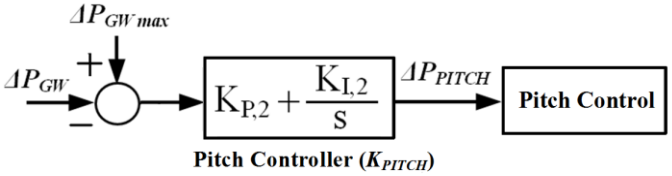

Figure 5.4 Block diagram of pitch controller (K_{PITCH}).

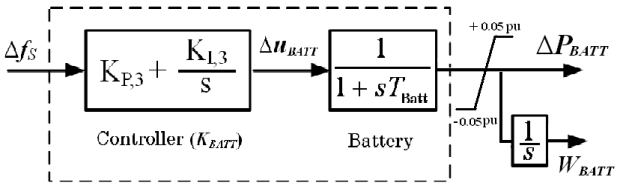

Figure 5.5 Block diagram of battery with the controller (K_{BATT}).

As shown in Fig. 5.3 and Fig. 5.4, the governor controller (K_{GOV}) and the pitch controller (K_{PITCH}) are represented by a simple 1st order PI controller which uses system frequency deviation (Δf_S) and output power of wind power (ΔP_{GW}) as a feedback input signal, respectively. Moreover, the battery block diagram is depicted in Fig. 5.5. The battery diagram consists of two transfer functions, i.e. the battery model and the PI based frequency controller. Based on [18], the battery can be modeled by the first-order transfer function with time constant T_{BATT} = 0.3 sec. In this work, the battery controller is presented by practically a 1st order PI controller with

single feedback input signal, system frequency deviation (Δf_S). The rated capacity of inverter is 15 kW (0.05 pu), and the rated capacity of battery is 30 kWh. Note that the system in (1) is a multi-input multi-output (MIMO) system.

5.5 Optimization Problem

In this study, the objective function is formulated to minimize the infinite norm of $\|G/(1+GK)\|_\infty$. Therefore, the robust stability margin of the closed-loop system will increase to achieve near optimum, and the robust stability of the power system will be improved. In addition, the problem constraints are the controller parameters bounds. Another objective is to limit the maximum overshoot by increasing the damping ratio of the hybrid wind-diesel power system in a D-shape region in the s-plane [20]. The conditions will place the closed-loop eigenvalues of the hybrid wind-diesel power system in the D-shape region characterized by $\zeta \geq \zeta_{spec}$ and $\sigma \leq \sigma_{spec}$ as shown in Fig. 5.6.

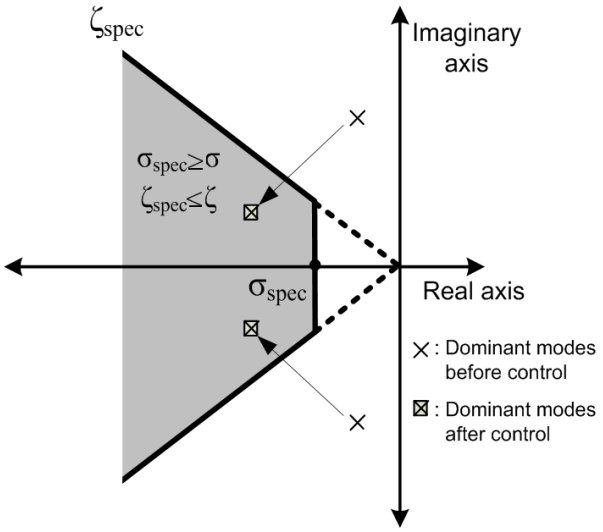

Figure 5.6 D-shape region in the s-plane where $\sigma \leq \sigma_{spec}$ and $\zeta \geq \zeta_{spec}$.

Therefore, the design problem can be formulated as the following optimization problem.

Minimize $\|G/(1+GK)\|_\infty$, (5.4)

Subject to $\zeta \geq \zeta_{spec}, \sigma \leq \sigma_{spec}$. (5.5)

$K_{P,i,\min} \leq K_{P,i} \leq K_{P,i,\max}$,

$K_{I,i,\min} \leq K_{I,i} \leq K_{I,i,\max}$, $i = 1,..,3$,

where ζ and ζ_{spec} are the actual and desired damping ratio of the dominant mode, respectively; σ and σ_{spec} are the actual and desired real part of the dominant mode, respectively.; $K_{P,min}$ and $K_{P,max}$ are the maximum and minimum controller gains, respectively; $K_{I,min}$ and $K_{I,max}$ are the maximum and minimum integral parameter of PI controllers, respectively. This optimization problem is solved by GA [21] to search the proposed PI controller parameters.

5.6. Designed Results

In the optimization, the ranges of search parameters are set as follows: ζ_{spec}, desired damping ratio, is set as 0.3, σ_{spec}, desired real part, is set as -0.3. $K_{P,i,min}$ and $K_{P,i,max}$, minimum and maximum gains of governor, pitch and battery controller, are set as 1 and 300, $K_{I,i,min}$ and $K_{I,i,max}$, minimum and maximum integral parameter of governor, pitch and battery controller, are set as 0.01 and 40. Moreover, the GA parameters are set as follows: crossover probability is 0.9, mutation probability is 0.05, population size is 100 and maximum generation is 100. Consequently, the convergence curve of the objective function can be shown in Fig. 5.7. The convergence curve shows that GA can bring the value of $\|G/(1+GK)\|_\infty$ for nominal operating condition down to 3.46 .

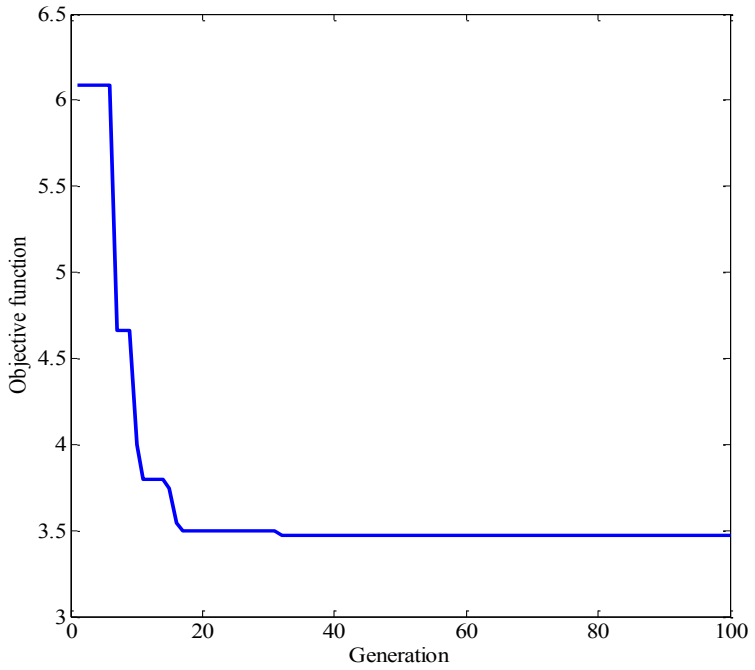

Figure 5.7 Objective function versus iteration.

As a result, the proposed PI controllers are given as follows,

$$K_{GOV} = -96.729 - \frac{9.27}{s}, \tag{5.6}$$

$$K_{PITCH} = 21.294 + \frac{2.063}{s}, \tag{5.7}$$

$$K_{BATT} = 72.069 + \frac{28.557}{s}. \tag{5.8}$$

In simulation studies, the performance and robustness of the proposed PI controllers are compared with those of PI-controller [7] and conventional PI controllers optimized without considering robustness. The conventional PI controller is referred to as "C-PI controller". Note that the control parameters of the C-PI controller and the proposed PI controller are optimized based on the same specification in the nominal operating condition. The design objective of the C-PI controller is to move the dominant mode to the D-shape region in the s-plane as shown in Fig. 5.6. The C-PI controller are given as follows,

$$K_{GOV} = -44.9108 - \frac{2.285}{s}, \tag{5.9}$$

$$K_{PITCH} = 24.39 + \frac{3.703}{s}, \tag{5.10}$$

$$K_{BATT} = 44.07 + \frac{13.307}{s}. \tag{5.11}$$

Table 5.1 Eigenvalue and damping ratio of dominant mode.

Cases	Eigenvalues, damping ratios
PI - controller [7]	-0.2746 ± *j* 2.0389, ζ= 0.133
C-PI controller	-0.4350 ± *j* 1.3604, ζ = 0.305
Proposed PI Controller	-0.4755 ± *j* 1.2929, ζ = 0.345

Table 5.1 shows the eigenvalues and damping ratios of dominant mode for nominal operating condition. Clearly, the desired damping ratio of dominant mode is achieved by the proposed PI controller and C-PI controller. Moreover, the damping ratio of both C-PI controller and proposed PI controllers are improved as designed in comparison with PI controller [7].

Next, to investigate the robustness and performance of the controllers, the locus of eigenvalue corresponding to dominant mode is shown in Fig. 5.8 when K_{IG} (fluid coupling) is varied from -90% to 90% of the nominal values. When fluid coupling increases, the dominant mode tends to move to the lack of the system damping. In the case of PI-controller [7], the dominant mode tends to move in the right direction or to the unstable region. The dominant mode of C-PI controller also moves to outside of the D-shape region in the s-plane. On the other hand, proposed PI controller is more robust against fluid coupling variation. Dominant mode of the proposed PI controller is still in the D-shape region for all K_{IG} variations. The result confirms that the proposed PI controller designed with considering system uncertainties is much superior to both PI-controller [7] and C-PI controller in terms of robustness.

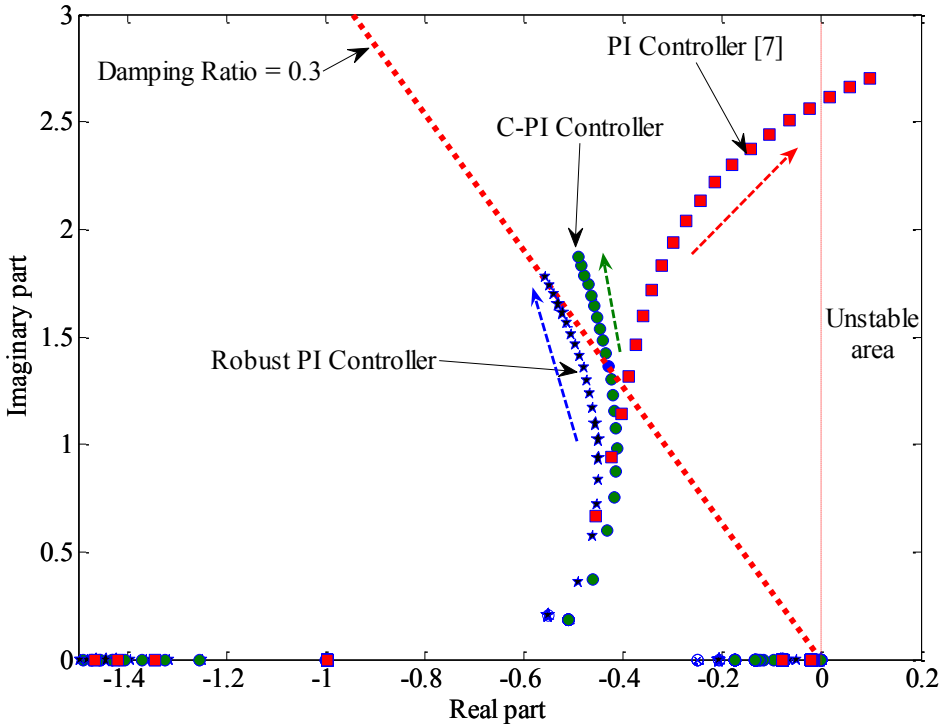

Figure 5.8 Root loci of dominant mode.

The eigenvalue analysis shows that the robust control design in this smart micro grid power system provides satisfactory performance for various operating conditions. As a result, adaptivity enhanced robust controller design is not necessary to be applied in this system.

5.7. Simulation Studies

The effectiveness, performance, and robustness of the proposed controllers are examined by simulation studies under three operating conditions as shown in Table 5.2.

Table 5.2 Operating conditions.

Cases	Disturbances
1	Step input of wind and load power
2	Random wind power input
3	Simultaneous random wind power and load change.

Case 1: Step input of wind and load power

In case 1, step increase of 0.01 pu on the system base of 300 kW in the wind power input and load change are applied to the system at $t = 5.0$ s. Fig. 5.9 and Fig. 5.10 show the system frequency deviation. In system with PI controller [7], the peak frequency deviation is very large and takes longer time to reach steady-state. This indicates that the pitch controller in the wind side and the governor in the diesel side do not work well. On the other hand, in case of the C-PI controller and the proposed PI controller are able to reduce frequency deviation significantly.

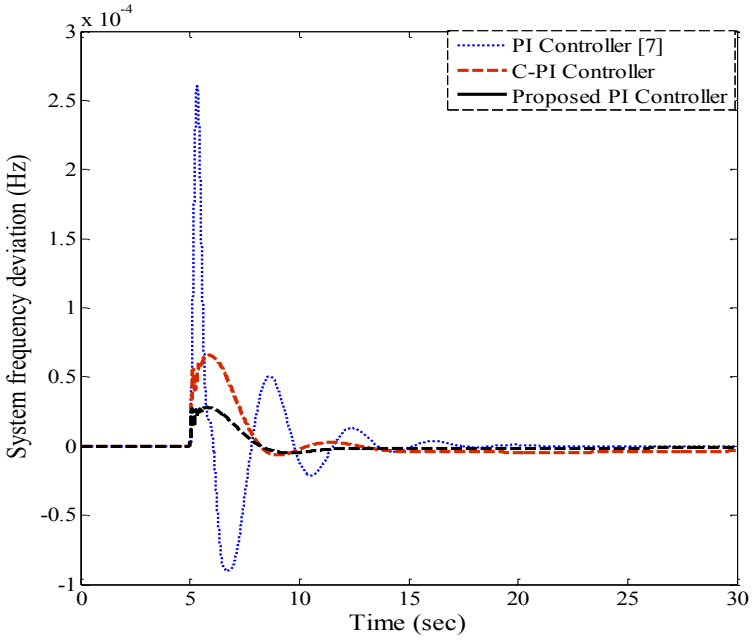

Figure 5.9 System frequency deviation against a step change of wind power.

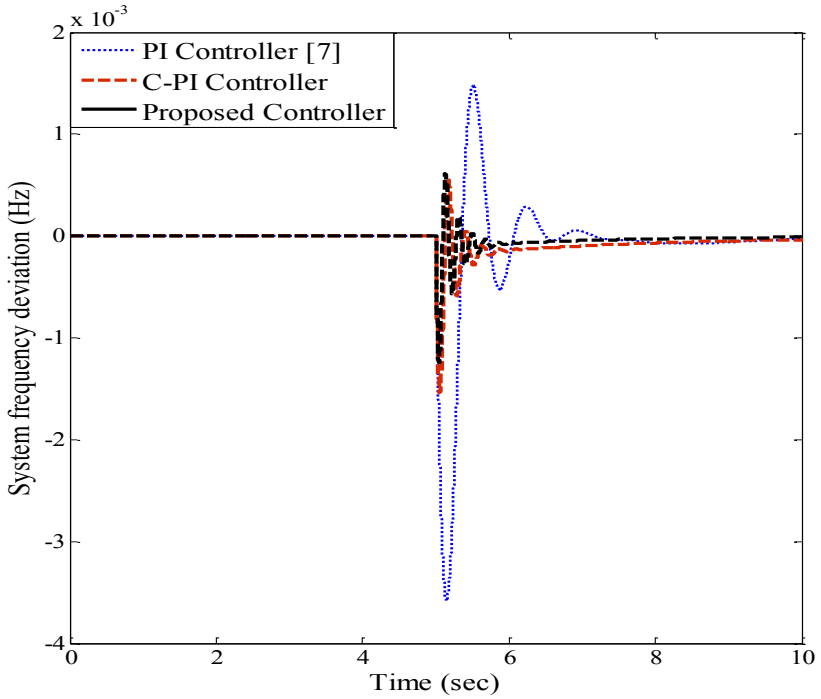

Figure 5.10 System frequency deviation against a step change of load power.

Case 2: Random wind power input.

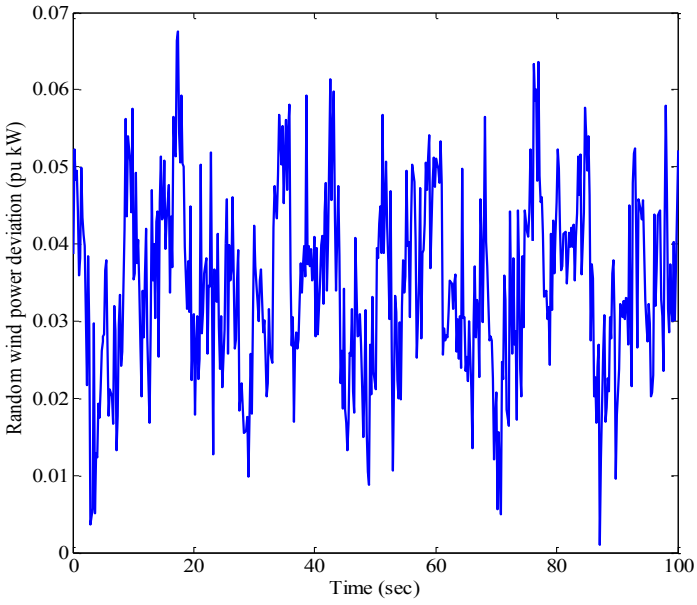

Figure 5.11 Random wind power input.

In this case, the system is subjected to the random wind power input as shown in Fig. 5.11. Under nominal operating condition, the system frequency deviation in this case is depicted in Fig. 5.12. The simulation result shows that the control effect of the proposed PI controller is better than the PI controller [7] and the C-PI controller. The frequency oscillation in the case of the proposed controller is damped very well.

When the fluid coupling (K_{IG}) is increased by 30 % from the nominal values, the C-PI controller is sensitive to this parameter change. It is still not able to work well as depicted in Fig. 5.13. In contrast, the proposed PI controller is able tolerate this condition.

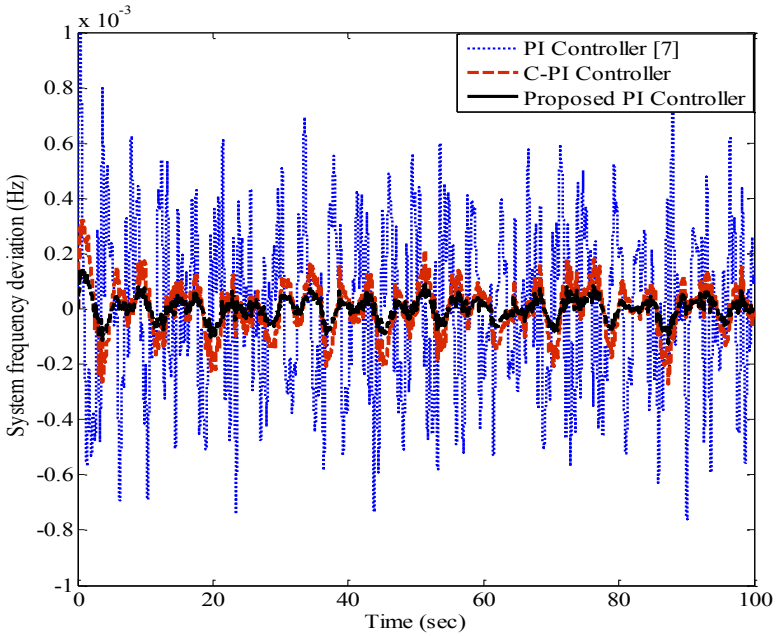

Figure 5.12 System frequency deviations under nominal system parameters.

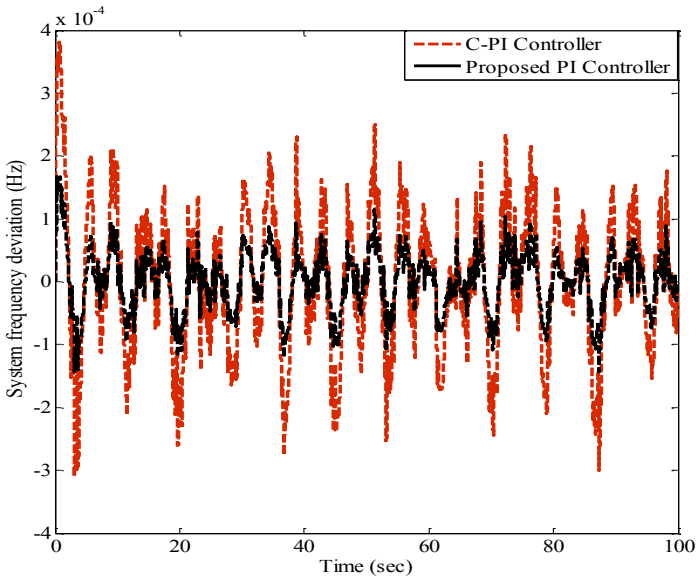

Figure 5.13 System frequency deviations under a 30 % increase in K_{IG}.

Next, the robustness of frequency controller is evaluated by an integral square error (ISE) under variations of system parameters. For 100 seconds of simulation study under the same random wind power in Fig. 5.11, the ISE of the system frequency deviation is defined as

$$ISE = \int_0^{100} |\Delta f_S|^2 \, dt \ . \qquad (12)$$

Figure 5.14 shows the values of ISE of system frequency under the variation of K_{IG} from -30 % to +30 % of the nominal values. As K_{IG} increases, the values of ISE in the case of the C-PI controller highly increase. On the other hand, the values of ISE in case of the proposed PI controller are much lower and almost constant.

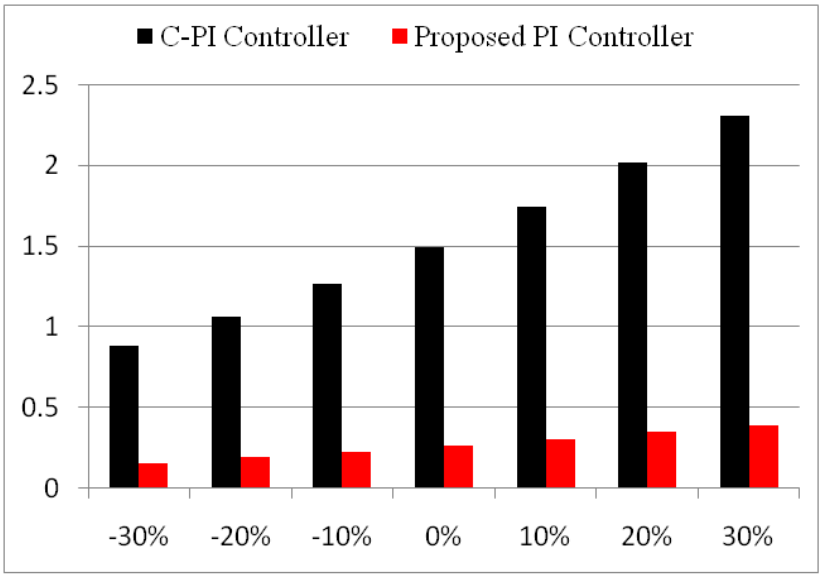

Figure 5.14 Variation of ISE under a change in K_{IG}.

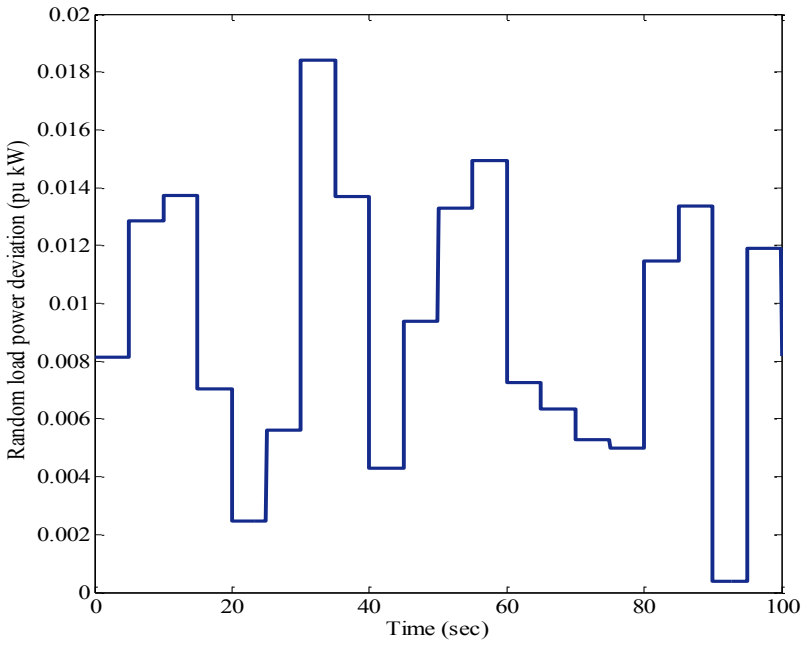

Figure 5.15 Random load change.

Case 3: Simultaneous random wind power and load change.

In case 3, the random wind power input in Fig. 5.11 and the load change in Fig. 5.15 are applied to the system simultaneously. Figure 5.16 shows the system frequency deviation under nominal system parameters. By the proposed PI controller, the frequency deviation is significantly reduced in comparison to that of the C-PI controller.

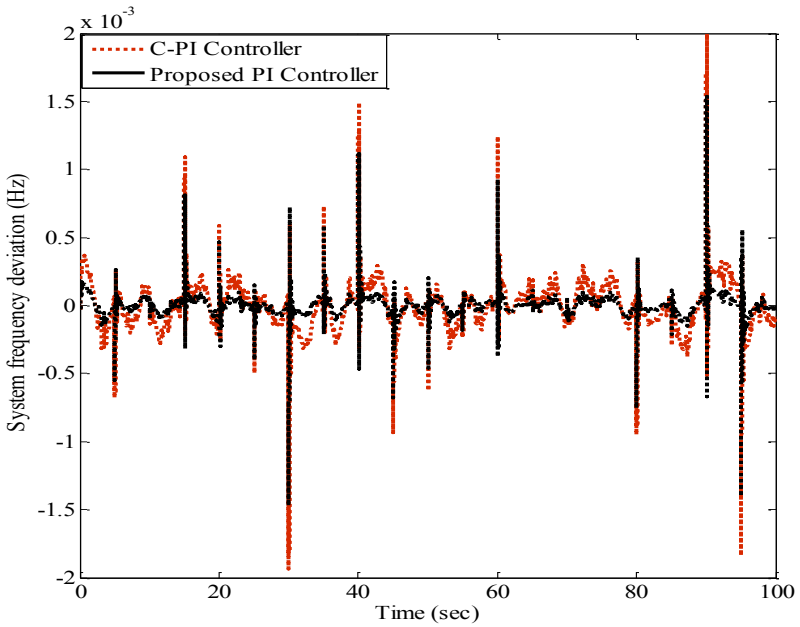

Figure 5.16 System frequency deviations under nominal system parameters.

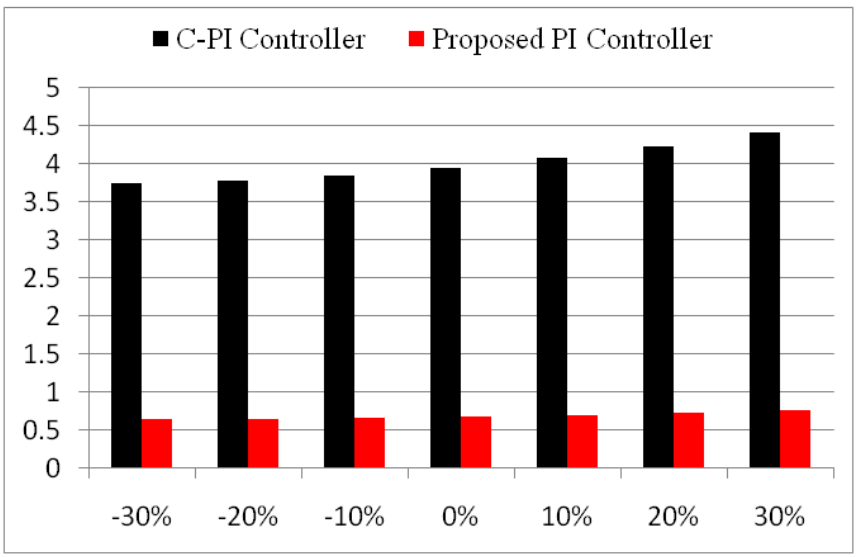

Figure 5.17 Variation of ISE under a change in K_{IG}.

Next, the values of ISE of system frequency are shown in Fig 5.17, under the variation of K_{IG} from -30 % to +30 % of the nominal values when the system is

subjected to the random wind power input in Fig. 5.11 and the load change in Fig. 5.15. Clearly, the ISE in case of the C-PI controller increases while K_{IG} is increased. This implies that the stabilizing effect of the C-PI controller is deteriorated at high fluid coupling of the system. On the other hand, the values of ISE in the case of the proposed PI controller are almost constant. These simulation results confirm the high robustness of proposed controller against the random wind power, load change, and system parameter variations.

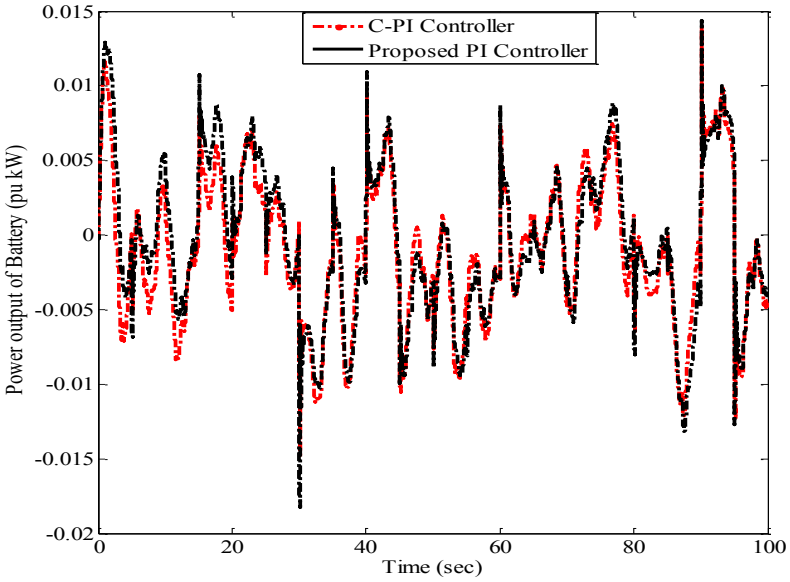

Figure 5.18 Power output of battery in case 3.

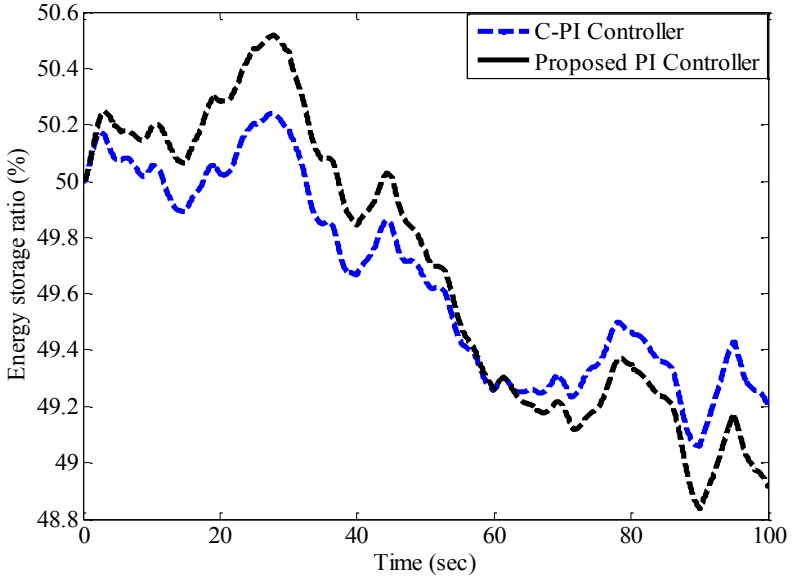

Figure 5.19 Energy storage ratio of battery in case 3.

Finally, the power output and energy storage ratio of battery for frequency stabilization are shown in Fig. 5.18 and Fig. 5.19, respectively. In this study, we assume that the reference of energy storage ratio is 50%. The simulation results show that both power output of the C-PI controller and the proposed PI controller can properly remain within the allowable limit. In addition, the energy storage ratio deviation in the case of proposed PI controller is smaller than that of C-PI controller. This indicates that the proposed PI controller can appropriately charge/discharge electrical energy with the power system. Accordingly, the frequency fluctuation stabilizing effect by the proposed PI controller is superior to that of the C-PI controller.

5.8 Conclusion

The robust PI–based coordinated frequency control of governor, pitch and battery controllers in the isolated wind-diesel hybrid power system has been proposed in this work. The controller of governor, pitch and battery are optimized simultaneously based on the proposed method. The inverse additive perturbation has been applied to model the power system with unstructured uncertainties. Moreover, the performance condition in the damping ratio of the dominant mode is applied to formulate the optimization problem. In this work, the structure of the proposed controllers of governor, pitch and battery is the first-order PI- controller. To get the proposed PI controller parameters, the genetic algorithm (GA) is employed to solve the optimization problem. Moreover, based on the eigenvalue analysis, the adaptivity enhanced control design is not necessary to be applied. Simulation studies have been done to confirm that the performance and robustness of the proposed robust PI- based controller of governor, pitch and battery is much superior to that of the conventional controller under random wind power input, load change and variations of system parameters.

REFERENCES

[1] T. Ackermann, "Wind power in power systems" , John Wiley & Sons Ltd (2005).

[2] M. Eduardo, A. Gouveia, A. Manuel and Matosb : " Evaluating operational risk in a power system with a large amount of wind power", Journal of Electric Power Systems Research , 79, pp. 734–739 (2009).

[3] A. Arulampalam, M. Barnes, Jenkins N and Ekanayake J.B : "Power quality and stability improvement of a wind farm using STATCOM supported with hybrid battery energy storage ", IEE Proceedings-Generation Transmission and Distribution,153, pp. 701–710 (2006).

[4] T. Senjyu, Sakamoto R., Urasaki N., Funabashi T., Fujita H. and Sakine H : Output power leveling of wind turbine generator for all operating regions by pitch angle control", IEEE Trans. on energy conversion, 21, pp. 467-475 (2006).

[5] T.S. Bhatti, Al-Ademi, A.A.F. and Bansal, N.K : " Dynamics and control of isolated wind-diesel power systems", Int J Energy Research, 19, pp. 729-740 (1995).

[6] E. Muljadi, and Butterfield, C.P : " Pitch-controlled variable speed wind turbine generation", IEEE Trans. ind appl, 37, pp. 240-246 (2001).

[7] T.S. Bhatti, Al-Ademi. A.A.F. and Bansal, N.K : " Load frequency control of isolated wind diesel hybrid power systems ", Energy Conversion and Managemen, 38, pp. 829-837 (1997).

[8] S. So, Haruka O and Shinichi I. : " A study of Load Frequency Control Combining a PID controller and a Disturbance Observer", Conference on IEEE T&D Asia 2009, (2009).

[9] A. Koji, Satoshi O and Shinichi I. : " New load frequency control method suitable for large penetration of wind power generations" Power Engineering society general meeting, pp.1-6 (2006).

[10] C. Chokpanyasuwan, Pothiya, S., Anantasate, S., Pattaraprakorn, W and Bhasaputra, P : "Robust Fuzzy logic-PID Controller for Wind-Diesel Power System using Particle Swarm Optimization", GMSARN International Conference on Sustainable Development: Issues and Prospects for the GMS (2008).

[11] R.W. Boom and Perterson H.A : " Superconducting energy storage for power systems", IEEE Trans Mag., 8, pp. 701-703 (1972).

[12] H.J. Boenig and Hauer J.F : " Commissioning tests of the Bonneville Power Administration 30 MJ superconducting magnetic energy storage unit ", IEEE Trans Power Appl Syst., 10, pp. 302–309 (1985).

[13] Y. Mitani, Tsuji K and Murakami Y : " Application of superconducting magnetic energy storage to improve power system dynamic performance ", IEEE Trans. Power Syst., 3, pp. 1418-25 (1988).

[14] J.B.X. Devotta and Rabbani M.G : " Application of superconducting magnetic energy storage unit in multi-machine power systems ", Energy Conv and Manag., 41, pp. 493-504 (2000).

[15] M.K. Abdelsalam, Boom R.W and Perterson H.A : "Operation aspects of superconducting magnetic energy storage (SMES)", IEEE Trans. Magnetics., 23, pp. 3275-3277 (1987).

[16] S.C. Tripathy, " Dynamic simulation of hybrid wind-diesel power generation system with superconducting magnetic energy storage", Energy Conv and Manag., 38, pp. 919-930 (1997).

[17] L. Xiangjun, Yu-Jin S and Soo-Bin H. :" Frequency control in micro-grid power system combined with electrolyzer system and fuzzy PI Controller", Journal of Power Sources, 180, pp. 468-475 (2008).

[18] T. Senjyu, Uehara, A., Yona, A., Funabashi, T : "Frequency control by coordination control of wind turbine generator and battery using $H\infty$ control ", IEEE T&D Asia (2009).

[19] P. Gu, Hr. Petkov and M.M. Konstantinov : Robust control design with MATLAB, Springer, London (2005).

[20] Y.L. Abdel-Magid, Abido M.A, AI-Baiyat S. and Mantawy A.H : "Simultaneous Stabilization of Multimachine Power Systems via Genetic Algorithm", IEEE Transactions on Power Systems, 14, pp. 1428-1439 (1999).

[21] GAOT , " A Genetic Algorithm for Function Optimization: A Matlab Implementation",
[Online] Available: http://www.ie.ncsu.edu/mirage/GAToolBox/gaot/ (1995).

CHAPTER 6

ROBUSTNESS AND ADAPTIVITY ENHANCED PSS DESIGN FOR STABILIZATION OF INTERCONNECTED SMART POWER SYSTEM WITH HIGH RENEWABLE ENERGY PENETRATION

This chapter applies the proposed control method to design of power system stabilizer (PSS) in a two-area four-machine power system by considering robustness and adaptivity. First, generator and exciter models, power system equipped with PSS are explained. To take system uncertainties such as various generating and loading conditions, system nonlinearities etc., into consideration, the concept of enhancement of inverse additive perturbation is formulated as the optimization problem of PSS parameters. The GA is applied to solve for PSS parameters. Eigenvalue analysis against variation of inertia constant and tie line power flow are used to evaluate whether an adaptive robust control design is necessary or not. An adaptive robust PSS design will be applied to improve performance of PSS whenever robust controller doesn't able to provide satisfactory performance. The performance and effectiveness of the proposed method have been investigated in an interconnected power system in comparison with a conventional PSS (CPSS). Nonlinear simulation studies are carried out to evaluate performance and robustness of the proposed PSS in comparison with that of PSS designed without considering robustness against several system uncertainties.

6. 1. Introduction

When large power output RE connected to grid, the number of conventional rotating type of generators in operation decreases, which results in the reduction of total inertia constant. This makes the power system stability weak [1, 2].

To handle the synchronous stability, power system stabilizer (PSS) has been selected as a cost effective device to provide the additional damping via the excitation system [3, 4]. However, the performance of PSS depends on the dynamic characteristic of the power system. When DREGs are connected to the grid, the uncertainty of RE generations may cause the dynamic characteristic of the power system changeable. Therefore, we need to re-estimate the system to adjust PSS parameters to enhance the stability of the power system.

Several approaches based on modern and robust control theories have been successfully applied to design PSS such as eigenvalue assignment [5], linear quadratic regulator [6], H_∞ control [7, 8], fixed structured robust control [9] etc., However, PSS was designed for normal operating condition and could not adapt to extreme power system conditions due to the high penetration of renewable energies. Moreover, all system parameters and exact mathematical models are needed in the design. It is difficult to be applied to the system which has no system parameters and exact mathematical model.

To overcome the problem, this chapter presents proposed technique that gives adaptivity as well as robustness to the conventional type of controllers. In adaptive control, the controller parameters are changed depending on the situations. However, it is not desirable that the parameters are changed too frequently. It is preferable that the parameter alteration is done at the right moment. Here a system identification technique and the robust controller design method described in chapter 4 are combined into an indirect adaptive controller design. The identified model is used to monitor discrepancy between the actual power system output and the expected output (model output). When a large discrepancy is detected, a new set of controller parameters is determined to adapt to the new situation. The effectiveness of proposed method is evaluated in interconnected power system with high renewable energy penetration against various line flow conditions and inertia constant in comparison with the conventional PSS and robust PSS (RPSS) without considering adaptivity.

6.2. Power System Modeling

6.2.1 Two-area four-machine interconnected power system

The configuration of a two-area four-machine interconnected power system [10] in Fig. 6.1 is used as the studied system. Each generator is equipped with a simplified exciter. The wind farms are located on buses 4 and 14, and PV generations are installed on buses 2 and 15 with maximum generating capacities 2,500 MW. In this study, the RE generations are modeled by the random active power source. Therefore, the changing of a dynamic characteristic of power systems may occur because of large amounts of power input from RE power generation or other extreme conditions such as some conventional generators being stopped when output power of RE generation significantly increases. To overcome this problem, readjustment of PSS parameters is highly needed.

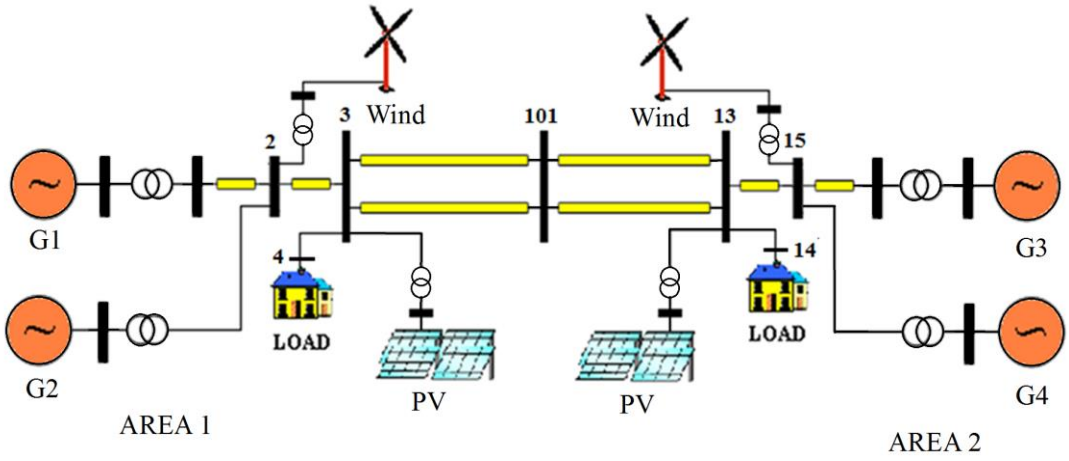

Figure 6.1 The configuration of a two areas four machines interconnected power system.

The generator in the systems is represented by the 5th -order model consisting of the swing equation, the generator internal voltage, and sub transient electro-magnetic fields (emfs) equation [11]. The swing equations can be written as

$$\dot{\delta} = \omega_r(\omega - 1), \tag{6.1}$$

$$\dot{\omega} = (P_m - P_e - D(\omega - 1))/M. \tag{6.2}$$

The internal voltage, $\dot{E}_q^{'}$ is given by

$$\dot{E}_q^{'} = (E_{fd} - (x_d - x_d^{'})i_d - E_q^{'})/T_{do}^{'}. \tag{6.3}$$

The sub transient emfs equations can be written as

$$\dot{E}_q'' = \left(E_q' - E_q'' + (x_d' - x_d'')i_d\right)/T_{d0}'', \tag{6.4}$$

$$\dot{E}_d'' = \left(-E_d'' + (x_q' - x_q'')i_q\right)/T_{q0}''. \tag{6.5}$$

where ω is the angular velocity, $\dot{\omega}$ is derivation of the angular velocity, δ is the rotor angle, $\dot{\delta}$ is derivation of the rotor angle, M is the inertia constant, D is the damping coefficient, P_m is the mechanical input to the generator, P_e is the electrical output, $\omega_r = 2\pi f$ is the rated angular velocity , f is the system frequency, E_d', E_d'' are direct axis transient and sub transient voltage, E_q', E_q'' are quadrature axis transient and sub transient voltage, E_{fd} is field voltage, x_d, x_d', x_d'' are synchronous, transient and sub transient direct axis reactances, x_q, x_q', x_q'' are synchronous, transient and sub transient quadrature axis reactances, T_{d0}', T_{d0}'' are transient and sub transient direct axis time constants, T_{q0}'' is sub transient quadrature axis time constants, i_d is direct axis component of stator current, and i_q is quadrature axis component of stator current. And the real power output of the generator is described as

$$P_e = (E_d'' i_d + E_q'' i_q) + (X_d'' - X_q'')i_d i_q \tag{6.6}$$

6.2.2 Excitation System

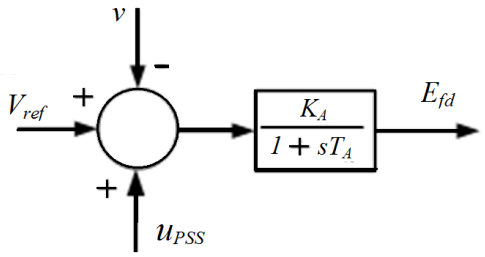

Figure 6.2 IEEE type-ST1 excitation systems.

The excitation system can be represented by the IEEE type-ST1 system as shown in Fig. 6.2, and is described by

$$\dot{E}_{fd} = \left(K_A(V_{ref} - v + u_{PSS}) - E_{fd}\right)/T_A, \tag{6.7}$$

$$v = \left(v_d^2 + v_q^2\right)^{1/2}, \tag{6.8}$$

$$v_d = x_q i_q, \tag{6.9}$$

$$v_q = E_q' - x_d' i_d, \tag{6.10}$$

where K_A is gain of the excitation system, T_A is time constant of the excitation system, E_{fd} is field voltage , v_d is direct axis component of terminal voltage, and v_q is quadrature axis component of terminal voltage, u_{PSS} is output signal of PSS and V_{ref} is reference voltage, respectively.

6.2.3 Power System Stabilizer Model

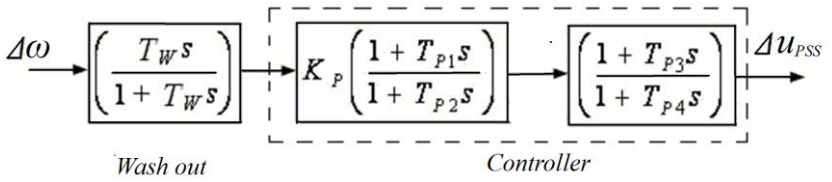

Figure 6.3 Block diagram of power system stabilizer (PSS).

As shown in Fig. 6.3, the PSS is modeled by two blocks diagram. The first block is wash out with time constant T_W=10s, the second block is a controller which represented by the 2nd order lead/lag controller [12], where $\Delta\omega$ is an angular velocity deviation as input signal of PSS, Δu_{PSS} is the control output signals of the PSS controller. K_P , T_{P1}, T_{P2}, T_{P3} and T_{P4} are gain and time constants of PSS.

6.3 Optimization Problem Formulation

6.3.1 Robust PSS Design

The objective function to improve the robustness of controller and to enhance the damping of dominant modes is formulated as follows,

$$\text{Minimize} \quad \|G/(1+GK)\|_\infty \tag{6.11}$$

$$\text{Subject to} \quad \zeta \geq \zeta_{spec}, \sigma \leq \sigma_{spec}, \tag{6.12}$$

$$K_{i,\min} \leq K_i \leq K_{i,\max},$$

$$T_{ij,\min} \leq T_{ij} \leq T_{ij,\max},$$

$$i = 1,2, \quad j = 1,2,$$

where ζ and ζ_{spec} are the actual and desired damping ratio of the dominant inter-area oscillation mode, respectively; σ and σ_{spec} are the actual and desired real part, respectively; $K_{i,\max}$ and $K_{i,\min}$ are the maximum and minimum controller gains, respectively; $T_{ij,\max}$ and $T_{ij,\min}$ are the maximum and minimum time constants, respectively. This optimization problem is solved by GA.

6.3.2 Adaptive Robust PSS.

The flow chart of the proposed adaptive robust PSS design is shown in Fig. 6.4. Each step of the proposed adaptive robust PSS design is explained as follows,

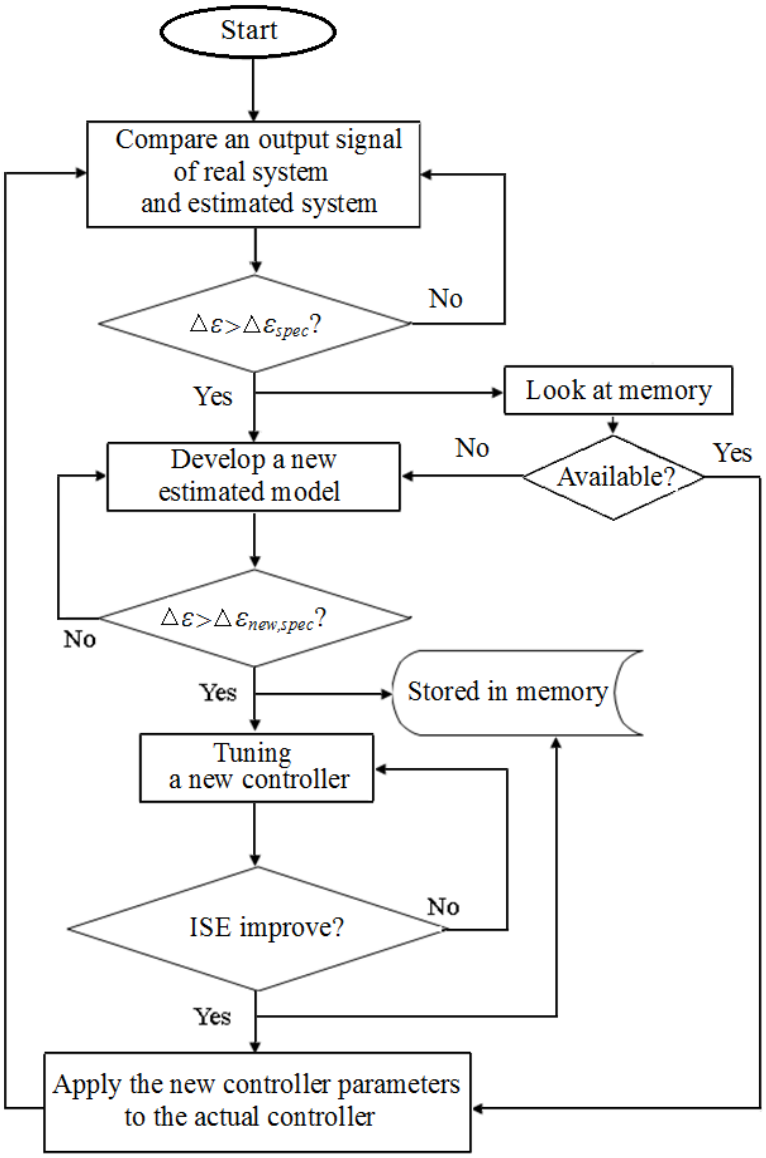

Figure 6.4 Flow chart of the proposed adaptive control design method.

Step 1. Comparison of the real system and the estimated model

In this step, we compare the output signal of both the real and the estimated system. The result of the comparison between the real and estimated model is called 'mismatch error'. The estimated model will be updated whenever the mismatch ($\Delta\varepsilon$), exceeds predetermined bound ($\Delta\varepsilon_{spec}$). $\Delta\varepsilon_{spec}$ is predetermined by the power control

designer according to the error tolerance required. A memory is used as "model and controller bank" to store a new estimated model and controller parameters. The system will look at memory to check the availability of the matching estimated when mismatch error exceeds $\Delta\varepsilon_{spec}$, re-uses the suitable model & controller parameters directly without model identification and controller parameters tuning. Otherwise, the system will develop a new estimated model and tune PSS parameter.

The mismatch ($\Delta\varepsilon$) is calculated by the following equation:

$$\Delta\varepsilon = y - \hat{y} \tag{6.13}$$

where y is the measured output of the real system (angular velocity deviation) and $\hat{y}$ is the output of the estimated model.

Step 2. Develop a new estimated model

Develop a new estimated model using output error (OE) system identification so that the mismatch error becomes less than or same as specification. If the mismatch error is greater than specification $\Delta\varepsilon_{New,spec}$, the engineer need to develop a new estimated model again using set of data. In this study, the estimated model is represented by a transfer function of 5th order identical to the order of the real synchronous generator modeled by Modelica/Dymola which uses the 5th order nonlinear model.

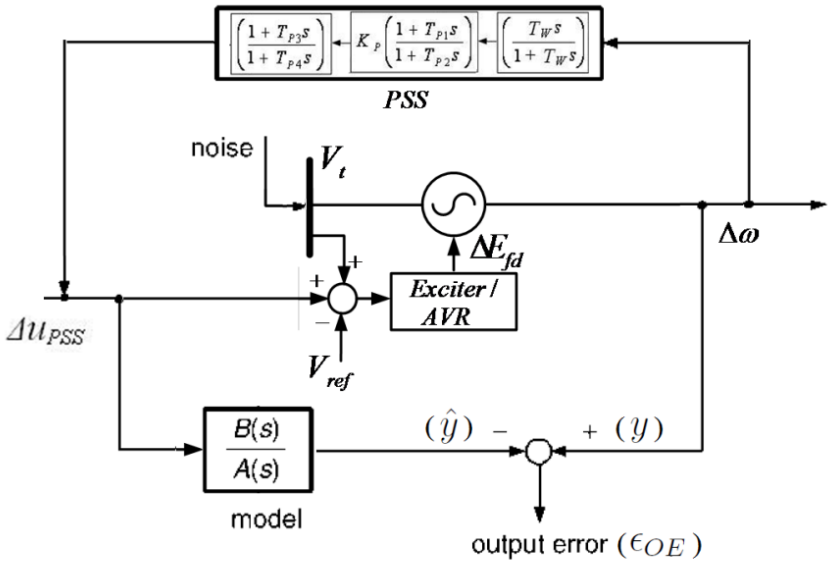

Figure 6.5. Structure of Output Error (OE) for single generator

Figure 6.5 depicts the structure of the OE model for each single generator model in the studied power system. The generator is fitted with the automatic voltage regulator (AVR), an excitation system, and the PSS. To construct estimated model, the input signal of OE model is the PSS's output signal, and the measured output of real system is the angular velocity deviation of the generator. Then OE identification will search the estimated model by minimizing the output error between the estimated model and real generator model. There are two sets of data. The first set of data is used to model identification, and the second set of data is needed as model validation. The length of each data is 60 s or 1 minute. Note that, the estimated model is representation of generator with AVR and an excitation system.

Step 3. Controller parameters tuning

Based on the new estimated model, parameters of the 'virtual controller' will be tuned by considering system uncertainties and increasing the damping ratio of the dominant mode of the power system. Note that, the 'virtual controller' parameters are tuned and that therefore the actual system behavior is not affected by the tuning. To tune controller parameters, the optimization problem in (6.11) and (6.12) is solved.

Step 4. Store the new estimated model and the new controller parameters in the memory.

After the new controller parameters are successfully obtained to improve the robustness and performance of the system, the new estimated model and the new controller parameters will be stored in the memory to be used in the similar situations in the future without model identification and controller parameters tuning.

Step 5. Apply the new controller parameters to the actual controller, and return to step 1.

6.4 Designed Results

In optimization, the ranges of search parameters and GA parameters are set as follows: desired damping ratio (ζ_{spec}) is set as 0.1, desired real part of the inter-area

oscillation mode (σ_{spec}) is set as -0.1, minimum and maximum gains of PSS ($K_{i,\min}$ and $K_{i,\max}$) are set as 1 and 30, minimum and maximum time constants of PSS ($T_{ji,\min}$ and $T_{ji,\max}$) are set as 0.01 and 1. Consequently, the robust control parameters (RPSS) are obtained as follows.

$$K_{PSS1} = 25.05\left(\frac{0.8638s+1}{0.7425s+1}\right)\left(\frac{0.8538s+1}{0.7227s+1}\right), \tag{6.14}$$

$$K_{PSS2} = 25.58\left(\frac{0.5395s+1}{0.3324s+1}\right)\left(\frac{0.5124s+1}{0.3175s+1}\right), \tag{6.15}$$

$$K_{PSS3} = 12.79\left(\frac{0.4940s+1}{0.2545s+1}\right)\left(\frac{0.4748s+1}{0.2675s+1}\right), \tag{6.16}$$

$$K_{PSS4} = 12.5\left(\frac{0.6235s+1}{0.1806s+1}\right)\left(\frac{0.6133s+1}{0.1350s+1}\right). \tag{6.17}$$

In simulation studies, the performance and robustness of RPSS are compared with Conventional PSS (CPSS) [13]. Then eigenvalue analysis is carried out to evaluate the robustness of both CPSS and RPSS. The loci of eigenvalue when tie line power flow is varied from 2.5 to 4.5 pu are depicted in Fig. 6.5. At the very high power flow condition, CPSS is not able to stabilize the first mode, its eigenvalues move to unstable region. On the other hand, RPSS is robustly able to stabilize all dominant modes.

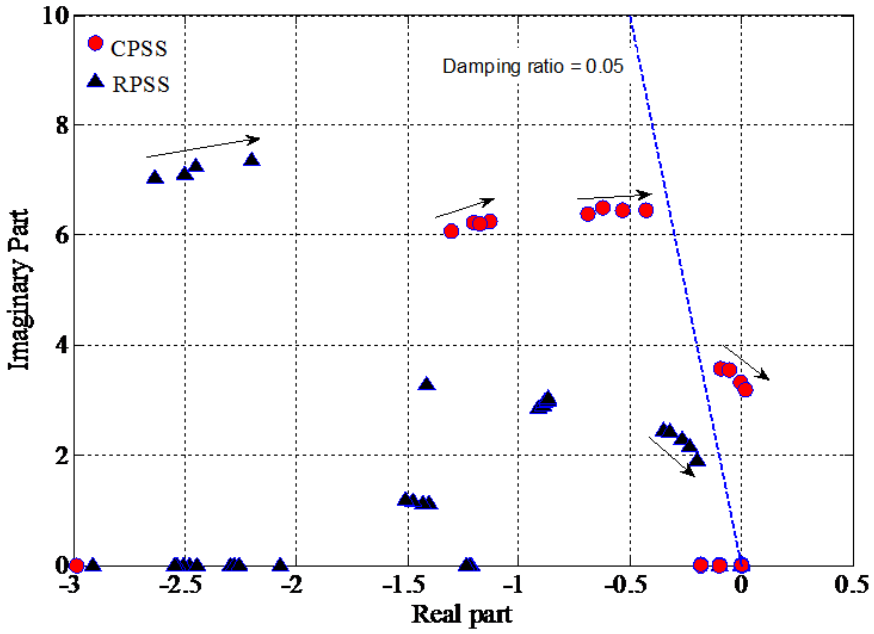

Figure 6.6 Root loci of dominant modes against P_{tie} variations.

Table 6.1 Operating Conditions.

Case	G1	G2	G3	G4	Load
Normal Condition (Case 1)	P_G =6.0	P_G =5.5	P_G =5.5	P_G =5.5	L_1=10, L_2 = 12
Heavy line load (Case 2)	P_G =7.5	P_G =6.0	P_G =4.5	P_G =4.0	L_1=10, L_2 = 12
Heavy line flow and weak line (Case 3)	P_G =9.0	P_G =4.5	P_G =5.0	P_G =4.0	L_1=12, L_2 = 13

Note: P_G = Generation power (pu), L=Load power (pu), Base = 900 MVA

Next the performance of PSSs is evaluated by simulation studies. Nonlinear simulations of three case studies in Table 6.1 are carried out under the penetration of wind power generations and PV generations penetrations.

In each case, the eigenvalue analysis against inertia constant variation is evaluated to check whether the adaptive robust PSS method is necessary or not. The inertia constant of all generators is varied from 4.0 p.u. to 6.5 p.u. Figure 6.7, Fig. 6.8 and Fig. 6.9 show the loci of eigenvalue in case 1, case 2 and case 3, respectively. These results show that the stability of the system becomes weak when the inertia constant decrease.

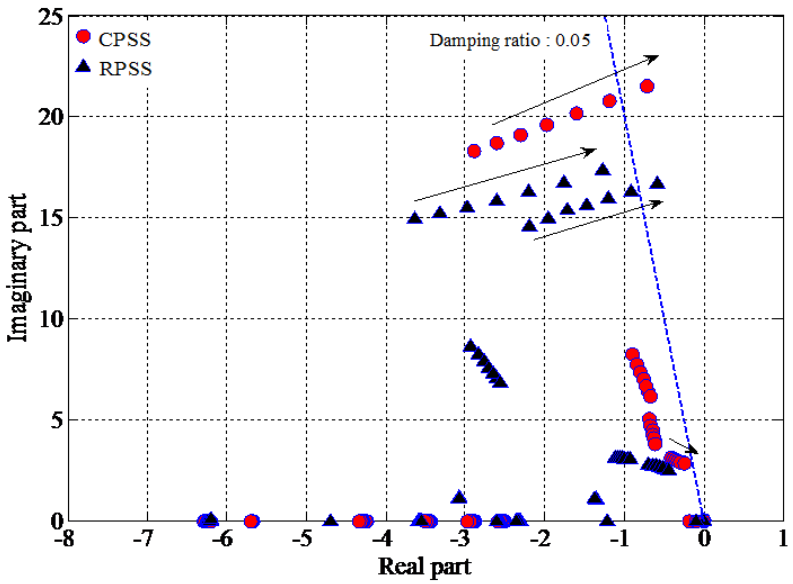

Figure 6.7 Root loci of dominant modes against inertia constant variations in case 1.

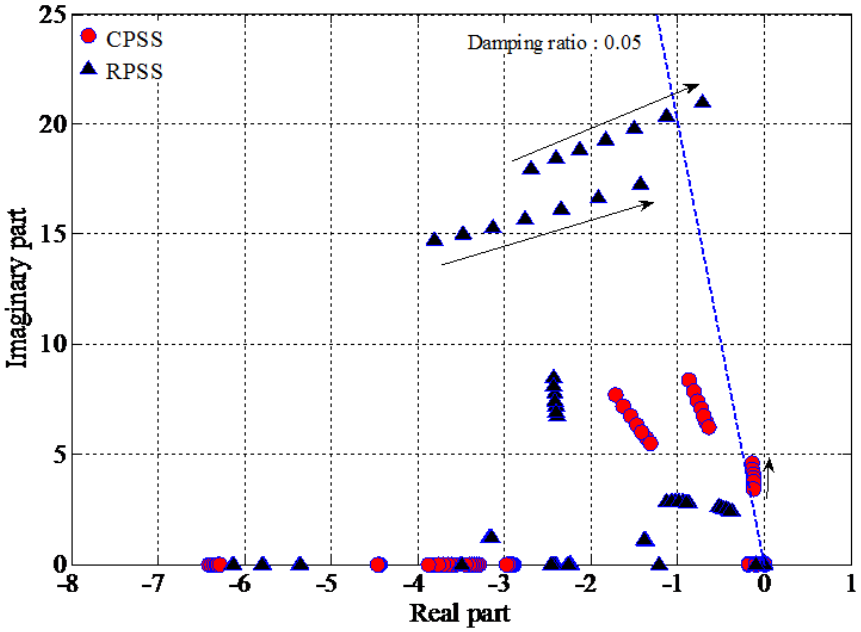

Figure 6.8 Root loci of dominant modes against inertia constant variations in case 2.

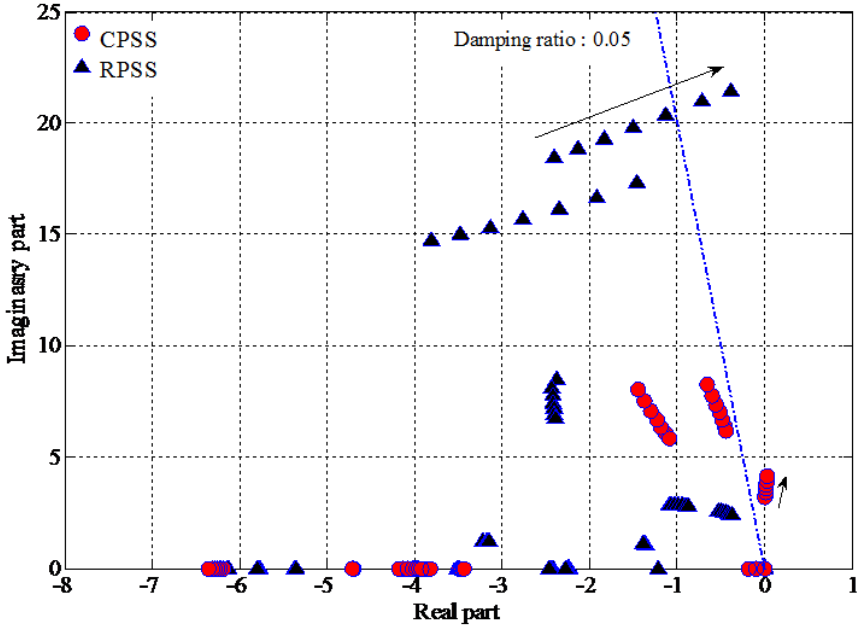

Figure 6.9 Root loci of dominant modes against inertia constant variations in case 3.

In practice, damping of rotor swings is considered to be satisfactory if the damping ratio $\zeta = 0.05$ [11]. Based on the eigenvalue analysis, the damping ratio of both RPSS and CPSS become less than 0.05 when the inertia constant go down till very low. Especially in case 3, the CPSS becomes unstable. On other hand, even though RPSS is able to keep all the dominant modes in stable area, the first dominant mode moves to outside of satisfactory damping ratio $\zeta = 0.05$. As a result, in the case that inertia

constant is very low due to high penetration of renewable energy, the performance of robustness is not enough; we need to combine the robustness with adaptivity to stabilize extreme conditions.

6.5 Simulation Results

Nonlinear simulation studies performed by Dymola with ObjectStab are carried out to evaluate the effectiveness and robustness of optimized RPSS when the system is subjected high RE penetrations and some faults are applied to the system. In the first part of this section, the author shows the simulation results with the robust and not adaptive controller. The simulation results are used to describe the difference between the robust control without adaptive and the adaptive robust control.

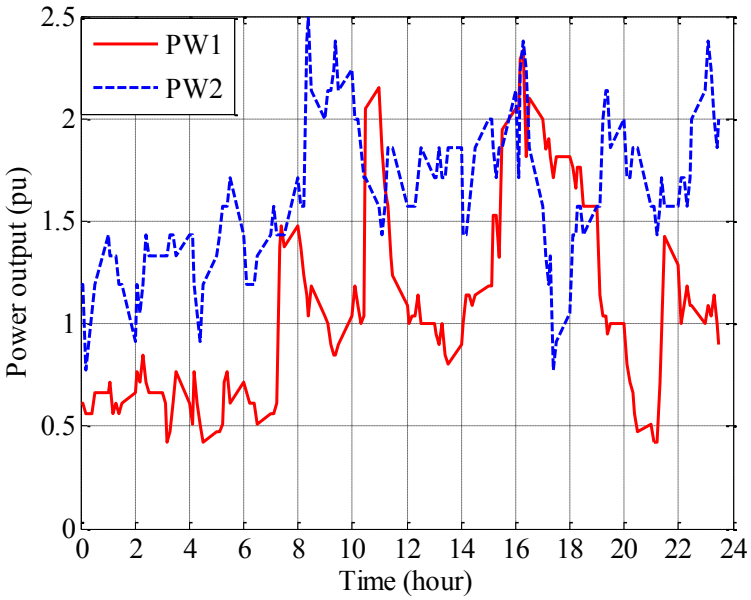

Figure 6.10 Wind power generation.

In simulation studies of all cases, wind power generations [PW1] and [PW2] as shown in Fig. 6.10, are injected to bus 4 and bus 14, respectively. And PV power generations [PV1] and [PV2] as shown in Fig. 6.11, are injected to bus 4 and bus 14, respectively. Simulation results under three case studies are carried out as follows:

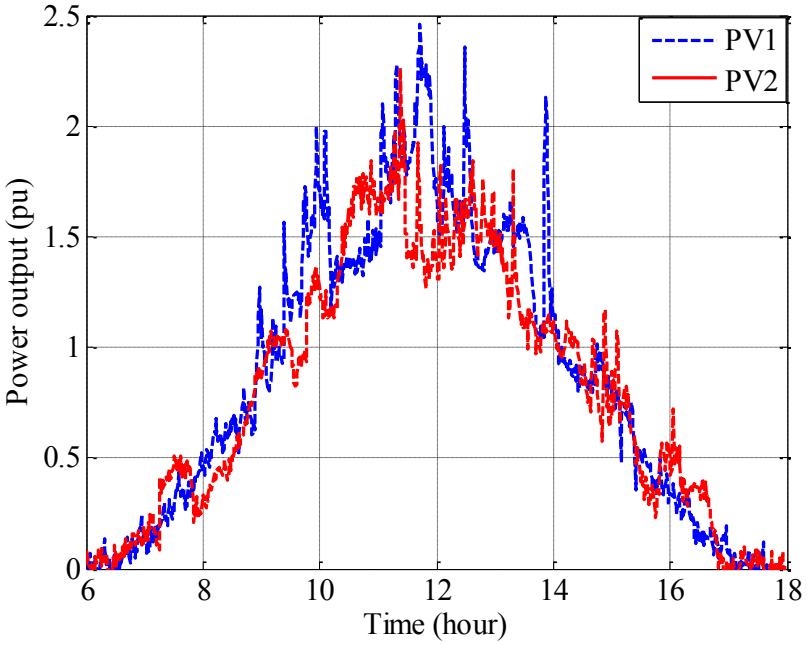

Figure 6.11 PV power generations.

Case 1: System with and without three phase faults on bus 101.

a) Without three phase faults

First, performance of controller at the system without three phase faults is evaluated. Fig. 6.12 and Fig. 6.13 show tie-line power deviation and angular velocity deviation in case 1, respectively. CPSS and RPSS are able to damp power oscillations due to RE power fluctuations.

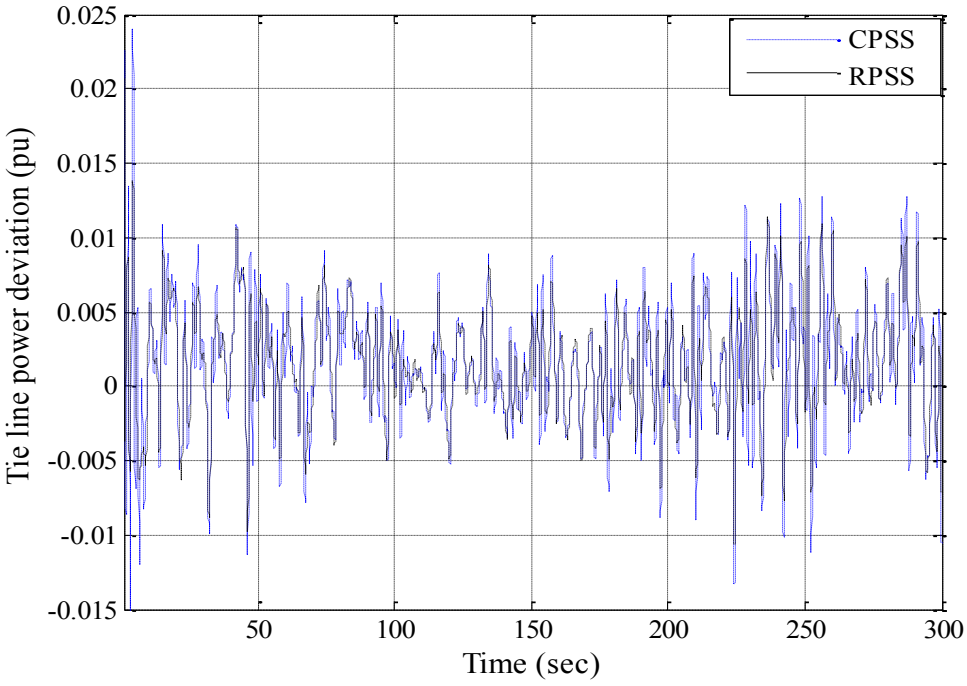

Figure 6.12 System responses of tie line power in case 1 without fault.

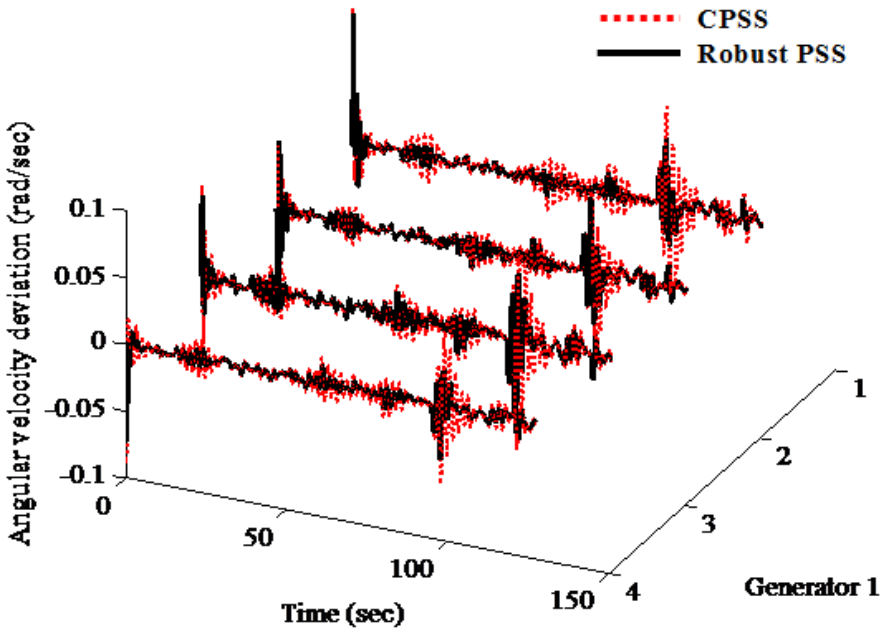

Figure 6.13 System responses of angular velocity deviation in case 1 without fault.

b) With three phase faults

Then a three phase fault is applied to the system on bus no. 101 at t = 5.0 s, Fig. 6.14 shows the responses of speed deviation of all generators. CPSS and RPSS are able to damp power oscillations. Nevertheless, the overshoot and setting time of power oscillations in the cases of RPSS are lower than those of CPSS. The angular velocity deviation oscillation reaches [illegible] the shortest period.

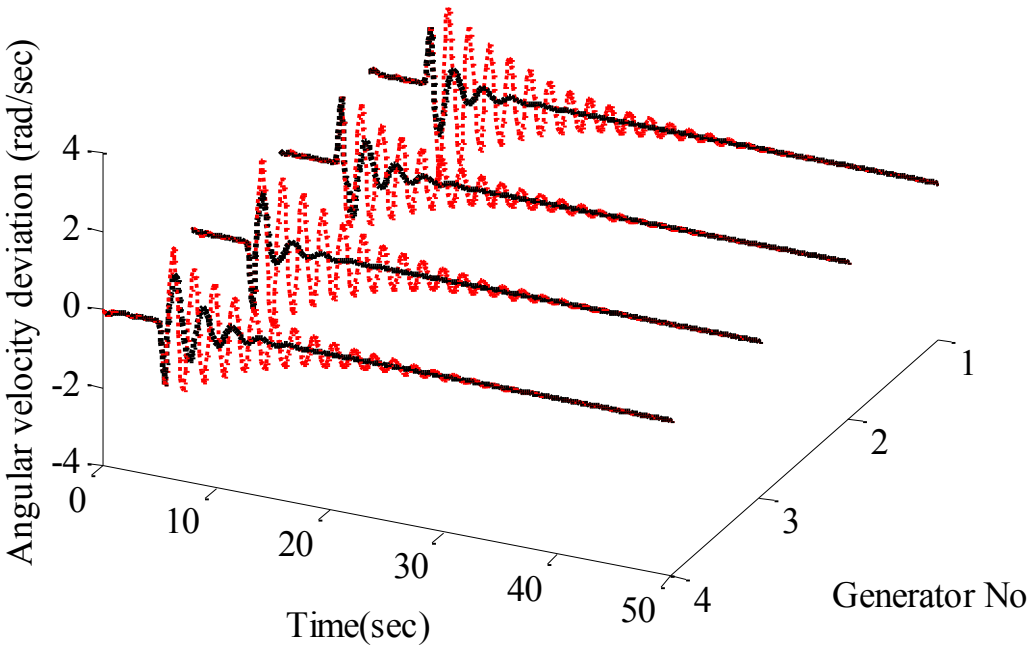

Figure 6.14 Simulation results of case 1 with 3 phase faults at Bus 101.

Case 2: The tie line power flow is increased from 2.5 pu to 4.5 pu.

a) Without fault.

The response of tie line power flow and angular velocity without fault are shown in Fig. 6.15 and Fig. 6.16, respectively. The figures depict that the RPSS provide more damping effects than CPSS [12]. The damping effect of CPSS is deteriorated. On the other hand, the power oscillations are effectively stabilized by RPSS. The RPSSs are rarely s

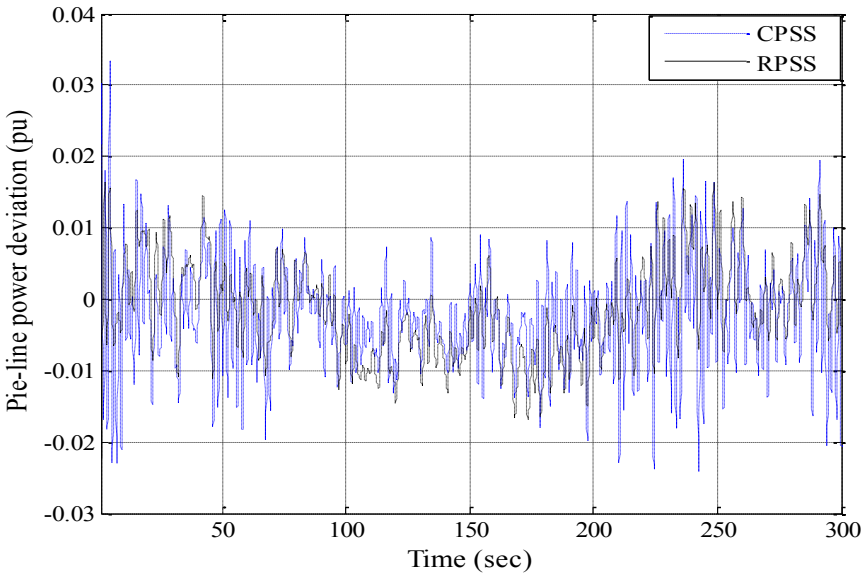

Figure 6.15 System responses of tie line power flow in case 2 without fault.

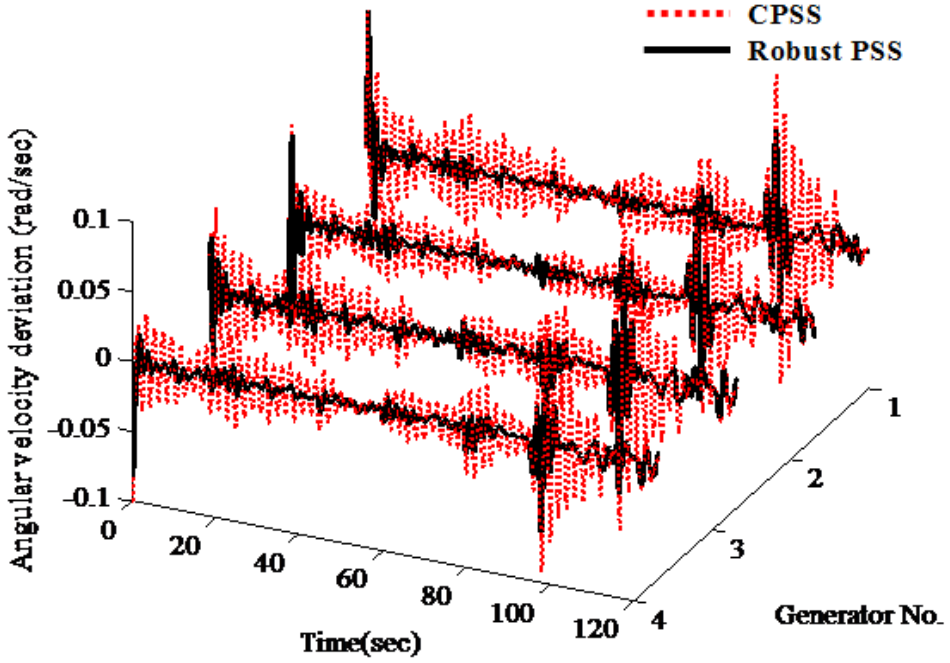

Figure 6.16 System responses of angular velocity in case 2 without fault.

b) With fault.

At first, the tie-line power transfers from areas 1 to 2 via two lines of tie-line 3-101, then one line is suddenly opened at 5 s and is cleared 70 ms later. Figure 6.17 shows the system response of angular velocity deviation in case 2 when the fault is applied. It can be seen that, when the tie-line flow is highly increased, the stabilizing effect of CPSS is significantly deteriorated. The power oscillation is very severe and takes long time to reach zero. In contrast, the RPSS is robustly able to damp the power oscillation.

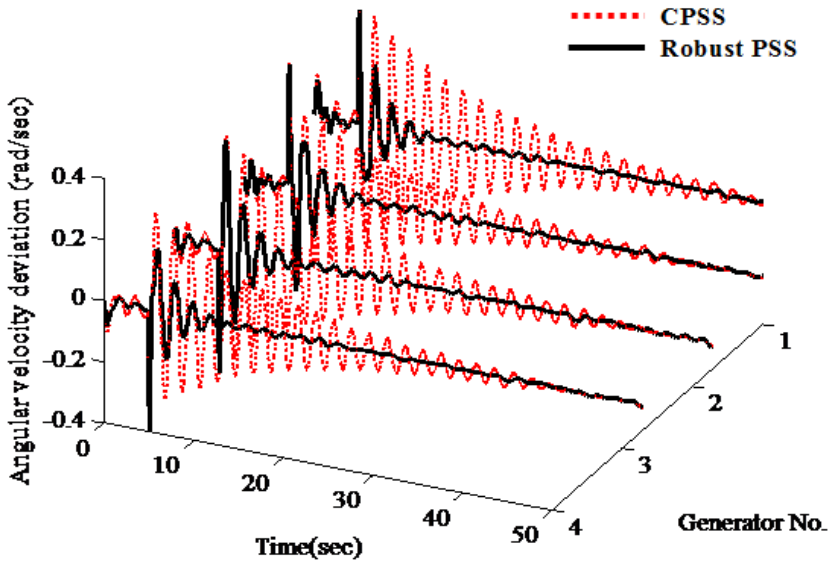

Figure 6.17 System responses in case 2 with fault in tie-line 3-101.

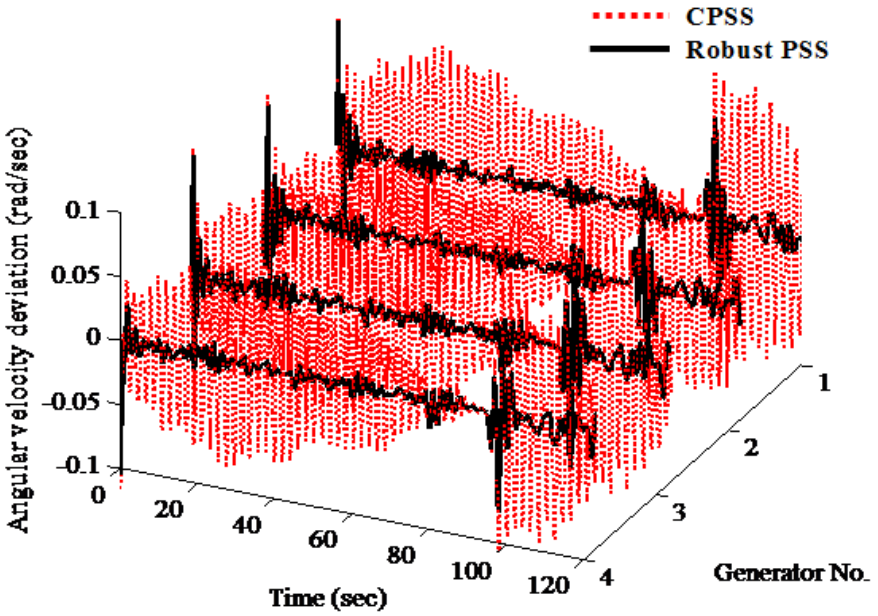

Figure 6.18 System responses of angular velocity in case 3 without fault.

Case 3: The system with and without fault on bus 101 with tie-line power 4.5 pu

a) Without Fault

The system response of angular velocity in case 3 without fault is shown in Fig. 6.18. CPSS fails to damp the angular velocity oscillation. On the other hand, the robust PSS can tolerate this situation.

b) With Fault

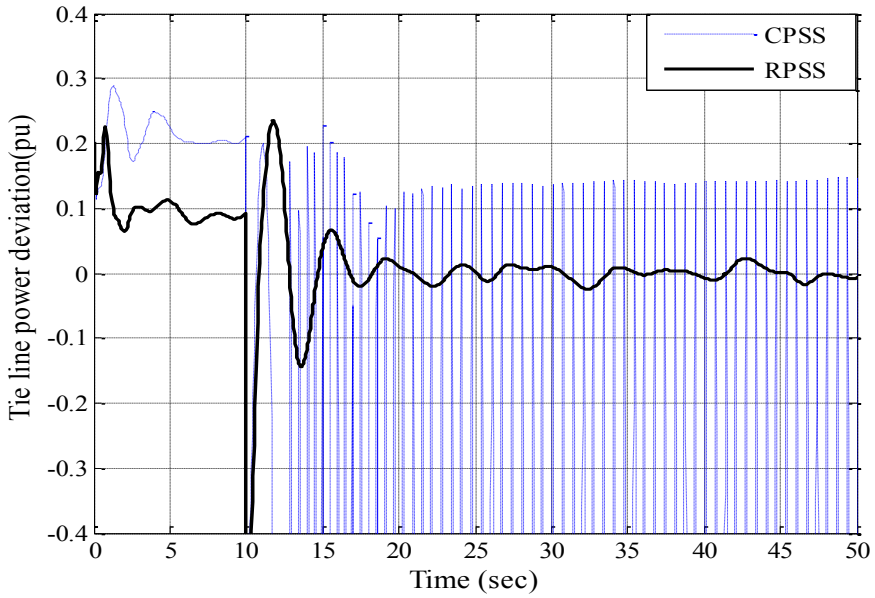

Figure 6.19 System responses of tie line power in case 3 with fault.

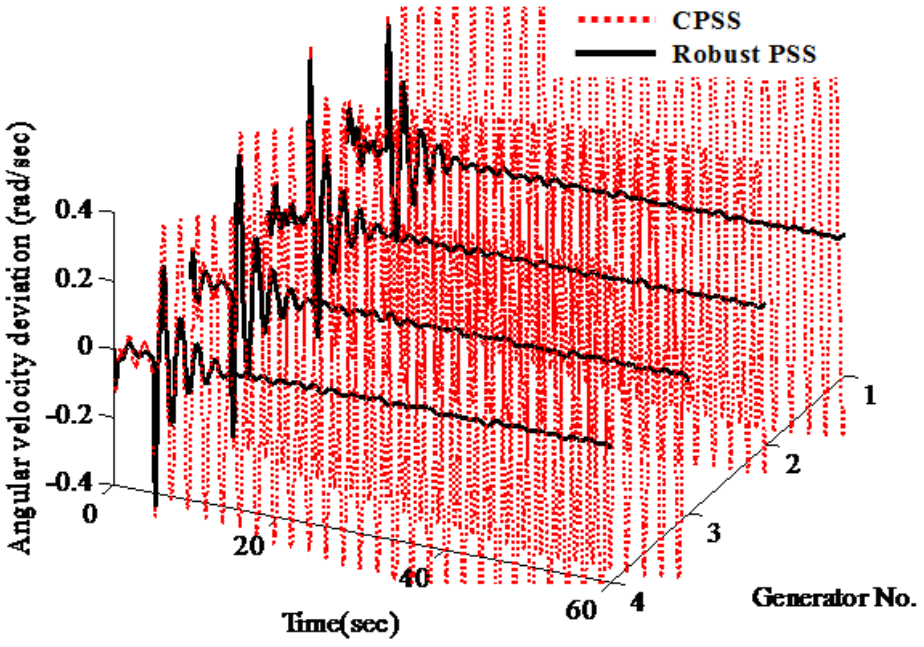

Figure 6.20 System response of angular velocity deviation in case 3 with fault.

In the heavy tie-line flow of case 3, the angular velocity deviation of all generator and tie-line power deviations are depicted in Figs. 6.19 and 6.20, respectively, when the temporary three phase fault occurs on bus 101 for 70 ms. The CPSS completely loses the stabilizing effect at both fault locations. The tie-line power flow severely oscillates and the system becomes unstable. On the contrary, the RPSS can robustly tolerate this situation. The power oscillations are absolutely damped. These results confirm that the robustness of RPSS is much superior to that of the CPSS under any line flow conditions and fault locations.

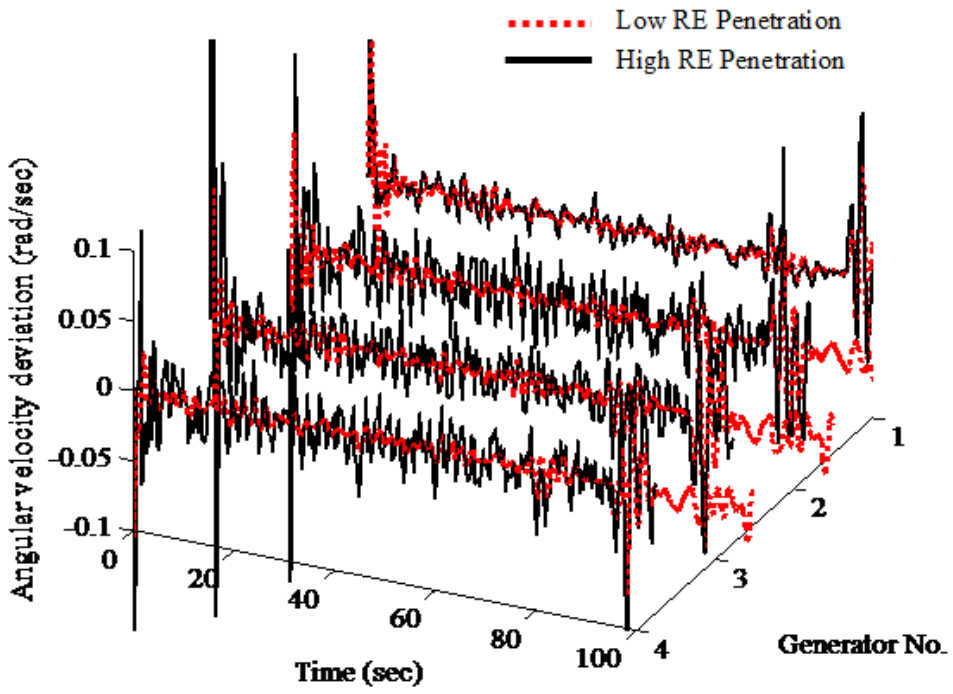

Figure 6.21 The system response of angular velocity in case 3 before and after high penetration of renewable energy.

Next, the high penetration of renewable energy to the system is used to evaluate the performance of RPSS. The response of angular velocity deviation in case 3 with low RE penetration and high RE penetration is shown in Fig. 6.21. The figure shows that the stability of power system becomes weak in the case of high RE penetration. The oscillation of angular velocity deviations of high RE penetration are significantly increase in comparison with that of low RE penetration. Therefore, the RPSS controller design by considering adaptivity is highly needed.

First, identification system should be applied to construct estimated model. In this study, the estimated model is represented by a transfer function of 5th order identical to the order of the real synchronous generator modeled by Modelica/Dymola which uses the 5th order nonlinear model. The period of data which be used in the identification is 60 s. After the OE model identification applied, the transfer function of the estimated model of each generator is obtained as follows,

$$G1 = \frac{16.29s^4 + 11.98s^3 + 1.412s^2 + 0.00433s - 1.66e^{-6}}{s^5 + 1.55s^4 + 4.47s^3 + 1.41s^2 + 0.0031s - 1.24e^{-6}}, \quad (6.18)$$

$$G2 = \frac{4.55s^4 + 1.16s^3 + 0.1377s^2 + 0.000197s - 6.6e^{-8}}{s^5 + 1.475s^4 + 1.03s^3 + 0.135s^2 + 0.00019s - 7.24e^{-8}}, \quad (6.19)$$

$$G3 = \frac{5.98s^4 + 1.657s^3 + 0.366s^2 + 0.00173s + 7.85e^{-7}}{s^5 + 2.65s^4 + 1.18s^3 + 0.366s^2 + 0.0015s + 6.6e^{-7}}, \quad (6.20)$$

$$G4 = \frac{16.48s^4 + 4.69s^3 + 0.85s^2 + 0.0016s + 1.2e^{-5}}{s^5 + 5.56s^4 + 2.74s^3 + 0.84s^2 + 0.00013s + 1.06e^{-5}}. \quad (6.21)$$

The eigenvalues of all estimated models are shown in Table 6.2:

Table 6.2 Eigenvalues of Estimated model

No	Eigenvalue	No	Eigenvalue
1	**0.00035**	8	-0.00359
2	**0.00031**	9	-2.19
3	-0.0025	10	$-0.6 \pm j1.9$
4	-0.345	11	$-0.655 \pm j0.6$
5	-0.00173	12	-0.228 ± 0.3
6	-0.164	13	$-0.0007 \pm j0.0035$
7	-0.00051	14	$-0.251 \pm j0.32$

Table 6.2 shows that there are two positive real eigenvalues. Both of the two real eigenvalues should be zero. Theoretically, the angle terms in the speed rows of the state matrix should sum to zero, i.e., the state matrix should be singular [14]. This singularity is caused by the fact that an equal change in each of the generator angles has no effect on the power flow in the interconnecting network. Round-off errors in calculation, and errors in the initial conditions determined by the iterative load flow solution, have made this sum nonzero [14]. In the case of the estimated model above,

the sum both of two real eigenvalues is 0.00004. It is a very small error. On the other hand, all the complex modes are stable. The result shows that the estimated model is acceptable.

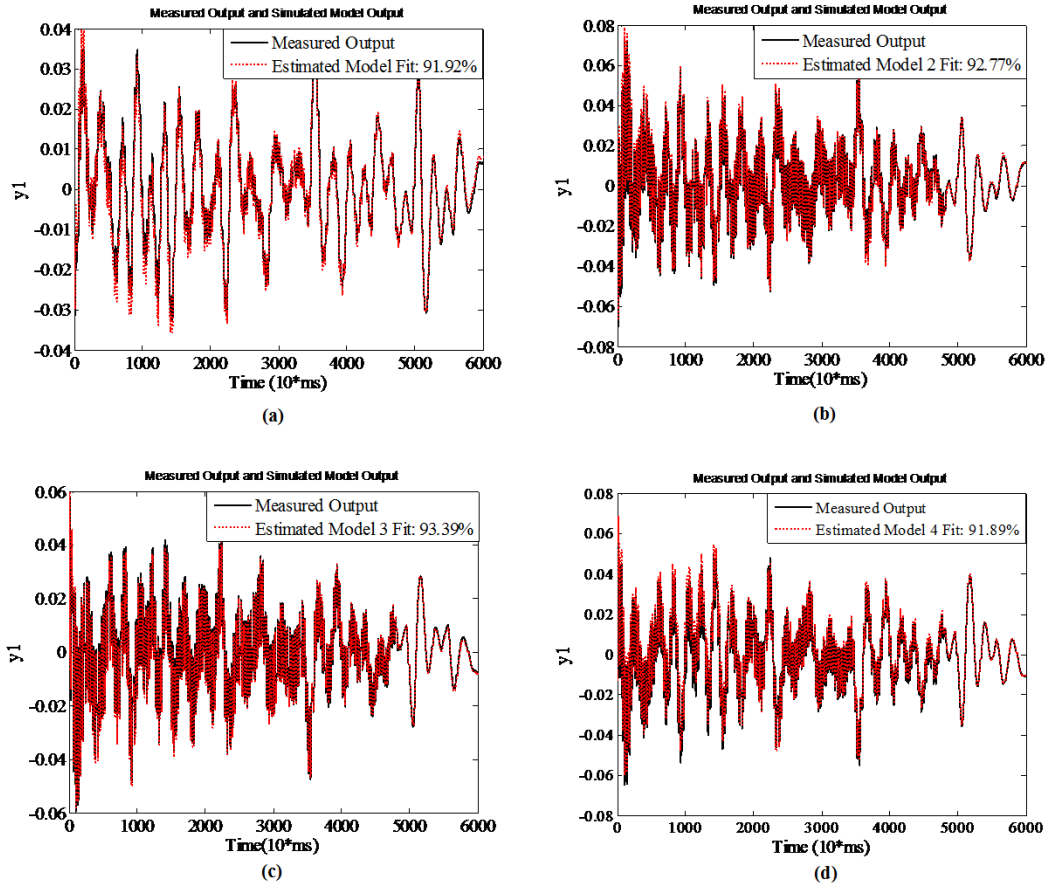

Figure 6.22 Validation of estimated model in case 3 with high RE penetration.

The estimated models are validated using a different set of data with the period of data 60 s. The simulation results of angular velocity deviation of each generator in case 1 using validation data are shown in Fig. 6.22. The simulation results show that the error between the measured output of the real system and the estimated model are smaller than specification, where the estimated model fit G1, G2, G3 and G4 are 91.92%, 92.77%, 93.39% and 91.89 %, respectively. The results confirm that the estimated model has a similar characteristic with the real system.

However, the set of data measurement is composed of many oscillatory components with different frequencies and contain noises. In general, noises occur at high

frequencies which are beyond the frequency of power system oscillations. To improve the quality of estimated model, the noises elimination technique is carried out prior to the detection of power oscillation modes.

To eliminate noises, the Discrete Fourier Transform (DFT) filtering is employed. The original measured oscillation data is filtered by low pass DFT filter to obtain the extracted frequency component. Then the extracted oscillation data is constructed by applying inverse DFT (IDFT) to the extracted frequency component. Meanwhile, the unwanted frequency components such as local oscillation data and noises with higher frequencies can be eliminated and the original signal can be filtered into signals containing mainly power oscillations. Finally, these data can be applied to construct estimated model using OE identification. The estimated models of each generator using low pass filter are shown in Figure. 6.23. The results show that the quality of estimated models is better than the estimated models without filtering.

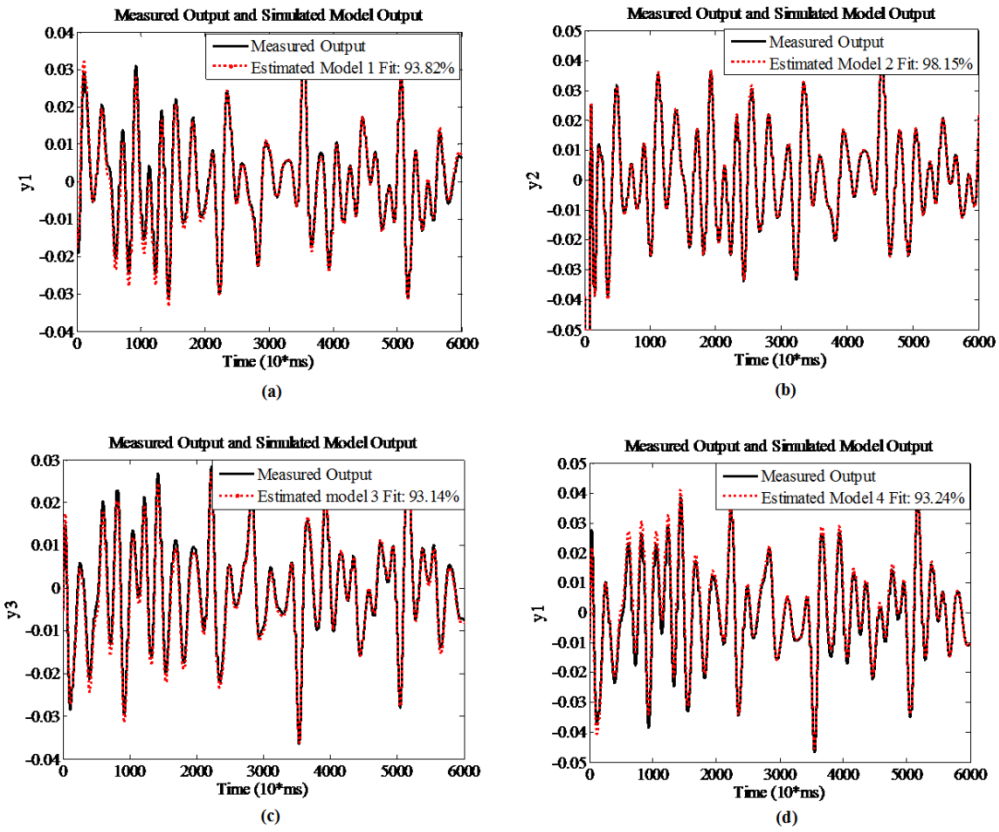

Figure 6.23 Validation of estimated model in case 3 using low pass filter.

Based on the new estimated model, PSS parameters are tuned using the proposed robust control design. In the optimization, the ranges of controller parameters are set

as follows: $K_{p,min}$ and $K_{p,max}$ are set as 1 and 30, $T_{p,i,min}$ and $T_{p,i,max}$ are set as 0.001 and 1, ς_{spec} is set as 0.1 and σ_{spec} is set as -0.1. As a result the PSS parameters are changed as follows,

$$K_{PSS1} = 11.81\left(\frac{0.8641s+1}{0.7395s+1}\right)\left(\frac{0.8495s+1}{0.7199s+1}\right), \tag{6.22}$$

$$K_{PSS2} = 12.02\left(\frac{0.8735s+1}{0.7404s+1}\right)\left(\frac{0.8524s+1}{0.7302s+1}\right), \tag{6.23}$$

$$K_{PSS3} = 13.10\left(\frac{0.8701s+1}{0.7521s+1}\right)\left(\frac{0.8502s+1}{0.7108s+1}\right), \tag{6.24}$$

$$K_{PSS4} = 10.5\left(\frac{0.8299s+1}{0.7403s+1}\right)\left(\frac{0.7998s+1}{0.7201s+1}\right). \tag{6.25}$$

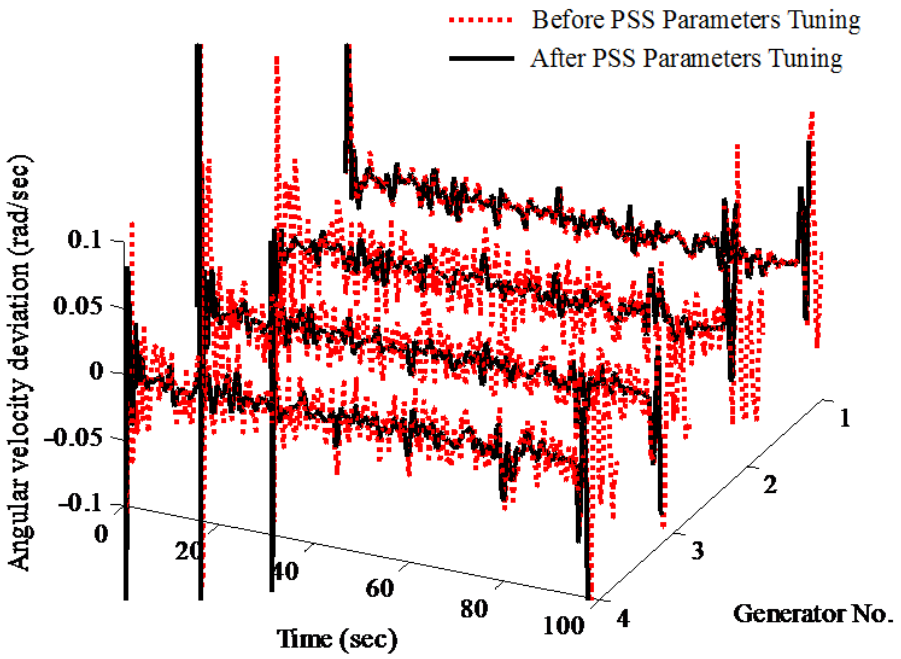

Figure 6.24 The system responses before and after PSS parameters tuning without fault.

The response of angular velocity deviation of each generator after applying the new PSS parameters is shown in Fig. 6.23. The overshoot and settling time of angular velocity deviations in the case of the after PSS parameters tuning are much lower than those of the before PSS parameters tuning. All simulation studies above show that the proposed technique gives adaptivity as well as robustness to the conventional type of controllers and is able to improve stability effectively.

6.6. Conclusions

Based on the results above, by applying adaptivity as well as robustness to the conventional type of controllers, the controllers are able to stabilize not only in low RE penetration, but also in extreme condition and high RE penetration. Without the availability of all system parameters and exact models, steady state data obtained from each generator can be used to construct estimated model by employing EO identification system. The estimated model can be used to tune PSS parameters. To take system uncertainties into consideration in the PSS optimization, the inverse additive perturbation has been applied to represent unstructured system uncertainties. To improve the system robust stability against system uncertainties, the PSS parameters have been automatically optimized by GA. A number of simulation tests in the two-area four-machine power system confirm that the proposed PSS control design is effective to stabilize the system against various line flow conditions and inertia constant due to RE penetration in comparison with the conventional PSS and RPSS without considering adaptivity.

REFERENCES

[1] A. Battaglini, Lilliestam J, Hass A, Patt A. Development of supersmart grids for a more efficient utilisation of electricity from renewable sources. J Cleaner prod 2009; 17: 911-8.

[2] G. Utsunomiya, Yoshida M, Tsuji T, Oyama T, Hashiguchi T, Goda T. A study on control effects of power system stabilizer on power system dynamics under a large penetration of PV generations. The international conference on electrical engineering 2012; July 8-12: Kanazawa, Japan: 630-4.

[3] F.P. DeMello, Concordia C. Concepts of synchronous machine stability as affected by excitation control, IEEE Trans. on PAS. 1969; 88: 316-29.

[4] E. Larsen, Swarm D. Applying power system stabilisers. IEEE Trans. on PAS. 1981; 100: 3017-46.

[5] E.Z. Zhou. Design of stabilizers for a multimachine power system based on the sensitivity of PSS effect. IEEE Power & Energy Society 1992; 7: 3: 606 - 13.

[6] M. Aldeen. Multimachine power system stabilizers design based on new LQR approach. Proc. of IEE Proc.-Gen. Tran. Dist. 1995; 142: 494-502.

[7] S. Chen S. H_∞ optimization-based power system stabilizer design. Procs. of IEE.-Gen. Tran. Dist. 1995; 142: 179-84.

[8] T.C. Yan. Applying optimization method to power system stabilizer design – Parts 1 & 2. Int. J. of Elect. Pwr. & Ener. Syst. 1997; 19: 29-43.

[9] A.N. Cuk Supriyadi, Design of Robust Power System Stabilizer using Genetic Algorithm-based Fixed-Structure H_∞ Loop Shaping Control. Proc. of the 17th World Congress The International Federation of Automatic Control 2008; July 6-11,Seoul, Korea: 11086-91.

[10] P. Kundur. Power system stability and control. McGraw Hill 1994.

[11] J. Machowski, J.W. Bailek, J.R. Bumby, Power System Dynamic and Stability, John Willey, Chichester, England, 1997.

[12] P.S. Rao, Sen I. Robust tuning of power system stabilizers using QFT. IEEE-Trans. on Control Systems Technology 1996; 4: 478-86.

[13] T. Elie, Poinot T, Ouvrard R, Abche A. Initialization of Output Error Identification Algorithms. PhD Thesis 2008; The university of Balamand, Lebanon.

[14] G. Rogers, " Power System Oscillations", Kluwer Academic Publisher, USA, 2000.

CHAPTER 7

CONCLUSION

7.1. Conclusion

In this thesis, the robustness and adaptivity enhanced controller design to improve dynamic stability in smart grid power system with high renewable penetration has been proposed. In this thesis, the existing controllers, most of which are PID or lead-lag controllers are optimized, so that they can exhibit better performance and that if this alone cannot attain desirable performance, new devices will be installed. The unstable outputs of renewable energy generation units cause frequency deviation from the rated value in micro grid power system. Moreover, when a large portion of the power demand is covered by the power from the renewable energy, the number of conventional rotating type of generators in operation decreases, which results in the reduction of total inertia constant. This makes the power system stability weak. To overcome this problem, improvement in the damping factor must be done. In order to achieve this, controller should properly function where robustness is much desirable against system uncertainties such as various generating and loading conditions, unpredictable network structures, variations of system parameters etc. However, when the variations of sensitive variables are large, giving robustness to the controllers is not enough. We need to make the controllers adaptive to the changes in operating conditions due to the high penetration of RE sources. Then a technique that gives adaptivity as well as robustness to the conventional type of controllers is proposed. The proposed robust control design has the following practical features.

1. Designing existing structure (PID or Lead/lag controller) by considering robustness and adaptivity. The existing structure of controller is easy to be implemented in utility and costless. In adaptive control, the controller parameters are changed depending on the situations. By considering the

robustness, it is not desirable that the parameters are changed too frequently. It is preferable that the parameter alteration is done at the right moment.

2. The identified model is equipped with virtual controller. The advantage of the feature is the parameter tuning of the controller can be done without disturb the real controller. The virtual controller is modeled by mathematical model for more flexibility and low cost.
3. The proposed control design method is able to store several good models and corresponding controller parameter sets in memory, and re-uses them in the similar situations without model identification and controller parameter re-tuning, Then we have "Model and Controller Bank"
4. Each control device is able to identify and tune controller parameters independently. As a result, no communications system necessary and cost of investment can be reduced.
5. Not only PSS and energy storage (ES) controller design, it can be applied to design damping controller of other FACTS controllers, high voltage direct current (HVDC) link etc.

A number of simulation tests for robust energy storage in hybrid wind-diesel power systems and adaptive robust PSS for stabilization in a two-area four-machine interconnected power systems with high renewable energy penetration confirm that the proposed controllers are very robust and gives satisfactory damping against various line flow conditions, inertia constant and fault locations.

7.2 Suggestion/Further research

There are a number of issues that are still to be addressed in the robustness and adaptivity enhanced controller design,

1. The identified/estimated model can be designed by other methods to get more accurate and much close to real system.
2. The proposed method can be extended to stabilize power systems containing a number of FACTS-based stabilizers.

3. It is possible to combine the robust control design with model free adaptive control in an interconnected power system with high renewable energy penetration.